Compatible and incompatible observables in the paradigmatic multislit experiments of quantum mechanics

Johannes Christopher Garbi Biniok

Doctor of Philosophy

University of York

Mathematics

September 2014

Abstract

The present investigation is about the quantum mechanics of multislit interference experiments. One of the cornerstones of our understanding of quantum mechanics is provided by the analysis of this type of experiments. Beginning with Bohr and Einstein, the discussion revolved mostly around single-slit diffraction and double-slit interference, probing the complementarity of path determination and the appearance of interference fringes, and contrasting the familiar with the quantum. Here, we are concerned with developing a systematic understanding and description of multislit interference experiments, i.e. setups in which a plurality of slits is illuminated. We provide a characterisation of a number of relevant observables, discussing those that are compatible and may be measured jointly, and also incompatible observables which cannot be measured jointly but instead display quantum uncertainty.

We begin with a discussion of a particular modification of the classic double-slit interference experiment which highlights the realisation of specific position and momentum observables which are jointly measurable. Although there are technical results regarding the coexistence of specific position and momentum observables, it may be surprising that ubiquitous experimental setups provide a preparation of such quantum states. We proceed with a discussion of the particular character of the incompatibility of certain measurements by building on an initial heuristic argument provided by Aharonov, Pendleton and Petersen. We prove, extend and discuss a formulation of uncertainty suitable for the context of multislit experiments. We conclude with a comparison of this formulation of uncertainty with an alternative uncertainty formulation developed by Uffink and Hilgevoord. Although these two uncertainty formulations are very different technically, we demonstrate that the same tradeoff is expressed independently.

Contents

List of Figures

Preface

The present doctoral dissertation is compiled from research that was performed between the years 2011 and 2014 at the University of York in the department of mathematics. The main topic of investigation is the quantum mechanics of multislit interference experiments. The general foundational interest of the physics community seems to focus on contrasting single-slit diffraction experiments and double-slit interference experiments, and the associated questions regarding complementarity. Here, a more general investigation of multislit interference experiments is presented. We provide a detailed study of the relevant observables, characterise interference quantum states and address quantum uncertainty.

At the time of writing, two scientific articles were published based on this research and a third one is being finalised for publication. The present text is, however, more detailed on several accounts. An introduction is provided to the relevant parts of the quantum mechanical formalism. Although this introduction may appear deceptively short, this accurately reflects the nature of the problems discussed: If phrased carefully, the answers can be put into simple terms. The main body of the text has been expanded by some additional discussion of relevant physics while detailed mathematical calculations are found in the Appendix. For going back and forth between different sections of the text, hyperlinks are provided. In particular, any reference of a specific part of the Appendix is a hyperlink, and in the Appendix a hyperlink is provided that leads back to the specific point, where the Appendix was referenced.

The first part comprises an analysis of a novel variety of multislit interference experiments that were interpreted as a violation of quantum complementarity since it appeared that incompatible quantum properties were being measured together [3]. It is argued that this type of experiment can be

understood, fully in line with quantum mechanics, as a joint measurement of compatible functions of the position and momentum observables. The analysis is based on earlier work of Busch and Lahti, who have shown that commuting functions of position and momentum exist [4].

The second part is an investigation of the quantum uncertainty in interference experiments based on an initial attempt by Aharonov, Pendleton and Petersen at modifying the so-called Heisenberg uncertainty relation in order to accurately express the relevant tradeoff [1]. The proposed uncertainty formulation was, however, never developed beyond a heuristic argument. We address technical issues, obtain a correct lower bound and discuss restrictions on the allowed quantum states. We develop the idea by introducing a refined observable, which allows precisely resolving the fine structure of the interference pattern.

The third part provides a comparison with an alternative uncertainty formulation developed by Uffink and Hilgevoord for single- and double-slit experiments [2]. However, in order to successfully apply their uncertainty formulation to multislit interferometry, arising issues need to be addressed. We generalise an underlying concept to fit the multislit context and find that additional considerations are necessary in order to express the relevant tradeoff. The comparison then becomes straightforward. Many of the results agree qualitatively, independently confirming that the relevant physical structure is captured.

For the purpose of a detailed and complete discussion, the Python code used to perform the referenced numerical calculations is provided in the Appendix.

Acknowledgements

A myriad of events led to the completion of this dissertation. The people directly involved in the chain of causation I wish to thank at this point.

The usual suspect is, of course, the supervisor. Indeed, I am extremely grateful to Paul Busch for the excellent guidance. Throughout the entirety of the last three years he has been available for questions and interested in discussing ideas. This made research very enjoyable, even at the times when it was frustratingly challenging—and then I could always count on Paul's expertise in phrasing a physics problem in mathematical terms or in plain words.

Jukka Kiukas, who is currently at the University of Nottingham, was immensely helpful in providing additional insight into a tricky problem. This enabled me to focus on the subject matter of my research, without getting sidetracked into a mathematical bog. I am very grateful for this.

I would also like to thank Kong K Wan of the University of St Andrews. In the winter semester of 2010 he taught a module dealing with the Foundations of Quantum Mechanics. His lectures fascinated me to the point that I asked for more, so he suggested contacting Paul Busch.

This leaves the people to acknowledge that make up the other part of my life: My family, including my partner Zoe. Thank you.

Declaration

I declare that the work presented here, except where otherwise stated, is based on my own research and has not been submitted previously for a degree at this or any other university.

All of the reported work was done in close collaboration with my supervisor, Paul Busch, while some of the work was done with a further collaborator, Jukka Kiukas of the University of Nottingham. Two scientific articles were published based on this research:

- J.C.G. Biniok and P. Busch, 'Multislit interferometry and commuting functions of position and momentum', Phys. Rev. A **87**, 062116 (2013)
- J.C.G. Biniok, P. Busch and J. Kiukas, 'Uncertainty in the context of multislit interferometry', Phys. Rev. A **90**, 022115 (2014)

Chapter 2 is based on the first publication, while Chapters 3 to 5 are based on the second publication. At the time of writing, a third manuscript is being prepared for submission:

- J.C.G. Biniok, 'Uncertainty formulations for multislit interferometry' (unpublished)

Some of the contents of Chapter 4 and the entirety of Chapter 6 are based on the third manuscript.

Chapter 1

The basic framework

Quantum mechanics is the general framework used to describe the physical world at the microscopic scale. This chapter serves as an introduction to those aspects of quantum mechanics that are relevant to the following investigation. The discussed results are all known very well, but reviewed here so that they may serve as a foundation to the following chapters.

1.1 Introduction

The nonclassical behaviour of microscopic objects is described by the mathematical framework called quantum mechanics. In a quantum mechanical description a given quantum object is characterised by a quantum state. According to quantum mechanics, the quantum state completely determines the properties of that object. The precise meaning of the quantum state, however, has been and continues to be a topic of debate. In particular, it is still disputed to what extent the properties of microscopic objects can be considered determined by quantum mechanics. The work of Einstein, Podolsky and Rosen played a major part in this discussion [7]. A more recent addition to the discussion, indicating continued interest and a lack of resolution, is the work of Pusey, Barrett and Rudolph [8].

The peculiar character of the quantum state is reflected in the equally peculiar predictions regarding the dynamical variables. The quantum mechanical treatment of the dynamical properties, the so-called observables, associated with a given physical system is unprecedented. In particular, the fact that a limited amount of information about a quantum system exists (according to the Copenhagen interpretation of quantum mechanics), rather than a limited amount of information being available, makes quantum mechanics intrinsically statistical. Substantial effort was expended to address this issue, most notably in the form of Bohmian mechanics and the Everett interpretation [9, 10].

A classical theory contains no restrictions on the existence or accessibility of observables, summarised by the following two statements: Every property of a given physical system

1. exists independently of its observation, and

2. exists independently of other observations.

At the microscopic level, however, very different behaviour is exhibited. The properties of a quantum object can change upon interaction with a different system or through evolution, to the point that the new properties of the quantum object might be in apparent contradiction with its original properties. We are forced to reject the first statement when speaking about microscopic systems. This is further complicated by the fact that an interrelationship exits between the physical properties of a single quantum object,

so that the observation of one property can have an effect on a different property. We are forced to reject the second statement as well. In this sense the classical concepts of "particle" and of "wave" are found insufficient for a quantum mechanical description. Quantum objects may display characteristics of either depending on the observation, whereas classical physics featured a clear classification of phenomena into either particle or wave. Certainly, a simple phenomenon, such as the propagation of a neutron through an interferometer or the detection of an electron, can be understood in terms of just particle or wave behaviour. More generally though, quantum mechanics requires aspects of both to be present in a description: A limited observation of a property associated with a particle may be possible at the same time as a limited observation of a property associated with a wave. This suggests that the concepts of particle and wave merely refer to two extremal cases with a continuous range of intermediate properties. We will be discussing such a case in the form of a modified multislit experiment in Chapter 2. The extent to which two observables may exist jointly is described by tradeoff relations, which are more commonly referred to as uncertainty relations. A particular mathematical formulation of an uncertainty relation for multislit experiments will be discussed starting with Chapter 3.

In the remainder of this chapter we discuss the mathematical formalism required to describe quantum systems as they are presented here. The quantum state and the observables are discussed in Sec. 1.2, along with the (canonical) commutation relation. This serves as the basis for the discussion of the principle of uncertainty and uncertainty relations in Sec. 1.3. Finally, we are going to address concepts relevant specifically to multislit experiments in Sec. 1.4, such as the evolution of a quantum state in a multislit setup.

1.2 Quantum states and observables

Quantum mechanics as presented here was formalised by John von Neumann [11]: With a given physical system we associate a complex Hilbert space $\mathcal{H}$. A particular physical state of that system, called (pure) quantum state, corresponds to a ray in $\mathcal{H}$. Quantum states, as elements of an abstract Hilbert space, are denoted using lowercase Greek characters, such as ψ or ϕ. More precisely, the particular Hilbert space of interest to the present discussion is the space of square-integrable complex-valued functions, denoted $L^2(\mathbb{R})$.

The dynamical properties of the given quantum object, more concisely referred to as observables, are represented by selfadjoint operators on $\mathcal{H}$. The pair of position $\mathcal{Q}$ and momentum $\mathcal{P}$ constitutes the classic example of observables. They are represented by operators Q and P respectively. In the following chapters, we will be dealing with measurements of Q and P as they occur in multislit experiments.

A Hilbert space being a generalisation of the Euclidean space, we have generalised concepts of length and angle in the form of a norm and an inner product. Given two quantum states ψ and ϕ, their inner product may be evaluated using their position representations $\psi(x)$ and $\phi(x)$,

$$\int_{-\infty}^{\infty} \psi^*(x)\ \phi(x)\ \mathrm{d}x\,. \tag{1.1}$$

It is common to refer to representations of quantum states in terms of L^2 functions using the term wavefunctions. This terminology originates from the solutions of the Schrödinger equation, which is a wave equation.

The norm of a state ψ is defined in terms of the inner product,

$$||\psi|| = \int_{-\infty}^{\infty} \psi^*(x)\ \psi(x)\ \mathrm{d}x\,. \tag{1.2}$$

The so-called expectation values are also defined by means of the inner product. For examples, in the position representation of ψ the expectation value of Q is given by

$$\langle Q \rangle_\psi = \int_{-\infty}^{\infty} \psi^*(x)\, x\, \psi(x)\ \mathrm{d}x\,. \tag{1.3}$$

The expectation value provides the link with experiments, quantifying the predicted statistics of the measured values of a particular observable in a given quantum state. We will be dealing mostly with the standard deviations, which are defined in terms of expectation values. We use $\Delta(Q,\psi)$ to denote the standard deviation of Q in state ψ,

$$\Delta(Q,\psi) = \sqrt{\langle Q^2 \rangle_\psi - \langle Q \rangle_\psi^2}\,. \tag{1.4}$$

In the following chapters, we will utilise position and momentum-space representations of quantum states. The Fourier transformation maps from position space to momentum space, while the inverse Fourier transformation

corresponds to the inverse mapping. The inverse Fourier transformation is defined by

$$\psi(x) = \frac{1}{\sqrt{2\pi\hbar}} \int_{-\infty}^{\infty} \mathrm{e}^{-\mathrm{i}\,xp/\hbar}\, \widehat{\psi}(p)\, \mathrm{d}p\,, \tag{1.5}$$

mapping the momentum representation $\widehat{\psi}(p)$ to the position representation $\psi(x)$. From now on we use units so that $\hbar = 1$.

Regarding the observables, as mentioned above, in the Hilbert-space formulation of quantum mechanics observables are associated with operators. The physical relationship between a pair of observables is mathematically described by the commutation relation of the operators involved. The two observables position $\mathcal{Q}$ and momentum $\mathcal{P}$, represented by two operators Q and P, form a canonically conjugate pair in that they satisfy the canonical commutation relation

$$[Q, P] = QP - PQ = \mathrm{i}\,. \tag{1.6}$$

According to von Neumann's theorem, a pair of observables is jointly measurable if the observables commute [11]. Hence the observables $\mathcal{Q}$ and $\mathcal{P}$ are said to be incompatible, precluding the existence of a complete set of joint eigenvectors. As will be seen in Sec. 1.3, this results in and is expressed by quantum uncertainty. The incompatibility of a pair of operators does not, however, exclude the existence of some common eigenvectors, allowing some (but not all) information about both observables to be measured; see Ref. [4] for more information regarding this point. This possibility is best illustrated considering the canonical commutation relation in a form due to Weyl [12]. The Weyl form of the canonical commutation relation is expressed in terms of (bounded) unitary operators $\mathrm{e}^{\mathrm{i}\,p\,Q}$ and $\mathrm{e}^{\mathrm{i}\,q\,P}$ and reads

$$\mathrm{e}^{\mathrm{i}\,p\,Q}\,\mathrm{e}^{\mathrm{i}\,q\,P} = \mathrm{e}^{-\mathrm{i}\,pq}\,\mathrm{e}^{\mathrm{i}\,q\,P}\,\mathrm{e}^{\mathrm{i}\,p\,Q}\,. \tag{1.7}$$

Observe that the operators commute for $pq = 2\pi n$ with $n \in \mathbb{N}$, because then $\mathrm{e}^{-\mathrm{i}\,pq} = \mathrm{e}^{-\mathrm{i}\,2\pi n} = 1$. Equivalently, this condition may be expressed in terms of the minimal periods of the operators, $T = 2\pi/q$ and $K_n = 2\pi/p$ respectively

$$T\,K_n = \frac{2\pi}{q}\frac{2\pi}{p} = \frac{(2\pi)^2}{2\pi n} = \frac{2\pi}{n}\,. \tag{1.8}$$

This result suggests that a function of position commutes with a function of

momentum if their relative periods are chosen accordingly [4]. If the period of the former is T, then the period of the latter must correspond to

$$K_n = \frac{2\pi}{n\,T} = \frac{4\pi}{mT}\,, \tag{1.9}$$

where we introduced $m = 2n$. We also define

$$K = \frac{2\pi}{T}\,. \tag{1.10}$$

This result about the commutativity of functions of position and momentum is central to much of the remainder of the present investigation. In Chapter 2 we will be dealing with commuting projection operators revealing information about both Q and P by way of the particular experimental implementation. The relative periods of these projection operators is specified by Eq. (1.10) for the particular experiment considered. Starting with Chapter 3, we will be discussing an expression of the incompatibility of the observables in multislit experiments in the form of an uncertainty relation. This involves decomposing the operators Q and P into mutually commuting and mutually noncommuting parts, according to the periods indicated in Eq. (1.9).

1.3 Uncertainty in quantum mechanics

In 1927 Heisenberg introduced the notion of a fundamental limit to the existence of precise values of a pair of observables represented by canonically conjugate operators [13]. Heisenberg presented a heuristic argument elucidating the physical principle now known as Heisenberg's principle of uncertainty. A number of mathematical formulations of uncertainty followed shortly thereafter [12, 14–16].

Kennard first published a tradeoff relation expressed in terms of the standard deviations of operators satisfying the canonical commutation relation of a single non-relativistic particle [14],

$$\Delta(Q,\psi)\,\Delta(P,\psi) \geq \frac{1}{2}\,. \tag{1.11}$$

Robertson established the uncertainty relation as a formal consequence of the non-commutativity of the operators involved [15]. For operators A and

B, we have

$$\Delta(A,\psi)\ \Delta(B,\psi) \geq \frac{1}{2}|\ \langle [A,B]\rangle_{\psi}\ |\,. \tag{1.12}$$

The Eqs. (1.11) and (1.12) are mathematical formulations of the principle of uncertainty. However, a particular mathematical formulation should not be regarded equivalent to the general principle. (A precise distinction between the uncertainty principle and its various formulations seems particularly important in light of recent claims regarding quantum uncertainty; see Ref. [17] and references therein.) In fact, in Chapter 3 we are going to argue that multislit experiments are outside the scope of Eq. (1.11), and that an alternative expression must be sought in order to successfully express the uncertainty principle in that context. We find that an alternative expression may be obtained using Eq. (1.12) after a suitable adaptation of the observables to the given experimental context.

1.4 A quantum mechanical description of multislit experiments

The quantum mechanical analysis of multislit experiments, which is developed in this section, is indispensable for the discussions in all following chapters, with the exception of Chapter E.

Multislit interference experiments have been very fruitful throughout the historical development of physics: Young's famous double-slit interference experiment conclusively displayed the wave behaviour of light. Möllenstedt and Jönsson first illustrated the wave-behaviour of a massive particle, namely the electron, in multislit interference experiments [18, 19]. More recently, the quantum mechanical behaviour of the much larger and heavier C_{60} molecule was demonstrated in multislit interference experiments [20].

A diagrammatic illustration of the simplest multislit experiment, the double-slit setup, is depicted in Fig. 1.1 and the associated interference pattern in Fig. 1.2. A quantum object traverses the experimental setup along the z-direction (from left to right). After passage of the aperture mask at location (i), the quantum object propagates freely until it is observed at location (ii) on a detection screen. For as long as the quantum object traverses the experimental setup from preparation to detection, the spatially extended wavefunction describing the object is present throughout the entire exper-

Figure 1.1: A typical multislit experiment, an ensemble of quantum objects is incident on the double-slit aperture mask at location (i), while at location (ii) an interference pattern is observed on a distant screen. An illustration of an interference pattern is provided in Fig. 1.2.

Figure 1.2: An illustration of the interference pattern observed in a double-slit experiment, such as the one depicted in Fig. 1.1. The regions where high intensity is detected form evenly spaced fringes (black fringes on white background). With increasing distance to the central fringe, the fringes become less visible as the overall intensity decreases.

imental setup. The detection event, though, registers a single object at a specific location, while an ensemble of such detections makes up an interference pattern typically associated with the behaviour of continuous waves.

1.4.1 Quantum interference and the complex numbers

Interference arises in quantum mechanics immediately from the Born rule, which postulates that probabilities are the expectation values of projections. In the present context, the Born rule amounts to a method for obtaining probabilities from the complex-valued wavefunctions by means of taking the (real-valued) modulus-square of the quantum amplitudes.

The following heuristic argument shows that interference phenomena follow immediately from the Born rule. Consider the experimental setup depicted in Fig. 1.1. There is a certain probability distribution associated with an illuminated slit A. We denote this probability distribution $\mathsf{P}(A)$. Analogously, there is a probability distribution $\mathsf{P}(B)$ associated with illumination of slit B. It is an *experimentally determined* fact that these probability distributions do not simply add up when both slits are illuminated. This phenomenon is called interference, and mathematically expressed by

$$\mathsf{P}(A \cup B) \neq \mathsf{P}(A) + \mathsf{P}(B) \; . \tag{1.13}$$

The probability distribution observed while both slits are open does not equal the sum of probabilities obtained from independent observations of each slit alone. This suggests the presence of an additional term, the so-called interference term $I(A, B)$

$$\mathsf{P}(A \cup B) = \mathsf{P}(A) + \mathsf{P}(B) + I(A, B). \tag{1.14}$$

It is emphasised that this is an experimental observation, which quantum mechanics must reproduce.

A quantum mechanical description is possible by means of a complex-valued function, while probabilities are identified with the square-modulus of that function by means of the Born rule. The detection probability of a quantum object with slit A open can be expressed in terms of a complex-valued function. We express this function in terms of a real $f(x)$ and a complex phase $\mathrm{e}^{\mathrm{i}\,\alpha\,x}$ where α is a (real) constant, both of which may depend

on the location along the axis of the screen x. The probability distribution associated with illuminating a single slit is obtained easily

$$\mathsf{P}(A) = \left| f(x)\, \mathrm{e}^{\mathrm{i}\,\alpha\, x} \right|^2 = f(x)^2. \tag{1.15}$$

Let us now consider simultaneous (and equal) illumination of both slits, i.e. two slits A and B open simultaneously. In this case, we require two functions but there can only be a difference in phase,

$$\Psi_A(x) = f(x)\, \mathrm{e}^{\mathrm{i}\,\alpha x}\,, \tag{1.16}$$

$$\Psi_B(x) = f(x)\, \mathrm{e}^{\mathrm{i}\,\beta x}\,, \tag{1.17}$$

where β is another (real) constant. As we assume equal illumination of the two slits, the quantum states can only differ in phase. We proceed to calculate the probability of joint passage of slit A and slit B

$$\mathsf{P}(A \cup B) = |\Psi_A(x) + \Psi_B(x)|^2 \tag{1.18}$$

$$= |\Psi_A(x)|^2 + |\Psi_B(x)|^2 + \Psi_A^*(x)\, \Psi_B(x) + \Psi_B^*(x)\, \Psi_A(x) \tag{1.19}$$

$$= f(x)^2\, (2 + 2\cos{(\alpha - \beta)x}) = 4\, f(x)^2 \cos\!\left(\frac{\alpha - \beta}{2} x\right)^2 . \tag{1.20}$$

The Born rule was used to obtain the final expression of the first line. The following calculation is straightforward, leading to a final result that indeed shows interference.

Quantum mechanics clearly describes the two-path interference exhibited in the double-slit experiment.

1.4.2 Modelling the multislit setup

The previous discussion of multislit experiments was heuristic, highlighting the observed phenomena. This section and the following section serve to make the discussion more precise. Again, let us consider the double-slit setup as depicted in Fig. 1.1, consisting of two slits forming an aperture mask on which a propagating quantum object is incident.

The quantum object propagates through the device depicted in Fig. 1.1 along the z-axis (from left to right). We model its wavefunction as a product, $\Psi(x, y, z) = \phi(x)\, \eta(y)\, \zeta(z)$. As is detailed in the following section and used later on, in the appropriate limit this problem can be simplified so that only

$\phi(x)$ needs to be considered: The state $\zeta(z)$ is a means of keeping track of the times of passage through the experimental setup, but any explicit time dependence can be removed while retaining an identification of the quantum state at different times with distinct locations in the setup. The state $\eta(y)$ is assumed to be entirely negligible. This enables us to focus solely on $\phi(x)$, the component along the transversal (vertical) direction.

The quantum state ϕ is diffracted at location (i). The action of the aperture mask at (i) is modelled by the following transmission function that gives the wavefunction $\psi(x)$ (up to normalisation) after passage through the aperture:

$$\phi(x) \to \chi_A(x)\,\phi(x) \equiv C\,\psi(x). \tag{1.21}$$

The indicator function $\chi_A(x)$ of set A takes the value 1 for $x \in A$ and 0 otherwise; A being the set that describes the effective aperture mask. The normalisation of ψ is provided by the constant $C = 1/||\chi_A\phi||$. Incidentally, Eq. (1.21) defines the action of an operator that is defined as a function $\chi_A(Q)$ of the position operator Q,

$$\left(\chi_A(Q)\,\phi\right)(x) := \chi_A(x)\phi(x).$$

This operator has eigenvalues 1 and 0 with associated eigenfunctions given by functions $\phi(x)$ either localised within A or within the complement of A. Thus, the state vector ϕ is projected onto an eigenvector of the *spectral projector* $\chi_A(Q)$ of Q associated with the set A. A single illuminated slit is assumed to prepare a quantum state described by an isolated peak, while coherent illumination of a general aperture mask is assumed to yield a suitable superposition of those.

The aperture mask at location (i) prepares a quantum state represented by the wavefunction $\psi(x)$, which then propagates freely until it arrives at (ii). In the Fraunhofer limit, upon arriving at (ii) the wavefunction has evolved so as to have a profile approximately proportional to that of the Fourier-transform $\widehat{\psi}(k)$ of $\psi(x)$. The following section provides the details.

1.4.3 Determining the momentum distribution via a late-time position measurement

From classical optics it is known that the interference pattern of a wave passing through an aperture mask can be described by the Fourier transformed aperture profile. Additional analysis is necessary to justify the same application in quantum mechanics. In particular, it is required to show that after free evolution the position representation of the state ψ_t at location (ii) is, up to scaling, approximated by the momentum representation of ψ_0, at the aperture at (i):

$$\psi_t \propto \mathcal{F}\psi_0 = \widehat{\psi}_0 \quad \text{(approximately)},$$

where $\mathcal{F}$ denotes the unitary operator effecting the Fourier transform,

$$\widehat{f}(k) = (\mathcal{F}f)(k) = \frac{1}{\sqrt{2\pi}} \int_{-\infty}^{\infty} f(x)\, \mathrm{e}^{\mathrm{i}\,k\,x}\, \mathrm{d}x. \tag{1.22}$$

Also see Eq. (1.5) regarding the inverse Fourier transform. We recall a simple 'rough and ready' argument here to show how this approximation can be obtained. The formal solution of the Schrödinger equation for free evolution, which may be obtained using the well known technique involving Green's function, is given by

$$\psi_t(x) = \sqrt{\frac{m}{2\pi \mathrm{i} t}} \int_{-\infty}^{\infty} \psi_0(x')\, \exp\left(\mathrm{i}\, \frac{m(x-x')^2}{2t}\right) \mathrm{d}x'\,. \tag{1.23}$$

With the limits of integration bounded by the apertures, the actual integration takes place from $-(T+a)/2$ to $(T+a)/2$, where a denotes the slit width. In the limit of large t then, the term depending on $(x')^2$ in the exponential can be neglected to a good approximation, because it is bounded by the finite dimensions of the aperture mask. The result is the following approximation

$$\psi_t(x) \approx \sqrt{\frac{m}{2\pi \mathrm{i} t}} \int_{-\infty}^{\infty} \psi_0(x')\, \exp\left(\mathrm{i}\, \frac{mx^2}{2t}\right) \exp\left(\mathrm{i}\, \frac{mx}{t} x'\right) \mathrm{d}x'\,. \tag{1.24}$$

After trivial rearranging, the desired expression is obtained:

$$\psi_t(x) \approx \sqrt{\frac{m}{\mathrm{i} t}}\, \exp\left(\mathrm{i}\, \frac{mx^2}{2t}\right) \frac{1}{\sqrt{2\pi}} \int_{-\infty}^{\infty} \psi_0(x')\, \exp\left(\mathrm{i}\, \frac{mx}{t} x'\right) \mathrm{d}x' \tag{1.25}$$

$$\approx \sqrt{\frac{m}{\mathrm{i}t}}\, \exp\left(\mathrm{i}\,\frac{mx^2}{2t}\right) \widehat{\psi}_0\left(\frac{m}{t}x\right) \tag{1.26}$$

The parameter t may be eliminated using $\frac{p_z}{m}t = L$, where L denotes the distance to the detection screen and p_z the longitudinal momentum component. In doing so, the limit of large t becomes a limit of large distance L in relation to the aperture size. Considering the typical dimensions of such a setup this seems reasonable. Compare, for example, the dimensions reported in Ref. [3], where the centre-to-centre separation of the two pinholes is $0.25 \cdot 10^{-3}\,\mathrm{m}$ and distance to the detection screen is $0.5\,\mathrm{m}$. Furthermore, as p_x/p_z will be small given these dimensions, we can also substitute p_z approximately with the magnitude of the mean momentum, p_0 so that for the mean wavelength λ of the packet we can use the value $\lambda = 2\pi/p_0 \approx 2\pi/p_z$, and so $t \approx mL\lambda/(2\pi)$. This gives the probability as

$$|\psi_t(x)|^2 \approx \frac{2\pi}{L\lambda}\, \left|\widehat{\psi}_0\left(\frac{2\pi}{L\lambda}x\right)\right|^2 . \tag{1.27}$$

1.4.4 Simple multislit wavefunctions

A single illuminated slit is assumed to prepare a quantum state described by a rectangular function of slit width, while a general aperture mask yields a suitable superposition of those. We consider superposition states of m coherently illuminated slits, where m is an even positive integer. These quantum states are but a subset of the quantum states that a multislit aperture mask can prepare, but they describe the important cases of the double-slit – illustrated in Fig. 1.3 – and the periodic aperture mask. They are of the form

$$\psi_n(x) = \frac{1}{\sqrt{2n}} \sum_{j=1}^{n} \Big[\mathrm{rec}_a\left(x + (2j-1)T/2\right) + \mathrm{rec}_a\left(x - (2j-1)T/2\right)\Big], \tag{1.28}$$

where the function $\mathrm{rec}_a(x)$ is of rectangular shape,

$$\mathrm{rec}_a(x) = \begin{cases} 1/\sqrt{a} & \text{for } x \in [-a/2, a/2] \\ 0 & \text{for } x \notin [-a/2, a/2] \end{cases} . \tag{1.29}$$

For uniformly illuminated aperture masks, the number of illuminated slits m is related to n via $m = 2n$. Furthermore, n is directly related to the

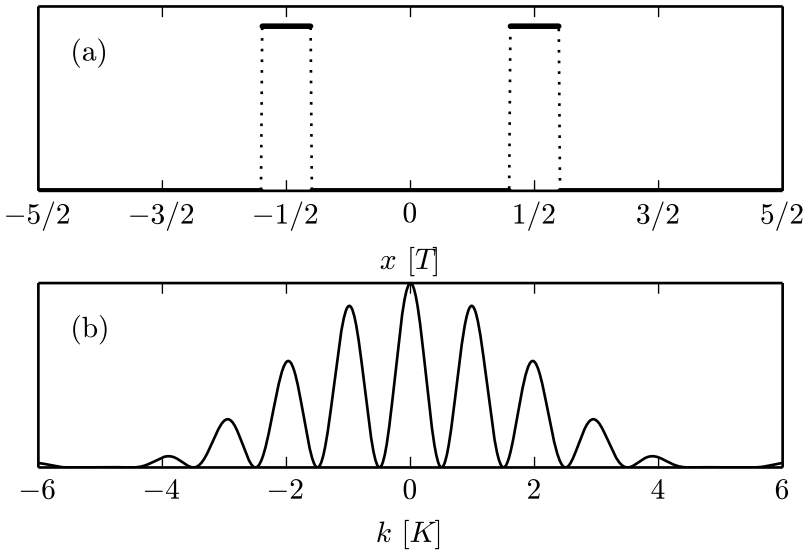

Figure 1.3: The probability distributions associated with the double-slit state ψ_1 are depicted, position space in (a) and in (b) momentum space. Note in particular that $\widehat{\psi}_1(k)$ vanishes at $k = (j + 1/2)K$, with integer j. Compare Fig. 1.2. The parameters were chosen such that $a/T = 0.2$.

support of the principal maxima of $\widehat{\psi}_n(k)$ via Eq. (1.9); see the explicit expression below. The rectangular function is a popular choice for describing the wavefunction profile across a single slit, although one may argue that it might not be the most physical choice. We are going to address the relevance of this choice for multislit experiments in Chapter 4, arguing that for purely multislit considerations this choice is acceptable. Only when (also) considering single-slit experiments, the rectangular function is unsuitable for technical reasons.

The interference pattern of a uniformly illuminated multislit is described by a wavefunction that can be computed analytically by means of a Fourier transform of the spatial wavefunction. The momentum-space wavefunction $\widehat{\psi}_n(k)$ (the Fourier transform of ψ_n) is given by

$$\widehat{\psi}_n(k) = \sqrt{\frac{a}{n\pi}}\,\mathrm{sinc}\Big(\frac{a}{2}k\Big)\sum_{j=1}^{n}\cos\bigg((2j-1)\,\frac{T}{2}k\bigg). \tag{1.30}$$

The following calculation is relatively trivial, but included so as to allow for easy comparison with an alternative way of obtaining an expression for the

Fourier transform of the wavefunctions discussed in Chapter 4.

$$\widehat{\psi}_n(k) = \mathcal{F}\psi_n(x) \tag{1.31}$$

$$= \frac{\mathcal{F}}{\sqrt{2n}}\left(\mathrm{rec}_a(x) * \sum_{j=1}^{n}\left[\delta\left(x + (2j-1)\frac{T}{2}\right) + \delta\left(x - (2j-1)\frac{T}{2}\right)\right]\right)$$

$$= \frac{1}{\sqrt{2n}}\sqrt{\frac{a}{2\pi}}\mathrm{sinc}\Big(\frac{a}{2}k\Big)\cdot\sum_{j=1}^{n} 2\cos\,(2j-1)\frac{T}{2}k \tag{1.32}$$

$$= \sqrt{\frac{a}{n\pi}}\,\mathrm{sinc}\Big(\frac{a}{2}k\Big)\sum_{j=1}^{n}\cos\,(2j-1)\frac{T}{2}k \tag{1.33}$$

Noting that the Fourier transform of a convolution is equal to a product of Fourier transforms, this calculation decomposes into two straightforward Fourier transformations. The computation proceeds by combining a sum of two complex phases into a real *sinc*, and a sum of two complex phases into a sum of real *cosines*. The latter identification happens symmetrically across the origin as indicated in Eq. (1.28).

For future reference, we define

$$f_n(y) = \sum_{j=1}^{n}\cos((2j-1)\,y), \tag{1.34}$$

and introduce at this point the dimensionless variable

$$\kappa = Tk/2\,, \tag{1.35}$$

which proves particularly useful for integrations.

By way of particular examples, let us consider an aperture mask consisting of two rectangular slits of width a at locations $\pm T/2$, and an incident wavefunction $\Psi(x)$ of constant real-valued amplitude passing through the aperture mask. The intensity profile of the interference pattern of the prepared double-slit superposition state ψ_1 is given by

$$\left|\widehat{\psi}_1(k)\right|^2 = \frac{a}{\pi}\,\mathrm{sinc}\Big(\frac{a}{2}\,k\Big)^2\cos\left(\frac{T}{2}\,k\right)^2, \tag{1.36}$$

The *sinc* function provides an envelope, while the *cosine* describes the fine structure, i.e. the interference fringes. At this point, it is not obvious how the identification of envelope and fine structure should be generalised to capture

ψ_n for $n > 1$. That question is addressed in Chapter 4.

Comparing Eq. (1.36) to the diffraction pattern resulting from the illumination of a single slit only, we observe that no *cosine* fringes are present in the momentum-space wavefunction of ψ_0,

$$\left|\widehat{\psi_0}(k)\right|^2 \propto \frac{a}{2\pi}\,\mathrm{sinc}\Big(\frac{a}{2}\,k\Big)^2 . \tag{1.37}$$

Note that although $n = 0$ denotes the single-slit state ψ_0, its support properties are unrelated to Eq. (1.9) because ψ_0 is not an interference state, but the result of diffraction.

Chapter 2

Compatible position and momentum observables

The present chapter comprises an analysis of a novel variety of multislit interference experiments that were interpreted as a violation of quantum complementarity since it appeared that incompatible quantum properties were being measured together [3]. In this experiment, information about spatial localisation is retained while information about interference is obtained.

It is argued here that this type of experiment can be understood, fully in line with quantum mechanics, as a joint measurement of compatible functions of the position and momentum observables. It is thus possible to subsequently gain information about the momentum distribution by means of the particular experimental setup with negligible impact on the position distribution, because the observation is of compatible coarse-grained versions of the complementary position and momentum observables. This explanation goes beyond addressing the question whether complementarity has been violated or not, namely by providing a better understanding of all quantum states prepared in multislit setups. The particular setup discussed in this chapter merely serves as a convenient illustration.

The analysis is based on earlier work of Busch and Lahti, who have shown that commuting functions of position and momentum exist [4].

2.1 Introduction

In traditional multislit experiments, as discussed in the previous chapter, the momentum distribution is captured on a detection screen. However, this procedure clearly destroys the quantum state. Establishing the existence of an interference pattern indirectly, i.e. without destroying the quantum state, is possible by removing the screen and replacing it by a wire grating, each wire carefully placed at the location of a node in the interference pattern [3]. The existence of an interference pattern may be deduced from the practically undiminished intensity passing the wire grating.

Using a lens, a geometric image of the aperture mask is produced such that the quantum state can be detected on the very set of positions it was prepared on—after it was subjected to the described momentum measurement. While indirectly observing an interference pattern without changing the localisation properties of a system may not be surprising from the point of view of classical physics, it is rather curious when considered in terms of quantum mechanics: Information about a quantum state was obtained, but apparently without changing the properties of that quantum state. In particular, information about a pair of incompatible observables was obtained; in this context, the measurement seems *classical*, revealing already existing information without changing the system properties.

This observation indicates that the experiment should be described in terms of two commuting observables which yield information about position and momentum respectively. In Sec. 1.6 we already addressed this matter, briefly pointing out that functions of position may commute with functions of momentum, although position and momentum do not commute. Indeed, as will be shown here, the experiment can be considered an approximate realisation of a joint eigenstate of mutually commuting functions of position and momentum. In the following two sections, the experimental setup and joint eigenstates of periodic sets of position and momentum are discussed in detail. This is followed by a description of multislit experiments in terms of joint eigenstates.

2.2 The modified multislit setup

The setup illustrated in Fig. 2.1 depicts a simplified version of the interference experiment reported in [3]. The experiment was performed using a double-pinhole, here the simpler double-slit setup is considered. A particle propagates through the device along the z-axis (from left to right). We model its wavefunction as a product, $\Psi(x, y, z) = \phi(x)\,\eta(y)\,\zeta(z)$, and focus on the component $\phi(x)$. This simplification was discussed in detail in Sec. 1.4.2.

The quantum state ϕ is diffracted at location (i) of Fig. 2.1, where the aperture mask is located. A wire grating is placed at location (ii), where the interference pattern would be observed. The separation of the wires depends on the spacing of the slits in the aperture mask via the indicated reciprocal correspondence $T \leftrightarrow 2\pi/T = K$, although in practice the wavelength of the source and the aperture-to-screen distance must be taken into account; compare Eq. (1.27).

A lens is placed immediately behind the wire grating for the purpose of producing at location (iii) the geometric image of the original aperture mask. The image is registered using appropriately placed detectors. Although this setup is sequential, with the aperture mask at (i) and the grating at (ii), it actually constitutes a joint (projective) measurement of the incident quantum state.

The aperture mask at location (i) prepares the quantum state represented by the wavefunction $\psi(x)$, which then propagates freely until it arrives at (ii). The action of the aperture mask is modelled by the transmission function that was specified in Sec. 1.4.2, Eq. (1.21), giving the wavefunction $\psi(x)$ (up to normalisation) after passage through the aperture mask. In the Fraunhofer limit, upon arriving at (ii) the wavefunction has evolved so as to have a profile proportional to that of the Fourier transform of the wavefunction at (i), denoted $\widehat{\psi}(k)$. Details regarding this approximation were discussed in Sec. 1.4.3.

The effect of the wire grating is modelled by a transmission function similar to the one specified in Eq. (1.21), but with a set B of intervals complementing the regions occupied by the wire grating:

$$\widehat{\psi}(k) = (\mathcal{F}\psi)(k) \to \chi_B(k)\,\widehat{\psi}(k) \equiv \left(\chi_B(P)\,\widehat{\psi}\right)(k), \tag{2.1}$$

where the arrow indicates passage through the wire grating and $\chi_B(P)$ de-

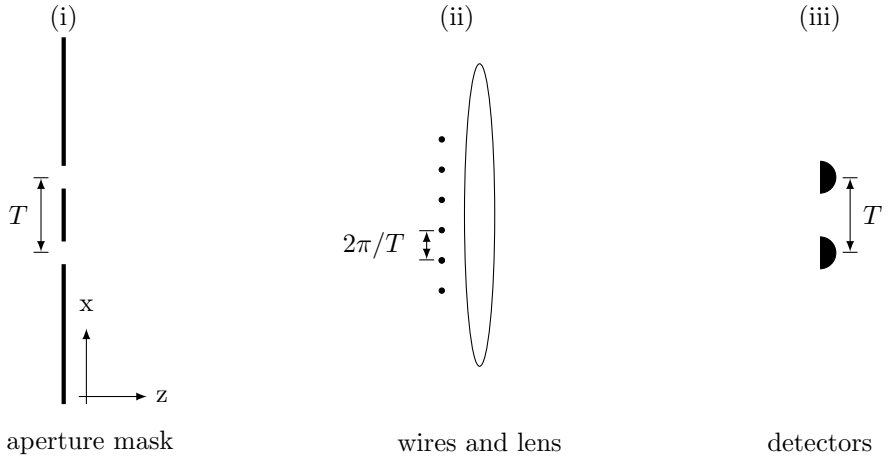

Figure 2.1: The modified double-slit interference experiment.

notes the spectral projector of momentum P associated with the set B and $\mathcal{F}$ denotes the unitary operator effecting the Fourier transformation, Eq. (1.22). Formally, the Fourier transform of ψ is denoted $\widehat{\psi}$.

Traversing the experiment from (i) to (iii), the action of the lens located at (ii) is modelled as spatial inversion, expressed by mappings $Q \mapsto -Q$ and $P \mapsto -P$, for the position and momentum respectively. This corresponds to the unitary parity transformation, which coincides with the square of the Fourier transformation $\mathcal{F}$. As a result, the divergent wave rays emerging from the aperture mask and arriving at the wire grating and lens are inverted so as to be refocused into an image of the original aperture mask.

This setup is realised by Afshar *et al.* in the form of a double-pinhole experiment with a total of six wires, each with a diameter of 0.127 mm and a separation of 1.3 mm [3].

2.3 Commuting functions of Q and P

While the canonical commutation relation, Eq. (1.6), represents the fact that the position and momentum observables are incompatible in a strong sense, a function of position may commute with a function of momentum. A first characterisation of commuting functions of position and momentum was given by Aharonov *et al.* in the context of an analysis of interference experiments, with the aim of explaining non-local momentum transfers in the Aharonov-Bohm effect [1]; we revisit this analysis in Chapter 3. A first

full proof of necessary and sufficient conditions for the commutativity of functions of position and momentum was reported by Busch and Lahti, who were unaware of the work of Aharonov *et al.* [4]. A first construction of a set of joint eigenstates was given by Reiter and Thirring [21]. Here, we present a construction of joint eigenstates that is readily identified with multislit interferometry. In Appendix A.1 an alternative, rigorous construction is included that generalises the one given by Reiter and Thirring. It is possible to show that these states are dense in the set of all possible states prepared in interference experiments. A technical manuscript detailing this is currently being prepared [22].

The existence of commuting functions of Q and P is suggested when considering the canonical commutation relation in the form due to Weyl, Eq. (1.7). We already noted in Sec. 1.6 that the operators $\mathrm{e}^{\mathrm{i}\,p\,Q}$ and $\mathrm{e}^{\mathrm{i}\,q\,P}$ commute for $pq = 2\pi n$ with $n \in \mathbb{N}$; or equivalently for respective periods T and $2\pi/(nT) = K_n$. Here, we focus on the case $n = 1$, which is denoted by K, as this is not only simpler but also reflects the experiment we wish to discuss. We conclude that, although Q and P do not commute, the spectral projections $\chi_X(Q)$ and $\chi_Y(P)$ onto periodic sets X and Y commute if the sets have periods T and K, respectively:

$$[\chi_X(Q), \chi_Y(P)] = 0.$$

(A set X is called periodic with (positive minimal) period T, if T is the smallest positive number by which X can be shifted such that the shifted set $X + T = X$, or equivalently, if its indicator function is a periodic function with minimal period T.)

Physical systems exhibiting such doubly periodic behaviour occur naturally. The electron in a crystal lattice constitutes a well known example: In position space, the electron is periodically localised in accordance with the periodic potential that is due to the crystal lattice. In momentum space, the electron is localised periodically in the so-called reciprocal lattice, i.e. a periodic lattice of reciprocal spacing. While solid state physics often deals with systems containing a very large (and essentially infinite) number of lattice points, it is argued below that even finite multislit experiments can be regarded as an approximate realisation of joint eigenstates of $\chi_X(Q)$ and $\chi_Y(P)$ over periodic sets.

The following construction of a class of joint eigenvectors has heuristic value and also makes the identification with multislit experiments more intuitive. It is carried out using the Dirac comb Ш_T,

$$\text{Ш}_T(x) = \sum_{j=-\infty}^{\infty} \delta(x - T/2 - jT)\,, \tag{2.2}$$

where δ denotes the delta-distribution. We denote the Dirac comb (or Shah function) using the Cyrillic letter 'sha' as is occasionally done in electrical engineering. We note that under a Fourier transformation the (shifted) Dirac comb Ш_T with period T is mapped onto a Dirac comb with period K,

$$\widehat{\text{Ш}}_K(k) = \frac{\sqrt{2\pi}}{T} \sum_{j=-\infty}^{\infty} (-1)^j \delta(k - jK)\,. \tag{2.3}$$

The sought joint eigenstates of $\chi_X(Q)$ and $\chi_Y(P)$ must have position and momentum representations that are localised in the periodic sets X and Y, respectively. Their construction makes use of the following identity involving functions W and M which will be suitably chosen:

$$\mathcal{F}[W * (\text{Ш}_T \cdot M)](k) = \widehat{W} \cdot \left(\widehat{\text{Ш}}_K * \widehat{M}\right)(k)\,. \tag{2.4}$$

The order of the two operations in Eq. (2.4), convolution ($*$) and multiplication, may be chosen freely, although the result is different in general. Here, both orders appear naturally because of the Fourier transformation present. A special case of Eq. (2.4) is applied in Ref. [23] for the construction of functions invariant under Fourier transformation, by choosing $W = M$.

We now choose W and $\widehat{M}$ to be square-integrable functions that are localised on (that is, vanish exactly outside) intervals of lengths strictly less than T, resp. K. For a precise definition it is convenient to use the mathematical term *support (of a function)* when speaking of the smallest closed set on which the function is localised.) In choosing W and $\widehat{M}$ square-integrable, it is ensured that the quantum state ϕ,

$$\phi(x) = \Big[W * (\text{Ш}_T \cdot M)\Big](x)\,, \tag{2.5}$$

$$\widehat{\phi}(k) = \left[\widehat{W} \cdot \left(\widehat{\text{Ш}}_K * \widehat{M}\right)\right](k)\,, \tag{2.6}$$

defined via Eq. (2.4) is indeed square-integrable. This is shown explicitly in Appendix A.2. The wavefunction $\phi(x)$ is localised on a periodic set X with period T, while its Fourier transform $\widehat{\phi}(k)$ is localised on a periodic set Y with period K. These sets are indeed obtained by placing equidistant copies of the supports of W and $\widehat{M}$, respectively. It follows in line with the result of Ref. [4] that ϕ is a joint eigenstate of the associated spectral projections of position and momentum. A mathematically rigorous construction of such joint eigenstates without the use of Dirac combs is included in Appendix A.1.

The quantum state ϕ thus does not change under the action of the spectral projections $\chi_X(Q)$ and $\chi_Y(P)$. In general, for any quantum state Ψ, the projected wavefunction $\chi_Y(P)\chi_X(Q)\,\Psi$ is a joint eigenstate of the two projectors. In fact, all eigenstates with eigenvalue 1 may be obtained as the projection onto the intersection of the ranges of $\chi_X(Q)$ and $\chi_Y(P)$, which is given by the product $\chi_X(Q)\chi_Y(P) = \chi_Y(P)\chi_X(Q)$. In the analysis below we model the action of the aperture mask and the wire grating as projections in this sense.

2.4 Joint eigenstates of Q and P on periodic sets

As reported in Ref. [3], an initial double-slit superposition state ψ_1 – see Eqs. (1.28), (1.30), and (1.36) – propagates through the experimental setup nearly undisturbed, namely the quantum state is nearly entirely detected on the same set of positions it was prepared on. By contrast, there is an effect on the image of the single-slit state ψ_0, defined in Eq. (1.37), detected at location (iii) in Fig. 2.1: In addition to the expected intensity peak many smaller peaks are found, such that each peak is separated by a distance T from its immediate neighbours. The detected signal is qualitatively illustrated in Fig. 2.3 (a), while the actual signal detected by Afshar *et al.* can be found in Ref. [3], Figs. 1 (c) and (d) therein. It should be noted that for a single-slit diffraction pattern the wire grating would not be in the exact centre, but shifted sideways by a small amount. The experimental setup reported in Ref. [3] features a single-slit diffraction pattern of the order of tens of millimetres, while the misalignment would be 0.25 mm.

These two observations can be understood in terms of joint eigenstates of Q and P on periodic sets. First, the superposition state ψ_1 remains unchanged to a good approximation, because ψ_1 is already prepared at (i) as

a good approximation to a joint eigenstate of periodic characteristic functions of position and momentum with appropriate periodic sets X, Y. This means ψ_1 is an approximation to an eigenstate of the momentum projector associated with the gaps in the wire grating, and hence ψ_1 passes virtually undisturbed. This can be described symbolically by the approximate equations

$$\psi_1 = \chi_X(Q)\psi_1 \to \chi_B(P)\psi_1 \approx \chi_Y(P)\psi_1 = \psi_1' \approx \psi_1.$$

Here $\psi \approx \psi'$ is taken to mean $\|\psi - \psi'\| \ll 1$ for (sub-)normalised vectors, the arrow denotes passage through the wire grating. Here, B denotes the set that is complementary to the set of wires, and is hence such related to the grating. The set Y is the complement to an idealised, infinitely-extending grating.

Second, the single-slit state ψ_0 does not remain unchanged. However, the finite wire grating imposes nodes in a manner that approximates the action of $\chi_Y(P)$ to a high degree, because ψ_0 remains an eigenstate of $\chi_X(Q)$; symbolically expressed by

$$\psi_0 = \chi_X(Q)\psi_0 \to \chi_B(P)\psi_0 \approx \chi_Y(P)\psi_0 = \psi_0' = \chi_X(Q)\psi_0' \not\approx \psi_0\,.$$

Considering that the experimental setup in Ref. [3] involves merely six wires, this may seem surprising. It suggests that the part of the wavefunction not penetrating the wire grating must have comparatively small amplitude.

While all quantum states that pass the aperture mask are eigenstates of $\chi_X(Q)$, the combined effect of aperture mask and wire grating represents a preparation procedure for approximate joint eigenstates of $\chi_X(Q)$ and $\chi_Y(P)$: All quantum states are projected onto the range of $\chi_X(Q)\chi_Y(P) = \chi_Y(P)\chi_X(Q)$ to a good approximation. The superposition state ψ_1, though, is already an approximate eigenstate of both projections, so that the effect of the wire grating is much smaller than on the single-slit state ψ_0 and even negligible to a good accuracy.

Using Eqs. (2.5) and (2.6), we now proceed to construct an example of a joint eigenstate of commuting periodic functions of Q and P. For this, the two localised functions $W, \widehat{M}$ need to be chosen appropriately. The function W describes the quantum amplitude of a single slit. We assume constant amplitude across the slit and model the associated wavefunction using the

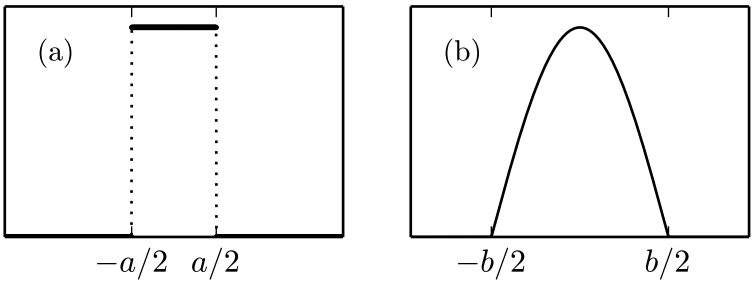

Figure 2.2: The functions $W(x)$, Eq. (2.7), and $\widehat{M}(k)$, Eq. (2.10) are depicted. These two functions are used to construct wavefunctions via Eqs. (2.5) and (2.6).

rectangular function of Eq. (1.29),

$$W(x) = \mathrm{rec}_a(x)\,, \tag{2.7}$$

where a is the slit width; for an illustration see Fig. 2.2 (a). The Fourier transform of W is easily calculated,

$$\widehat{W}(k) \propto \mathrm{sinc}(ak/2)\,. \tag{2.8}$$

The function $\widehat{W}$ is an envelope that accounts for the modulation of the interference pattern $I(k)$.

In the special case of a double-slit interference experiment with slit separation $T > a$, the interference pattern $I_{ds}(k)$ is well known and of the form

$$I_{ds}(k) \propto \mathrm{sinc}^2(ak/2)\,\cos^2(Tk/2). \tag{2.9}$$

The *cosine* describes a periodic pattern, which should be reproduced when the parameters of the joint eigenstate are chosen appropriate. This suggests that we choose $\widehat{M}$ to correspond to a single instance of this pattern

$$\begin{aligned}\widehat{M}(k) &= \cos\bigl(\pi k/K'\bigr)\ \chi_{[-K'/2,K'/2]}(k)\\ &= \begin{cases}\cos(\pi k/K') & \text{for } k \in [-K'/2, K'/2]\\ 0 & \text{for } k \notin [-K'/2, K'/2]\end{cases},\end{aligned} \tag{2.10}$$

where we have defined $K' < K$. In effect this is a half *cosine* pulse strictly contained in every interval K, and illustrated in Fig. 2.2 (b). For the K-

periodic set

$$Y = \bigcup_{j=-\infty}^{\infty} [jK - K'/2, jK + K'/2]$$

to be different from the whole real line, it is required that $K' < K$, so that the interval $[-K'/2, K'/2]$ is strictly contained in the interval $[-K/2, K/2]$.

Combining the expressions obtained for $\widehat{W}, \widehat{M}$ the interference pattern is described by

$$\left|\widehat{\phi}(k)\right|^2 \propto \mathrm{sinc}^2(ak/2) \sum_{j=-\infty}^{\infty} \cos^2\left(\frac{\pi}{K'}(k + jK)\right) \chi_{[-K'/2,K'/2]}(k + jK) \ . \tag{2.11}$$

This is a sum of non-overlapping terms, and the support of this function is the periodic set Y that is made up of equidistant copies of the interval $[-K'/2, K'/2]$. For the quantum state in position space, W is as defined in Eq. (2.7), and M follows from $\widehat{M}$ as defined in Eq. (2.10), yielding

$$\phi(x) \propto (W * [\mathrm{III}_T((\,\cdot\,) - T/2) \cdot M])(x) = \sum_{j=-\infty}^{\infty} M((j - 1/2)T)\, \chi_{[(j-1/2)T-a/2,(j-1/2)T+a/2]}(x). \tag{2.12}$$

The Dirac comb is shifted by $T/2$, in correspondence with the experimental setup. (This shift becomes a phase factor in momentum space and does not affect the momentum distribution.)

A suitable choice of the parameter K' renders ϕ an eigenstate of the two projections that occur in the experimental setup, namely the aperture mask and the wire grating, such that ϕ traverses from location (i) to location (iii) unchanged. An example of such a quantum state is depicted in Fig. 2.3. The wavefunction in momentum space, depicted in (b), is supported periodically on an interval of size $K' = K/2$. Similarly, the spatial wavefunction is supported on a periodic set, although most of the quantum state is contained in only four slits.

There are two important limiting cases. The spectral projection $\chi_Y(P)$ is over a strictly periodic set Y. In contrast, the dimensions of any experiment are necessarily finite. The particular experiment reported in Ref. [3] was performed with a total of six wires only, preparing the state $\chi_B(P)\psi$, where B is the complement to the region occupied by the wires. A model calcu-

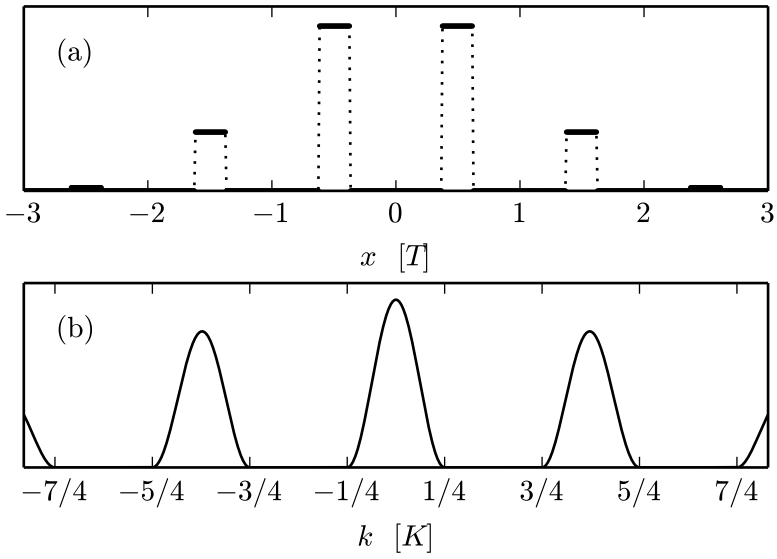

Figure 2.3: A joint eigenstate of commuting functions of Q and P is depicted. It is constructed according to Eqs. (2.5) and (2.6). Compare Fig. 1.3.

lation shows that the difference between the states $\chi_B(P)\psi$ and $\chi_Y(P)\psi$ is undetectable given the accuracy of the experiment at hand.

We may consider the limiting case of K' approaching K, modelling a scenario in which the wires become negligibly thin. When $K' = K$ the function M is zero at every delta peak of the periodic Dirac comb, except for two locations: $x = \pm T/2$. Hence it follows that for this particular choice of $W, \widehat{M}$, the quantum state ψ_1 exists solely in the two slits and is an approximation to a joint eigenstate defined on periodic sets. The aperture mask at location (i) in Fig. 2.1 prepares ψ_1 as an eigenstate of $\chi_X(Q)$ on the periodic set X. However, passage through a periodic wire set Y will cause a projection of the state onto one that is a joint eigenstate of periodic position and momentum sets. This projective measurement action causes a disturbance of the incoming wavefunction, which manifests itself in the observed position distribution when the state is finally detected at location (iii) in Fig. 2.1: In an ideal setup with dimensions identical to those reported in Ref. [3], approximately 1% of the total probability would not be found in the two detectors, where it would otherwise be expected. Instead, this one per cent of probability would be distributed over the remainder of the periodic set X. According to Ref. [3], experimentally it was found that about 2% probability

were found outside of the main peaks.

2.5 Conclusion

A description of multislit experiments was presented in this chapter in terms of quantum states that are defined on periodic intervals of position and momentum. These quantum states, themselves not periodic, represent a class of joint eigenstates of periodic functions of position and momentum. In our investigation we focused in particular on the modified double-slit experiment, which is similar to the double-pinhole experiment performed by Afshar *et al.* [3]. Using a description in terms of joint eigenstates it was possible to account for the two observations reported in Ref. [3] concerning the behaviour of a double-slit input state and a single-slit input state.

First, an incoming double-slit superposition state is virtually unaffected by the indirect measurement of the interference pattern performed by the wire grating, with each of the wires placed at a node. This is, of course, because the superposition state evolves into a momentum-space wavefunction with interference fringes. An explanation in terms of joint eigenstates over periodic sets, though, goes further and makes it possible to explain why a superposition state can be localised on essentially the same set of positions after it was subjected to such a measurement—after all, measuring the existence of an interference pattern corresponds to obtaining information about the momentum distribution. This joint measurement is (approximately) implemented by commuting projection operators: The experimental setup constitutes a good approximation to a joint determination of compatible coarse-grainings of position and momentum. It follows that there is no conflict with the principle of complementarity.

Second, an incoming single-slit state does not remain unchanged after passage of the wire system, but is instead detected on a set of locations expected of a joint eigenstate of periodic position and momentum projectors. Additional intensity peaks are found, such that each peak is separated by the same distance from its immediate neighbours as the two slits in the aperture mask. This agrees with the interpretation that the single-slit state was projected onto an approximate joint eigenstate of spectral projections of position and momentum on periodic sets through the projective action of the wire grating.

The fact that a single-slit state is affected by the wire grating in such a way that the detected output state is found to be localised in many periodically spaced intervals is a demonstration of the mutual disturbance of measurements of incompatible observables. The projector $\chi_A(Q)$ onto a state localised in a single slit is not compatible with the projector $\chi_B(P)$ onto a state localised in the set B of intervals in momentum space defined by the gaps in the wire grating or its idealised substitution by a periodic set. Consequently, a state originally prepared to be localised in a single slit is changed by the projective action of the wires so as to be instead localised on a periodic set of positions.

In this way the present experiment serves as a beautiful, new demonstration of complementarity that complements the existing illustrations. Usually one considers a perfect interference setup and then shows how the interference pattern is degraded by the introduction of a path-marking interaction with a probe system storing (partial) path information. See, for example, Ref. [24]. In the single-slit case one starts with a perfect path-marking setup which then, by introducing the wires, is changed into an interference experiment, degrading the accuracy of the path determination.

Finally, we presented a construction of a specific class of joint eigenstates of periodic sets of position and momentum. These states show explicitly that in an idealised experiment with periodically placed slits and wires the propagation of these states is entirely unaffected by the setup; the presence of the interference pattern would be established without disturbing the quantum state at all. The work of Corcoran and Pasch suggests that the construction of realistic approximations to such quantum states is possible experimentally as well [23].

To summarise, we have shown that it is appropriate to view the experimental setup reported in Ref. [3] – referring to both the aperture mask and the wire grating – as a preparation procedure for approximate joint eigenstates on periodic sets of position and momentum, regardless of the particular input state. The validity of this interpretation can be supported by numerical simulations of the experiment and variants of it (with different numbers and thickness of the wires).

Chapter 3

Uncertainty I: Modifying the Heisenberg Uncertainty Relation

This chapter is about the observables in multislit interference experiments, their incompatibility and the resulting quantum uncertainty that results in a tradeoff between spatial localisation and the appearance of fringes. The discussion focuses on a proposal presented by Aharonov *et al.*, who argued that a Heisenberg-type uncertainty relation in terms of particular position and momentum operators should exist [1]. These operators are intended to capture the relevant observables, because the operators present in the Heisenberg uncertainty relation do not. However, as the work of Aharonov *et al.* was not developed beyond the heuristic argument reported in Ref. [1], no accurate expression of such a tradeoff relation exists. Before we can derive such a relation, however, we need to address technical questions in the form of domain issues and arising restrictions on the allowed quantum states.

A decomposition of the observables $\mathcal{Q}$ and $\mathcal{P}$ into more suitable observables is central to the proposed adaptation of the Heisenberg relation to the multislit context.

The discussion presented here is going to be continued in Chapter 5, after the interlude of Chapter 4 in which a better understanding of simple multislit interference experiments is developed. This will allow us to develop the concepts and obtain a precise formulation of uncertainty in Chapter 5.

3.1 Introduction

Heisenberg's principle of uncertainty expresses the notion of a fundamental limitation of precise values for a pair of complementary observables for any quantum state. Mathematically the uncertainty principle is often expressed as a tradeoff between the standard deviations of the relevant observables. In its most common form, the so-called Heisenberg uncertainty relation, Eq. (1.11), a tradeoff is expressed between the standard deviations of the position Q and the momentum P of a single non-relativistic quantum object. In the context of multislit interferometry though, it is clear already from an intuitive point of view that the relevant complementary observables are not exactly position and momentum. Indeed, position should be replaced by "which slit" information, and momentum with fringe width. A mathematical representation of the former is clear (simply a coarse-grained position), but fringe width is less obvious. As is well known – see, for instance, Ref. [2] – and also argued here, the standard deviation of momentum cannot describe fringe width, rendering the Heisenberg relation unsuitable for expressing complementarity in the interferometric context. This may seem particularly surprising considering the important role played by the Heisenberg uncertainty relation in the historic Bohr-Einstein debate, which was concerned, *inter alia*, with the complementarity of path information and the appearance of interference.

It is not that the standard deviation as such is a poor measure though; it is the particular combination of standard deviation and the momentum operator P that is problematic. A more suitable expression of the uncertainty principle may be found by using observables that take into account the periodic nature of the experimental setup. The idea is to modify the pair (Q, P) by making Q discrete and P periodic. When properly adjusted, the resulting pair will still have a "canonical" nature that leads to an uncertainty relation. We are going to derive commutation relations for such operators, which are formally similar to the standard Heisenberg relation. The derived relations, however, will be valid only for subset of wavefunctions. This subset is closely related to the wavefunctions that naturally occur in multislit experiments. A proper understanding of this limited validity of the uncertainty relations requires careful consideration of the mathematical subtleties of the problem, in particular of domain questions.

The adaptation of the observables Q and P to the interferometric context is due to Aharonov *et al.*, who also provided a heuristic argument that the uncertainty relations discussed here should exist [1]. However, their work was never developed beyond invoking an analogy to angle and angular momentum. Most importantly, the fact that the relations are only valid for specific wavefunctions was never made clear. This is perhaps due to insufficient mathematical development of the problem in their work and in related publications [1, 25, 26]. It was not until the work of Gneiting and Hornberger of 2011 that correct commutation relations were stated, but their discussion is mainly formal and of different focus [27]. In conclusion, a thorough analysis seems in order. We present here a precise derivation and discussion of these uncertainty relations. Furthermore, we address limitations and benefits of the uncertainty relations, and discuss an application to uniformly illuminated aperture masks and the asymptotic behaviour of the uncertainty product in this case.

Throughout we will emphasise the interplay between physics and mathematics leading to a derivation that is mathematically deceptively simple and physically insightful, although occasionally subtle on both accounts.

3.2 Observables of multislit interferometry

The traditional approach to quantum uncertainty, employing the Heisenberg relation, Eq. (1.11), fails at quantifying the uncertainty of a double-slit superposition state ψ_1 (defined in Eq. (1.36) and illustrated in Fig. 1.3). The intensity profile of the interference pattern of ψ_1 is expressed by the product of a *cosine*, which describes the fringes, and a *sinc* function, which provides an envelope. As $\Delta(P, \psi_1)$ diverges, the Heisenberg relation provides no information. The presence of fringes, or lack thereof, has no impact on the result. This is particularly apparent when considering the single-slit state ψ_0, for which again $\Delta(P, \psi_0)$ diverges. The root of this problem is the combination of standard deviation and operator P. For instance, the moments of P are insensitive to the relative phase between two path states, or even to the absence of a phase relation in the case of a mixed state. This led Aharonov *et al.* to instead consider unitary shift operators for a description of interference, as these can be used to create overlap and thus establish sensitivity to relative phase. They then proposed a decomposition of the

noncommuting operators Q and P into commuting parts $Q_{\rm mod}$ and $P_{\rm mod}$ (periodic) and noncommuting parts Q_T and P_K, and presented a heuristic argument that an uncertainty relation of the same form as the Heisenberg relation should exist.

The following observation illustrates this idea: Q being the shift generator for quantum states in momentum space and P being the shift generator for position space, the unitary shift operators considered by Aharonov *et al.* are, in fact, identical to the operators in Weyl's commutation relation, Eq. (1.7). This observation suggests a decomposition of Q into a T-periodic part and a remainder, and P into a K-periodic part with remainder. More precisely,

$$Q = Q_{\rm mod} + Q_T, \tag{3.1}$$

$$P = P_{\rm mod} + P_K, \tag{3.2}$$

yielding a pair of commuting operators

$$[Q_{\rm mod}, P_{\rm mod}] = 0\,. \tag{3.3}$$

The subscript "mod" was chosen to reflect the terminology of Aharonov *et al.*, who refer to these observables as "modular variables". We require the following definitions

$$Q_{\rm mod}(x) = Q(x) \mod T\,, \tag{3.4}$$

$$P_{\rm mod}(k) = (P(k) + K/2 \mod K) - K/2\,. \tag{3.5}$$

Note that $P_{\rm mod}$ is shifted by $K/2$, i.e. by half the fringe separation, in order to avoid overlap of the fringes with the points of discontinuity of $P_{\rm mod}(k)$. This shift is crucial for avoiding anomalous behaviour of $\Delta(P_{\rm mod}, \psi_n)$, as will become evident shortly; Aharonov *et al.* appear to have neglected it [1, 25, 26]. The definition of the operator Q_T follows from Eqs. (3.1) and (3.4), while P_K follows from Eqs. (3.2) and (3.5).

Q_T corresponds to a discretised position observable, while P_K is a discretised momentum observable. Illustrations of Q_T and $P_{\rm mod}$ are displayed in Fig. 3.1.

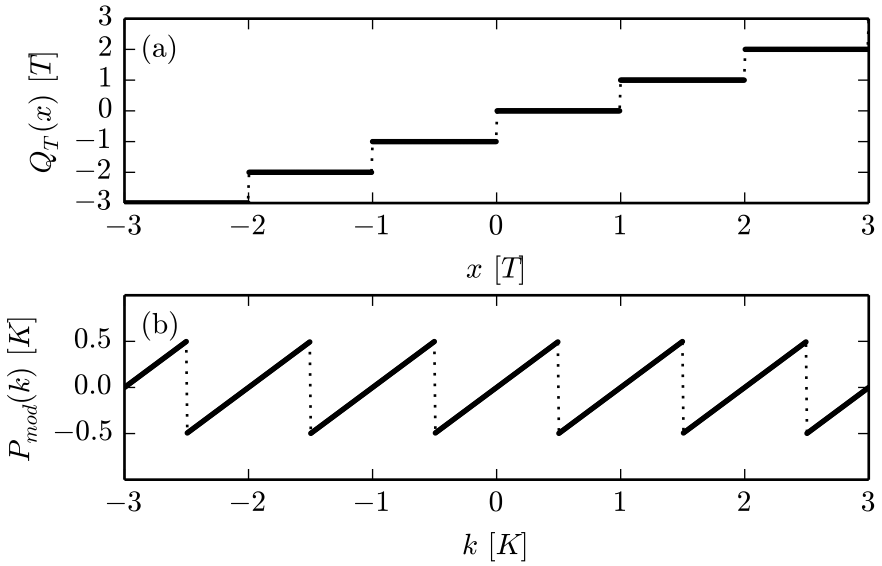

Figure 3.1: In (a) Q_T is depicted in position space; it is defined indirectly through relations Eq. (3.1) and Eq. (3.4), whereas (b) illustrates P_{mod} in momentum space, as defined in Eq. (3.5).

3.3 Uncertainty relations for multislit setups

Conceptually the periodic quantity P_{mod} seems appropriate for measuring the fine structure of the momentum distribution. Similarly, Q_T appears suitable for measuring the localisation property as it corresponds to a coarse position observable—the spatial localisation should not critically depend on the exact shape of the slits, and Q_T does not depend on the slit shape at all, as is shown below. Moreover, the fact that Q_{mod} and P_{mod} commute suggests that the canonical nature of the pair (Q, P) is "transferred" to the pairs (Q_T, P_{mod}) and (Q_{mod}, P_K), the only problem being that Q_T and P_K have discrete spectrum and so cannot be canonical operators in the strict sense. In fact, it is possible to obtain the following two commutators for general quantum states [6, 27]

$$[Q_T, P_{\mathrm{mod}}] = \mathrm{i}\,\mathbf{1} - \mathrm{i}\,K\,\widehat{\mathrm{III}}_K((\cdot) - K/2), \tag{3.6}$$

$$[Q_{\mathrm{mod}}, P_K] = \mathrm{i}\,\mathbf{1} - \mathrm{i}\,T\,\mathrm{III}_T. \tag{3.7}$$

The two Eqs. (3.6) and (3.7) are unsuitable for obtaining uncertainty relations resembling the state-independent Heisenberg uncertainty relation, because they feature state-dependent terms. Simplifying these commutators to a canonical form is only possible if the wavefunction vanishes at the locations of the delta peaks—this leads to the aforementioned restriction on the validity of the associated uncertainty relations.

A rigorous derivation of the two commutation relations, Eqs. (3.6) and (3.7), is rather long and technical, and provided in Ref. [22]. It proceeds by making precise the analogy with the angular momentum-angle case alluded to by Aharonov *et al.* in their heuristic argument. In fact, relations of the form of Eqs. (3.6), (3.7) were known for the angular momentum and angle pair since the 1960s [28–30].

Here we present an alternative argument that immediately leads to the desired commutators by exploiting the properties of the relevant quantum states from the beginning. For the detailed discussion we focus on the pair Q_T and P_{mod} as it is more natural to considerations in multislit interferometry; an analogous argument holds for P_K and Q_{mod}. In order to determine the commutator

$$[Q_T, P_{\mathrm{mod}}]\,\psi = (Q_T P_{\mathrm{mod}} - P_{\mathrm{mod}} Q_T)\,\psi \tag{3.8}$$

it is necessary to ensure that

$$\psi \in \mathcal{D}(Q_T)\,, \tag{3.9}$$

$$P_{\mathrm{mod}}\,\psi \in \mathcal{D}(Q_T)\,. \tag{3.10}$$

Here $\mathcal{D}$ denotes the domain of the indicated operator. Since the operator P_{mod} is bounded, its domain is the whole Hilbert space and hence does not lead to restrictions.

Recall that the *domain* of an operator is a subspace of square-integrable wavefunctions (elements of the Hilbert space $L^2(\mathbb{R})$), which, upon application of the operator, yield wavefunctions that are still square integrable. In particular, the domains of Q and P are

$$\mathcal{D}(Q) = \left\{\psi \in L^2(\mathbb{R}) : \int_{-\infty}^{\infty} x^2\,|\psi(x)|^2\,\mathrm{d}x < \infty\right\}, \tag{3.11}$$

$$\mathcal{D}(P) = \left\{\psi \in L^2(\mathbb{R}) : \psi \text{ absolutely continuous }, \psi' \in L^2(\mathbb{R})\right\}\,. \tag{3.12}$$

First, note that the domains of Q and Q_T are equal,

$$\mathcal{D}(Q_T) = \mathcal{D}(Q), \tag{3.13}$$

ecause these two operators differ by the bounded Q_{mod}. Second, noting that Q acts as a differentiation operator in momentum space, a wavefunction in its domain is required to be absolutely continuous. While Eq. (3.9) thus amounts to the standard continuity assumption, Eq. (3.10) is peculiar to the present setup and requires more care. Since

$$P_{\mathrm{mod}}\,\widehat{\psi}(k) = (k - jK)\widehat{\psi}(k) \qquad \text{for } k \in \big((j-\tfrac{1}{2})K, (j+\tfrac{1}{2})K\big] \tag{3.14}$$

where $j \in \mathbb{Z}$, this function is discontinuous at $k = jK + K/2$, *unless* $\widehat{\psi}(k)$ vanishes at these points. This gives the aforementioned restriction on the allowed wavefunctions explicitly,

$$\widehat{\psi}((j+1/2)K) = 0 \text{ for each } j \in \mathbb{Z}\,. \tag{3.15}$$

Since $\widehat{\psi}$ is absolutely continuous by Eq. (3.9), this restriction is also sufficient for the commutator $[Q_T, P_{\mathrm{mod}}]\,\psi$ to be defined.

Note that if $P_{\mathrm{mod}}\widehat{\psi}(k)$ were not continuous, the derivative would not approach a finite limit value at the point of discontinuity; more precisely, we could describe the point of discontinuity by a step function, whose (distributional) derivative is a delta function. This line of reasoning would eventually lead to the state-dependent correction terms in Eqs. (3.6) and (3.7).

The wavefunctions that naturally appear in the interferometric context typically have periodically-spaced *nodes*, i.e. they vanish periodically. As is evident from comparing Figs. 1.3 and 3.1 and discussed in more detail below, our specific choice of P_{mod} in Eq. (3.5) has the discontinuity points of $P_{\mathrm{mod}}(k)$ aligned with the nodes of the particular wavefunctions considered here. We emphasise once more that a wavefunction with periodic but non-vanishing values at the discontinuity points of P_{mod} is unsuitable because of boundary effects that lead to a state-dependent commutator.

Condition (3.15) suggests a decomposition of the (dense) subspace of the

admissible wavefunctions into a direct sum of subspaces

$$\mathcal{D}_j = \big\{\widehat{\psi} \in L^2(jK + [-K/2, K/2]) : \widehat{\psi}(jK - K/2) = \widehat{\psi}(jK + K/2) = 0\big\}, \tag{3.16}$$

where $j \in \mathbb{Z}$. Note that a restriction to any of the subspaces $\mathcal{D}_j$ corresponds to a quantum object confined to a ("momentum") box, carefully discussed in Ref. [31] by Bonneau, Faraut and Valent; below we point out parallels.

We are now able to derive the commutator of Q_T and P_{mod}, and hence the lower bound of the uncertainty relation. With the restriction (3.15) on the wavefunction, P_{mod} corresponds to P on each interval $jK + [-K/2, K/2]$ up to a constant, see Eq. (3.14). This enables us to perform the following formal manipulations in order to obtain the commutator

$$\begin{aligned}
[Q_T, P_{\mathrm{mod}}] &= [Q - Q_{\mathrm{mod}}, P_{\mathrm{mod}}] && && (3.17)\\
&= [Q, P_{\mathrm{mod}}] && && (3.18)\\
&= [Q, P] && \text{on each } \mathcal{D}_j && (3.19)\\
&= \mathrm{i} && && (3.20)
\end{aligned}$$

While the algebraic manipulations are trivial, the penultimate expression may only be obtained by way of the domain considerations above. Hence, for each wavefunction in the dense subspace given by Eq. (3.15) (together with the domain conditions (3.9) and (3.10)), we have

$$[Q_T, P_{\mathrm{mod}}]\,\psi = \mathrm{i}\,\psi\,. \tag{3.21}$$

By means of the Robertson relation, Eq. (1.12), the desired uncertainty relation now follows immediately

$$\Delta(Q_T, \psi)\ \Delta(P_{\mathrm{mod}}, \psi) \geq \frac{1}{2}\,. \tag{3.22}$$

This uncertainty relation is of Heisenberg-type, yet the observables have been adapted to capture the relevant features of quantum states prepared in multislit interference experiments. We are going to explore the benefits of this relation in the following section.

For completeness, we point out that this discussion proceeds analogously

for wavefunctions restricted similarly in position space, yielding

$$[Q_{\mathrm{mod}}, P_K]\,\eta = \mathrm{i}\,\eta, \tag{3.23}$$

and ultimately

$$\Delta(Q_{\mathrm{mod}}, \eta)\;\Delta(P_K, \eta) \geq \frac{1}{2}, \tag{3.24}$$

for wavefunctions η from a suitably restricted dense subspace.

3.4 Uniformly illuminated aperture masks

For our detailed discussion we focus on Eq. (3.22), the uncertainty relation that describes the tradeoff between the spatial localisation of a quantum state incident on a multislit aperture mask and its fringe width.

We consider states obtained as follows: A single illuminated slit is assumed to prepare a quantum state described by a rectangular function of slit width, while a general aperture mask yields a suitable superposition of those. As the eigenspaces of Q_T are excluded – analysis of single-slit states is beyond the scope of this approach – we consider superposition states of m coherently illuminated slits, where $m = 2n$ is an even positive integer. These quantum states are but a subset of the quantum states that a multislit aperture mask can prepare, but they include important examples, and they have a structure that makes a discussion of uncertainty both simple and insightful. These states were introduced in Sec. 1.4.4 as superpositions of rectangular wavefunctions. The rectangular function is a popular choice for describing the profile across a single slit, although one may argue that it might not be the most physical choice. For the present uncertainty relation, Eq. (3.22), this choice is actually entirely irrelevant as will become evident shortly.

The standard deviation $\Delta(Q_T, \psi_n)$ is easy to compute analytically, one obtains [27]

$$\Delta(Q_T, \psi_n) = \frac{T}{2}\sqrt{\frac{4n^2-1}{3}}. \tag{3.25}$$

We note that for uniformly illuminated aperture masks the standard deviation of Q_T increases linearly with the number of illuminated slits $m = 2n$. This result is simple and intuitive. However, $\Delta(P_{\mathrm{mod}}, \psi_n)$ requires some technical effort.

It is shown in Appendix B.1 that $\Delta(P_{\mathrm{mod}}, \psi_n)$ is independent of the slit width a, and the related *sinc* envelope. This result is desired on the basis of the detailed physical considerations presented in Chapter 4, and proves extremely useful for related considerations and calculations. The derivation provided in Appendix B.1 is very detailed; suffice it to say here that the result follows because of the periodicity of Eq. (1.34), i.e. $f_n(k)^2 = f_n(k + jK)^2$ (with integer j), and because of a result on infinite sums provided in Ref. [32]. This integration is performed using a conveniently rescaled variable $\kappa = Tk/2$, which renders the integrand dimensionless. We obtain

$$\begin{aligned} \Delta(P_{\mathrm{mod}}, \psi_n)^2 &= \int_{-\infty}^{\infty} P_{\mathrm{mod}}(k)^2 \, \psi_n(k)^2 \, \mathrm{d}k \\ &= \frac{2^3}{T^2 n \pi} \int_{-\pi/2}^{\pi/2} \kappa^2 \, f_n(\kappa)^2 \, \mathrm{d}\kappa \end{aligned} \tag{3.26}$$

We proceed to calculate explicitly the value assigned to the fine structure of the double-slit superposition state ψ_1, we obtain

$$\Delta(P_{\mathrm{mod}}, \psi_1) = \left(\frac{2^3}{T^2 \pi} \int_{-\pi/2}^{\pi/2} \kappa^2 \cos(\kappa)^2 \, \mathrm{d}\kappa \right)^{1/2} = \frac{1}{T} \sqrt{\frac{\pi^2 - 6}{3}} \tag{3.27}$$

Regarding the asymptotic behaviour, it is shown in Appendix B.2 that

$$\Delta(P_{\mathrm{mod}}, \psi_n) \approx \frac{\sqrt{2 \ln 2}}{T} \frac{1}{\sqrt{n}} \qquad \text{for large } n \,. \tag{3.28}$$

Numerically computed values of $\Delta(P_{\mathrm{mod}}, \psi_n)$ are depicted in Figs. 3.2 and 3.3, illustrating this result. We conclude immediately that the asymptotic behaviour of the uncertainty product is divergent, i.e. that

$$\lim_{n \to \infty} \Delta(Q_T, \psi_n) \, \Delta(P_{\mathrm{mod}}, \psi_n) \propto \lim_{n \to \infty} \sqrt{n} = \infty \,. \tag{3.29}$$

The uncertainty product associated with the state ψ_1 follows immediately from Eqs. (3.25) and (3.27),

$$\Delta(Q_T, \psi_1) \, \Delta(P_{\mathrm{mod}}, \psi_1) = \frac{1}{2} \sqrt{(\pi^2 - 6)/3} \approx 0.568 \,. \tag{3.30}$$

This is surprisingly close to the lower bound already, and in fact equal to the value of the conventional Heisenberg uncertainty product, Eq. (1.11),

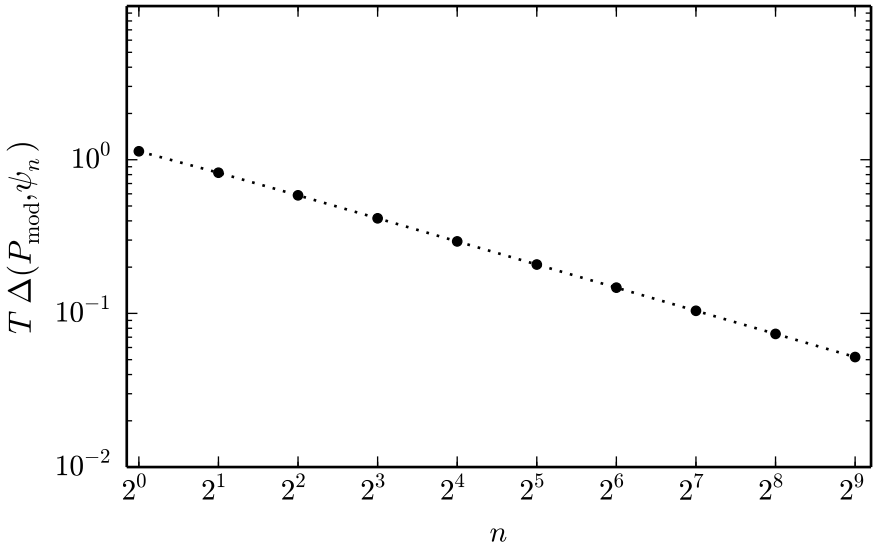

Figure 3.2: The standard deviation of P_{mod} in state ψ_n is depicted for various values of n. The values of $\Delta(P_{\mathrm{mod}}, \psi_n)$ are multiplied by T, removing the dependence on the slit separation.

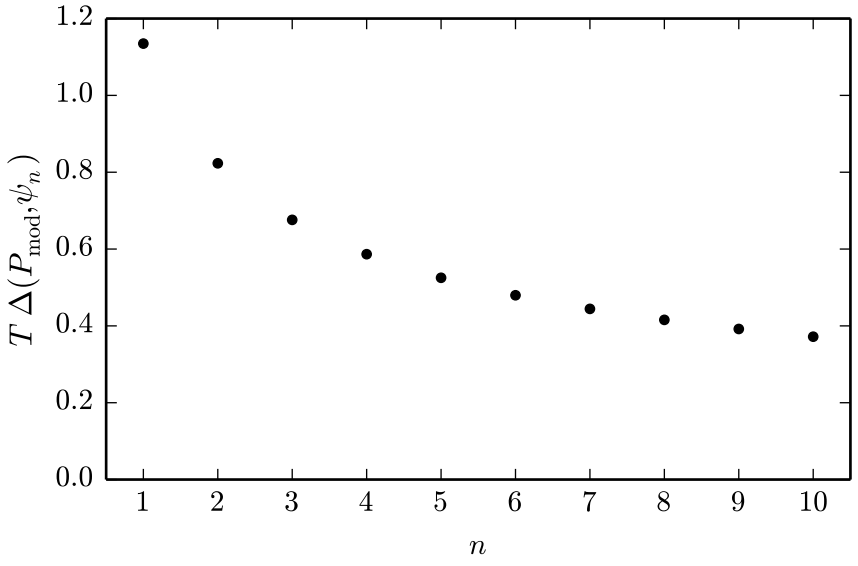

Figure 3.3: The standard deviation of P_{mod} in state ψ_n is depicted for various values of n. The values of $\Delta(P_{\mathrm{mod}}, \psi_n)$ are multiplied by T, removing the dependence on the slit separation.

assigned to a particle confined to a box (in one dimension). This is not a coincidence, the central idea of the formulation of uncertainty discussed here is that a direct sum of such "boxes" is considered. More explicitly, for the particle in a box the spatial wavefunction of the lowest energy eigenstate is described by a half *cosine* pulse, whereas a single fringe of the double-slit state is described by a half *cosine* pulse. (See Fig. 2.2 (b) for an illustration of a half *cosine* pulse.) In these two considerations position space and momentum space are interchanged: A spatial wavefunction is (typically) considered for the particle in the box, whereas a wavefunction in momentum space is considered here.

In the following chapter a better understanding of quantum states prepared by uniformly illuminated aperture masks is developed. An argument is presented which formalises the naive understanding of fringe width prevalent in the present chapter, explaining why the asymptotic behaviour of the uncertainty product in Eq. (3.29) does not reflect the observed physical structure. A solution is presented in Chapter 5 in the form of a more apt decomposition of the momentum operator.

3.5 Discussion

This section contains a number of conceptual and technical points and some critical observations on the work of Aharonov *et al.* [1, 25, 26].

While the pairs of operators appearing in Eqs. (3.22) and (3.24) are more appropriate for multislit interferometry than Q and P appearing in the Heisenberg uncertainty relation, it must be stressed that these inequalities are valid only for quantum states ψ and η, respectively, which vanish at the points of discontinuity of P_{mod}, see Eqs. (3.15), and Q_{mod}. Notable exceptions are the eigenstates of Q_T and P_K. In particular, the uncertainty relation (3.22) is inappropriate for a description of single-slit states. This point is particularly intriguing, because it is the adaptation of the observables to multislit interferometry that rules out the description of single-slit states. This seems to point to a fundamental qualitative difference between the quantum mechanics of interference and of (singe-slit) diffraction.

The heuristic argument provided by Aharonov *et al.* refers to the analogy between the pair (Q_T, P_{mod}) and the pair of angular momentum and angle operators, the latter being understood as in the review of Carruthers and

Nieto, Ref. [30]. The analogy can be made precise by observing that the restriction of the Weyl commutation relations to a discrete set of position variables and a periodic set of momentum variables defines a representation of the Weyl relations on the group $\mathbb{Z} \times \mathbb{T}$, where $\mathbb{T}$ is the circle group. This representation is reducible, corresponding to the fact that the eigenspaces of Q_T are infinite-dimensional, and can be decomposed into a direct sum of copies of the angle-angular momentum pair. This topic will be investigated in detail in a more technical work [6].

Finally, we feel obliged to point out that in the later publications by Aharonov *et al.*, their heuristic uncertainty relation, as claimed in Ref. [1], is instead presented as an actual inequality of the form

$$\Delta(Q_T, \Psi)\, \Delta(P_{\mathrm{mod}}, \Psi) \geq 2\pi$$

in units where $\hbar = 1$. This is, of course, incorrect as the claimed lower bound is easily violated. The double-slit state (among others) violates the lower bound claimed. There is no indication that these authors are considering a non-standard definition of the standard deviation. On the contrary, the explicit definitions in Ref. [26] indeed confirm that standard deviations are used. Furthermore, the definition of $P_{\mathrm{mod}}(k)$ implicit in Aharonov *et al.* [1, 25, 26] features an unsuitable choice of origin. It follows that the value assigned to the fringe width increases as the number of illuminated slits is increased, indicating that the relevant features of the fringe width are not captured. In contrast, our choice of Eq. (3.5) yields the expected asymptotic behaviour.

Chapter 4

The product form of multislit wavefunctions

In the present chapter an alternative way of expressing the wavefunctions prepared in certain multislit interference experiments is introduced. This elementary way of rewriting the momentum-space wavefunctions turns out extremely useful for physical considerations, yet it has apparently remained undiscovered.

A large part of the discussion of quantum uncertainty in Chapters 5 and 6 relies on the product form, because it highlights the structure of the quantum states prepared in multislit experiments and allows us to anticipate certain results. In particular, the product form yields a recursive relationship between quantum states prepared in multislit interference experiments. This recursive relationship provides a classification scheme for functions related to the envelope and those related to the fine structure. A general method for identifying these functions is required since at present there is no definition apart from the simple identification of envelope with *sinc* and fine structure with *cos* in the case of the double-slit interference experiment (which, of course, does not work for other multislit interference experiments).

Once the particular function governing the fine structure is identified, it becomes possible to discern the changes to the fine structure that result from illuminating additional slits. The precise change introduced to the fine structure must be reflected by a suitable measure of fringe width. The final part is the subject-matter of Chapter 5.

4.1 Introduction

From experimental observation it was concluded that the particular illumination of the aperture mask is related to the character of the fringes seen on a distant detection screen. The change in the interference pattern that results from illuminating more slits suggests that the spatial localisation (related to the number of illuminated slits) and the fringe property (related to the appearance and shape of the fringes) constitute a pair of incompatible observables, whose relationship is described by an uncertainty tradeoff. The precise character of this relationship or the particular form of the relevant observables, however, is not obvious. We develop these ideas using an alternative way of expressing the momentum-space wavefunctions. We consider multislit aperture masks with slit numbers corresponding to powers of 2, because only the wavefunctions prepared by these setups can be rewritten in product form.

Typically the momentum-space wavefunctions of quantum states prepared in setups with an even number of illuminated slits are expressed in terms of a sum; see in Eq. (1.30). The following examples of such wavefunctions are prepared by setups with a number of illuminated slits that correspond to a power of 2. There are two changes in notation as they substantially reduce the notational overhead: These quantum states are denoted ζ_d, indicating the number of illuminated slits $m = 2^d$. They relate to the previous notation via

$$\zeta_d = \psi_{2^{d-1}}, \tag{4.1}$$

i.e. $2^{d-1} = n$. Furthermore, the rescaled variable $\kappa = Tk/2$ is used.

$$\widehat{\zeta_0}(\kappa) = \sqrt{\frac{1}{\pi}\frac{a}{T}}\,\mathrm{sinc}\Big(\frac{a}{T}\,\kappa\Big)$$

$$\widehat{\zeta_1}(\kappa) = \sqrt{\frac{2}{\pi}\frac{a}{T}}\,\mathrm{sinc}\Big(\frac{a}{T}\,\kappa\Big)\cos(\kappa)$$

$$\widehat{\zeta_2}(\kappa) = \sqrt{\frac{2}{2\pi}\frac{a}{T}}\,\mathrm{sinc}\Big(\frac{a}{T}\,\kappa\Big)\,[\cos(\kappa) + \cos(3\kappa)]$$

$$\widehat{\zeta_3}(\kappa) = \sqrt{\frac{2}{4\pi}\frac{a}{T}}\,\mathrm{sinc}\Big(\frac{a}{T}\,\kappa\Big)\,[\cos(\kappa) + \cos(3\kappa) + \cos(5\kappa) + \cos(7\kappa)]$$

$$\widehat{\zeta_4}(\kappa) = \sqrt{\frac{2}{8\pi}\frac{a}{T}}\,\mathrm{sinc}\Big(\frac{a}{T}\,\kappa\Big)[\cos(\kappa) + \cos(3\kappa) + \cos(5\kappa) + \cos(7\kappa)\ldots$$
$$\cdots + \cos(9\kappa) + \cos(11\kappa) + \cos(13\kappa) + \cos(15\kappa)]$$

$$\vdots$$

$$\widehat{\zeta}_d(\kappa) = \sqrt{\frac{2}{2^{d-1}\pi}\frac{a}{T}}\,\mathrm{sinc}\Big(\frac{a}{T}\,\kappa\Big)\sum_{j=1}^{2^{d-1}}\cos((2j-1)\kappa) \qquad \text{(for } d \geq 1 \text{ only)} \tag{4.2}$$

Note though that the single-slit wavefunction $\widehat{\zeta}_0$ actually cannot be obtained from Eq. (4.2), but must be considered independently.

The above expressions are obtained naturally when performing a Fourier transform of the respective 2^d-slit wavefunction, pairing up the slits symmetrically around the origin and thus combining two phase factors into a single, real *cosine*. This straightforward calculation was already presented in Sec. 1.4.4. Observe that the number of terms in the general expression for $\widehat{\zeta}_d(k)$ goes linearly with the number of illuminated slits $m = 2^d$, where $d \in \mathbb{N}$.

Although this way of expressing the wavefunctions is obtained naturally, it is not particularly useful for developing a better understanding of the structure of the respective quantum state. For instance, it is difficult to determine the separation of the nodes or to identify the functions determining the envelope from the ones determining the fine structure. In particular, there is no justification for considering (just) the *sinc* function as the envelope. It is true that the *sinc* function is responsible for the square-integrability of the wavefunctions, but below we shall make an argument that the envelope is more complicated.

The same wavefunctions are now given in the alternative product form.

$$\begin{aligned}
\widehat{\zeta}_0(\kappa) &= \sqrt{\frac{1}{\pi}\frac{a}{T}}\,\mathrm{sinc}\Big(\frac{a}{T}\,\kappa\Big)\\
\widehat{\zeta}_1(\kappa) &= \sqrt{\frac{2}{\pi}\frac{a}{T}}\,\mathrm{sinc}\Big(\frac{a}{T}\,\kappa\Big)\cos(\kappa)\\
\widehat{\zeta}_2(\kappa) &= \sqrt{\frac{4}{\pi}\frac{a}{T}}\,\mathrm{sinc}\Big(\frac{a}{T}\,\kappa\Big)\cos(\kappa)\cos(2\kappa)\\
\widehat{\zeta}_3(\kappa) &= \sqrt{\frac{8}{\pi}\frac{a}{T}}\,\mathrm{sinc}\Big(\frac{a}{T}\,\kappa\Big)\cos(\kappa)\cos(2\kappa)\cos(4\kappa)\\
\widehat{\zeta}_4(\kappa) &= \sqrt{\frac{16}{\pi}\frac{a}{T}}\,\mathrm{sinc}\Big(\frac{a}{T}\,\kappa\Big)\cos(\kappa)\cos(2\kappa)\cos(4\kappa)\cos(8\kappa)\\
&\vdots
\end{aligned}$$

$$\widehat{\zeta}_d(\kappa) = \sqrt{\frac{2^d}{\pi}\frac{a}{T}}\,\mathrm{sinc}\Big(\frac{a}{T}\,\kappa\Big)\prod_{j=0}^{d-1}\cos\big(2^j\kappa\big) \tag{4.3}$$

It is immediately obvious that the product form provides a more compact way of expressing the wavefunction, involving only $\log_2 m = d$ factors compared to the $m = 2^d$ terms in the sum form. Also note that the general product form (4.3) yields the correct expression for the single slit ζ_0 when using the convention that an unevaluated product is the identity of multiplication.

We proceed to demonstrate the equivalence of Eq. (4.2) and Eq. (4.3) by means of mathematical induction. This is followed by an account of how the product form expresses the same physical structure differently, leading to an alternative mathematical expression of the wavefunctions.

4.2 Proving equivalence

The equivalence of the sum form of the interference wavefunction, Eq. (4.2), and its product form, Eq. (4.3), can be shown using mathematical induction. This is most conveniently done after dropping prefactors, as they are irrelevant to the calculation. Starting the induction at $d = 2$ (it holds trivially for $d = 1$ and $d = 0$), we calculate

$$\begin{aligned}
\prod_{j=0}^{2-1}\cos\big(2^j\kappa\big) &= \cos\big(2^0\kappa\big)\cos(2\kappa) && (4.4)\\
&= 2\left[\cos((2-1)\kappa) + \cos((2+1)\kappa)\right] && (4.5)\\
&= 2\left[\cos(\kappa) + \cos(3\kappa)\right] && (4.6)\\
&= 2\sum_{j=1}^{2^{2-1}}\cos((2j-1)\kappa) && (4.7)
\end{aligned}$$

Hence, for $d = 2$ the product form equals the summation form. We used the known trigonometric identity

$$2\cos(A)\cos(B) = \cos(A-B) + \cos(A+B) \tag{4.8}$$

going from Eq. (4.4) to Eq. (4.5). Now, assuming that the equivalence holds for the case d, i.e. that

$$2^{d-1}\prod_{j=0}^{d-1}\cos\big(2^j\kappa\big) = \sum_{j=1}^{2^{d-1}}\cos((2j-1)\kappa), \tag{4.9}$$

we proceed to show that this equivalence holds generally for the case $d+1$. We start the calculation and immediately use Eq. (4.9).

$$2^d\prod_{j=0}^{d}\cos\big(2^j\kappa\big) = 2\cdot 2^{d-1}\prod_{j=0}^{d-1}\cos\big(2^j\kappa\big)\cdot\cos\Big(2^d\kappa\Big) \tag{4.10}$$

$$= 2\cdot\left[\sum_{j=1}^{2^{d-1}}\cos((2j-1)\kappa)\right]\cdot\cos\Big(2^d\kappa\Big) \tag{4.11}$$

We now use the distributive property and then the trigonometric identity of Eq. (4.8) in order to evaluate each term of *cosine* products thus obtained. The terms are then rearranged.

$$\begin{aligned}
&= \cos\Big(2^d-1\Big)\kappa + \cos\Big(2^d+1\Big)\kappa + \cdots + \cos\kappa + \cos\Big(2^{d+1}-1\Big)\kappa \\
&= \cos\kappa + \cdots + \cos\Big(2^d-1\Big)\kappa + \cos\Big(2^d+1\Big)\kappa + \cdots + \cos\Big(2^{d+1}-1\Big)\kappa \\
&= \sum_{j=1}^{2^d}\cos\,(2j-1)\kappa
\end{aligned} \tag{4.12}$$

This is indeed the desired expression. We conclude that the following statement, linking the product form to the sum form, is true,

$$2^{d-1}\prod_{i=1}^{d}\cos\big(2^{i-1}\kappa\big) = \sum_{j=1}^{2^{d-1}}\cos((2j-1)\kappa)\,, \tag{4.13}$$

concluding the proof.

Note that the right-hand side of Eq. (4.13) can be viewed as a Fourier series of the periodic function on the left-hand side. This Fourier series has the special property that its coefficients are either 1 or 0. A more subtle observation relating to Eq. (4.13) is discussed in Appendix E, addressing the underlying mathematical structure. This also provides an alternative proof to the induction presented here. Appendix E is, however, of a purely

mathematical interest and unrelated to physical considerations.

4.3 Deducing the product form

We obtained the momentum-space wavefunction in Sec. 1.4.4 by means of a Fourier transform. The alternative product form, Eq. (4.3), can be obtained by performing the Fourier transform in a different way. A diagrammatic illustration is provided in Fig. 4.1. The different algebraic expressions leading to the sum or the product form are easily identified. We proceed with an example.

Assuming a uniformly illuminated aperture mask with eight slits, the Fourier transform is performed by considering each slit location as a delta function δ, and the aperture mask as a sum of such. The following expression is found to express the structure of the aperture mask

$$\begin{aligned} f_3(x) = &\left[\delta\left(x+1\right)+\delta\left(x-1\right)\right]+\left[\delta\left(x+3\right)+\delta\left(x-3\right)\right] \\ &+\left[\delta\left(x+5\right)+\delta\left(x-5\right)\right]+\left[\delta\left(x+7\right)+\delta\left(x-7\right)\right] . \end{aligned} \tag{4.14}$$

This is precisely the underlying structure of Eq. (1.28). The Fourier transform is easily computed, noting that the Fourier transform of a sum is the sum of Fourier transforms, giving

$$\widehat{f}_3(k) = \cos(\kappa)+\cos(3\,\kappa)+\cos(5\,\kappa)+\cos(7\,\kappa) . \tag{4.15}$$

Alternatively, the aperture mask may be described by the following convolutions

$$\begin{aligned} g_3(x) = &\left[\delta\left(x+1\right)+\delta\left(x-1\right)\right]*\left[\delta\left(x+2\right)+\delta\left(x-2\right)\right] \\ &*\left[\delta\left(x+4\right)+\delta\left(x-4\right)\right] . \end{aligned} \tag{4.16}$$

The Fourier transform of Eq. (4.16) is also computed easily, noting that the Fourier transform of a convolution is a product of Fourier transforms. This leads immediately to the promised product form

$$\widehat{g}_3(\kappa) = \cos(1\,\kappa)\cdot\cos(2\,\kappa)\cdot\cos(4\,\kappa) \tag{4.17}$$

Eqs. (4.15) and (4.17) were obtained by pairing up slits in two distinct ways

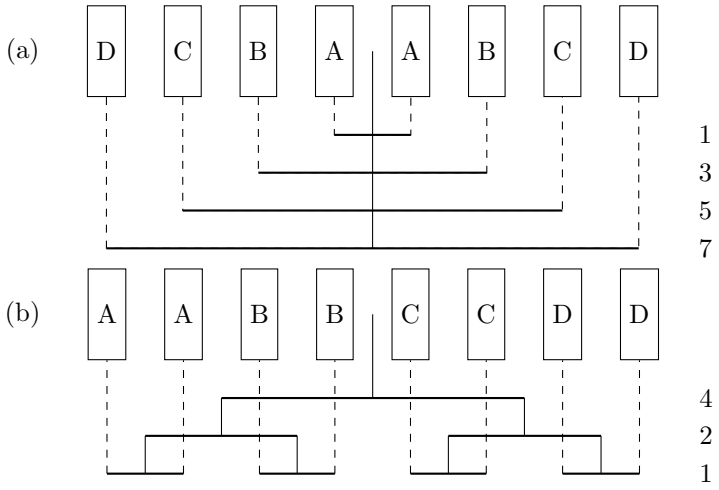

Figure 4.1: The two different ways of arranging the slits of an aperture mask in pairs are depicted for an example setup with eight slits. In (a), the usual way of pairing up slits across the origin is shown; this results in a sum. The numbers indicate the distance between the two members of the pair, they are in units of "slit separations". In (b) an alternative way of pairing the slits is shown, which underlies the product form. The numbers indicate the distance of the successive pairings in units of "slit separations".

as part of the Fourier transform. The common way of pairing up two slits results in Eq. (4.15): Two slits with equal distance to the origin are considered a pair and their complex phases are combined into a real *cosine*. This way of pairing up slits is illustrated in Fig. 4.1 (a). The four pairs in the depicted 8-slit setup are denoted A, B, C and D.

The procedure underlying the product form is different, it is illustrated in Fig. 4.1 (b). It entails successively dividing the aperture mask into halves, and the halves into quarters and so on, until pairs are left. In the illustrated example, dividing the initial aperture mask into halves results in a *cosine* factor scaled with the centre-to-centre distance of 4 (in units of "half slit separations") between the halves. Dividing each of the two halves results in quarters and gives a *cosine* factor scaled by 2, which is the centre-to-centre distance between the quarters. Finally, the pairs of slits yield a *cosine* factor scaled with unity. Observe that the centre-to-centre distances indicated on the right-hand side times the number of occurrences is constant, e.g. on the lowest level 4 pairs with a distance of unity are obtained whereas on the

highest level there is one division with a centre-to-centre distance of 4. This generalises trivially to larger interference setups.

This leads us to the following notion, the implications of which are discussed in the following section: Doubling the number of illuminated slits results in an additional *cosine* factor with doubled frequency, and it seems like a suitable definition of fringe width to regard a *cosine* of doubled frequency to have fringes of half the width.

4.4 Conclusions

In earlier sections, in particular the previous one, certain aspects of the structure of quantum states expressed in product form were briefly mentioned. Here, a detailed exposition is presented. We develop the concepts of the width of an interference pattern as well as its fine structure.

Consider the momentum-space wavefunction of the double-slit superposition state ζ_1; it is specified in Eq. (1.36) and illustrated in Fig. 1.3. This is the simplest interference wavefunction and its structure is easily read: The *sinc* provides an envelope while the *cosine* describes the fringes.

For higher-order wavefunctions additional functions appear and an identification with envelope and fine structure is not so simple anymore. However, once we have a recipe for identifying the additional functions, we could group them accordingly. Formally, this is done by grouping and collectively relabelling them according to the properties they determine: We define two functions, $\widehat{g}_d(\kappa)$ and $\widehat{f}_d(\kappa)$. The function $\widehat{g}_d(\kappa)$ describes an envelope, while the function $\widehat{f}_d(\kappa)$ describes the fine structure. The wavefunction would be expressed as

$$\widehat{\zeta}_d(\kappa) \propto \widehat{g}_d(\kappa)\, \widehat{f}_d(\kappa), \tag{4.18}$$

up to some normalisation factor. In the previous section, we discussed a recursive relationship between the wavefunctions,

$$\widehat{\zeta}_d(\kappa) \propto \widehat{\zeta}_{d-1}(\kappa) \cos 2^{d-1}\kappa\,, \tag{4.19}$$

Identifying the Eqs. (4.18) and (4.19), we obtain

$$\widehat{g}_d(\kappa) = \widehat{\zeta}_{d-1}(\kappa), \tag{4.20}$$

$$\widehat{f}_d(\kappa) = \cos 2^{d-1}\kappa\,. \tag{4.21}$$

According to Eq. (4.21), the fine structure of the momentum-space wavefunction $\widehat{\zeta}_d(\kappa)$ is determined by a simple *cosine*. In fact, this single *cosine* is all that differentiates $\widehat{\zeta}_d(\kappa)$ from $\widehat{\zeta}_{d-1}(\kappa)$. As this *cosine* does not change the overall localisation property of the interference pattern, $\widehat{\zeta}_d(\kappa)$ shares its localisation property with $\widehat{\zeta}_{d-1}(\kappa)$. Applying this argument repeatedly, we conclude that the localisation property of $\widehat{\zeta}_d(\kappa)$ is determined by $\widehat{\zeta}_0(\kappa)$.

The quantum state ζ_0 is prepared through illumination of a single aperture. However, the present investigation is about superposition states and the resulting interference phenomena; diffraction is an independent phenomenon. The given choice of aperture, which implies the particular shape of $\widehat{\zeta}_0(k)$, determines the overall localisation properties of the various $\widehat{\zeta}_d$. We refer to $\widehat{\zeta}_0$ as the fundamental envelope. While the fundamental envelope is, in general, only part of the effective envelope, it is qualitatively distinct in that it depends on diffraction. Accordingly, a measure of the fringe property should not depend on the fundamental envelope. In fact, there should not be any dependence on the effective envelope, but only dependence on the function actually determining the fine structure of the momentum-space wavefunction, i.e. Eq. (4.21). Note that any measure of fringe contrast necessarily has this unwanted dependence.

This recursive relationship is illustrated Fig. 4.2 for ζ_0, ζ_1, ζ_2 and ζ_3, i.e. for $n = 1, 2, 4, 8$. Note the following: The eight-slit wavefunction $\widehat{\zeta}_3(\kappa)$ depicted in Fig. 4.2 c) (solid line) is contained in an envelope $\widehat{\zeta}_2(\kappa)$ (dotted). Equally, the four-slit wavefunction $\widehat{\zeta}_2(\kappa)$ depicted in Fig. 4.2 (b) (solid line) is contained in an envelope $\widehat{\zeta}_1(\kappa)$ (dotted). This argument applies recursively, the spread of $\widehat{\zeta}_d(\kappa)$ is determined by $\widehat{\zeta}_{d-1}(\kappa)$, and in turn the spread of $\widehat{\zeta}_{d-1}(\kappa)$ is determined by $\widehat{\zeta}_{d-2}(\kappa)$, all the way up to the single-slit state $\widehat{\zeta}_0(\kappa)$. This is an excellent illustration that the spread of the interference pattern is independent of the number of illuminated slits; it instead depends on the slit shape. The uncertainty product should not depend on the spread of the interference pattern nor, consequently, on the particular choice of aperture.

Considering the fine structure we note that while the *sinc* is common to the single-slit wavefunction $\widehat{\zeta}_0(\kappa)$ and the double-slit wavefunction $\widehat{\zeta}_1(\kappa)$, the latter also possesses fine structure described by the *cosine*. Doubling the number of illuminated slits (from 1 to 2) results in a *cosine* of frequency 1. Doubling the number of illuminated slits once more (from 2 to 4) results in a *cosine* of double the frequency, i.e. 2, and hence a fringe width that is reduced

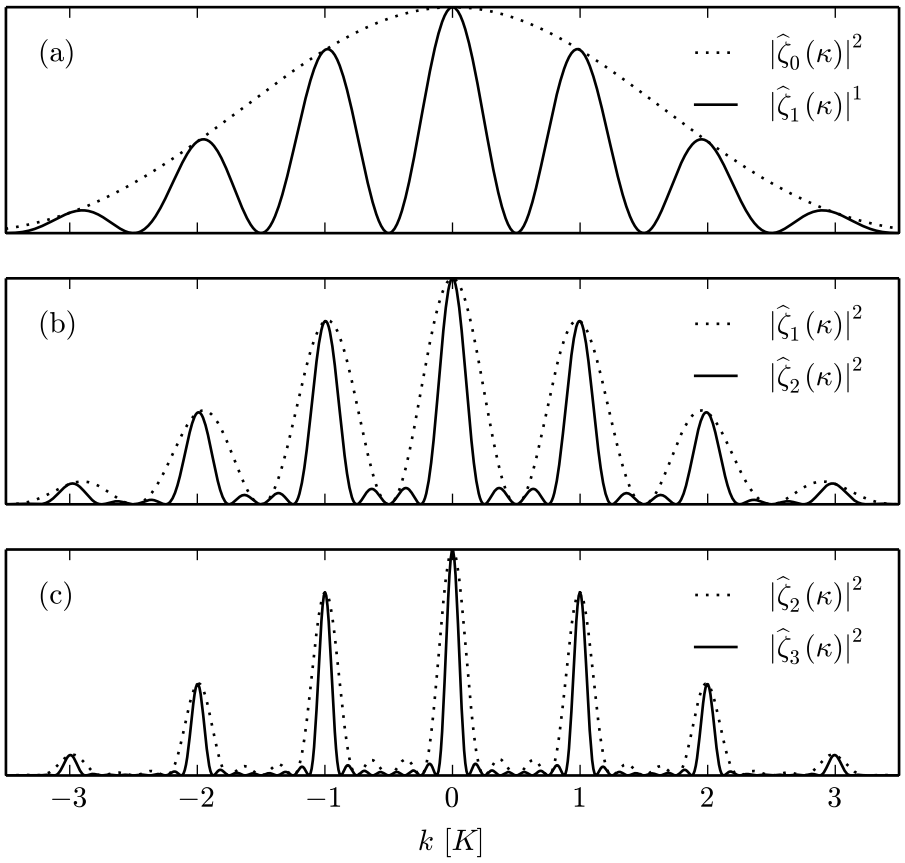

Figure 4.2: The interference patterns associated with ζ_1, ζ_2 and ζ_3 are depicted; their recursive relationship is illustrated. Figure 1 (a) shows $|\widehat{\zeta_1}(\kappa)|^2$, the first interference state, and the *sinc* envelope (dotted line). Figure 1 (b) shows $|\widehat{\zeta_2}(\kappa)|^2$ (solid line), $|\widehat{\zeta_1}(\kappa)|^2$ (dotted) serves as the envelope to $|\widehat{\zeta_2}(\kappa)|^2$. Figure 1 c) shows $|\widehat{\zeta_3}(\kappa)|^2$ (solid line), $|\widehat{\zeta_2}(\kappa)|^2$ (dotted) serves as the envelope to $|\widehat{\zeta_3}(\kappa)|^2$. Note that the depicted states are not normalised relative to each other so as to better demonstrate the shape and recursive relationship of the depicted states. The parameters are chosen such that $a/T = 1/4$.

by a factor of 2. We observe that our initial result for the fine structure, Eq. (3.28), depends on the square root of the number of illuminated slits. Yet we saw in this section that doubling the number of illuminated slits leads to a fine structure with doubled frequency; whatever measure might be used, this should be reflected. In the next chapter we discuss a modification of the uncertainty formulation of Chapter 3 that yields precisely the right asymptotic behaviour.

It follows naturally that the particular choice of slit shape is of little importance. The common choice of rectangular slit shape, $\mathrm{rec}_a(x)$, is often rejected on the basis of its diverging standard deviation, i.e. $\Delta(P, \mathrm{rec}_a) = \infty$. However, this concern is unnecessarily restrictive in the given context, and only important when (also) considering single-slit diffraction.

To summarise, we discussed in detail a certain subset of superposition states that can be expressed in a product form that provides an alternative way for expressing the momentum-space wavefunction of these states. The structure of interference wavefunctions in product form is easily read, which allows identifying the functions determining the spread of the interference pattern and the functions determining its fringe width. In particular, the constituent functions of the wavefunction can be identified with either the effective envelope or the fine structure. We found that the fine structure is determined by a single *cosine* only.

Chapter 5

Uncertainty II: A refined modification of Heisenberg uncertainty

We revisit the uncertainty formulation that was discussed in Chapter 3 in light of the results of Chapter 4.

In Chapter 4 we identified the function describing the fine structure and noted that doubling the number of illuminated scales this function by a factor of 2, i.e. reduces the fringe width by a factor of 2. This feature should be captured by any suitable measure of fringe width, but in its present form the uncertainty formulation of Chapter 3 does not meet this requirement.

Here, we refine the measure of fringe width by adapting the operator P_{mod} to the given experimental setup. This modification indeed leads to a measure of fringe width capable of resolving the fringe width precisely, demonstrated by fitting asymptotic behaviour of the fringe width, and to a converging uncertainty product.

The uncertainty of a different set of quantum states is also investigated. These quantum states are the joint eigenstates on periodic sets of Q and P, which were introduced in Chapter 2.

5.1 The refined modular momentum

In Chapter 3 we found that the measure of fringe width, $\Delta(P_{\text{mod}}, \psi_n)$, is related to the inverse square root of the the number of illuminated slits $m = 2n$. This asymptotic behaviour was obtained in Eq. (3.28). From the investigation of the previous section, however, we conclude that this is not the expected asymptotic behaviour.

According to the discussion of Chapter 4, doubling the number of illuminated slits should result in half the fringe width. More precisely, we found that the momentum-space wavefunction picks up a *cosine* of doubled frequency from doubling the number of illuminated slits. However, this is not reflected by $\Delta(P_{\text{mod}}, \psi_m)$,

$$\Delta(P_{\text{mod}}, \psi_{2n}) \neq \frac{1}{2}\Delta(P_{\text{mod}}, \psi_n)\,. \tag{5.1}$$

We address this issue by means of a refined operator,

$$P_{\text{mod}}(n) = (P + K_n/2 \mod K_n) - K_n/2\,, \tag{5.2}$$

which explicitly depends on the experimental setup by means of the dependence on n. It is important to note that $P_{\text{mod}}(n)$ commutes with Q_{mod}, because $K_n = 2\pi/(nT)$, ensuring that we again obtain the uncertainty relation

$$\Delta(Q_T, \psi)\ \Delta(P_{\text{mod}}, \psi) \geq \frac{1}{2}\,. \tag{5.3}$$

The derivation in Sec. 3.3 is extended to this more general case at the discretion of the reader.

The operator $P_{\text{mod}}(n)$ is adapted to the given experimental setup and reflects the minimal period of the nodes occurring in the given interference pattern of ψ_n. Calculating the asymptotic behaviour of this measure of fine structure, we find

$$\Delta(P_{\text{mod}}(n), \psi_n) = \left(\frac{2}{K_n}\int_{-K_n/2}^{K_n/2} k^2 \cos\left(\frac{\pi}{K_n}\,k\right)^2 \,\mathrm{d}k\right)^{1/2} \tag{5.4}$$

$$= \frac{K_n}{2\pi}\sqrt{\frac{\pi^2-6}{3}} = \frac{1}{nT}\sqrt{\frac{\pi^2-6}{3}} \tag{5.5}$$

We obtain a result that depends inversely on n (while we found dependence

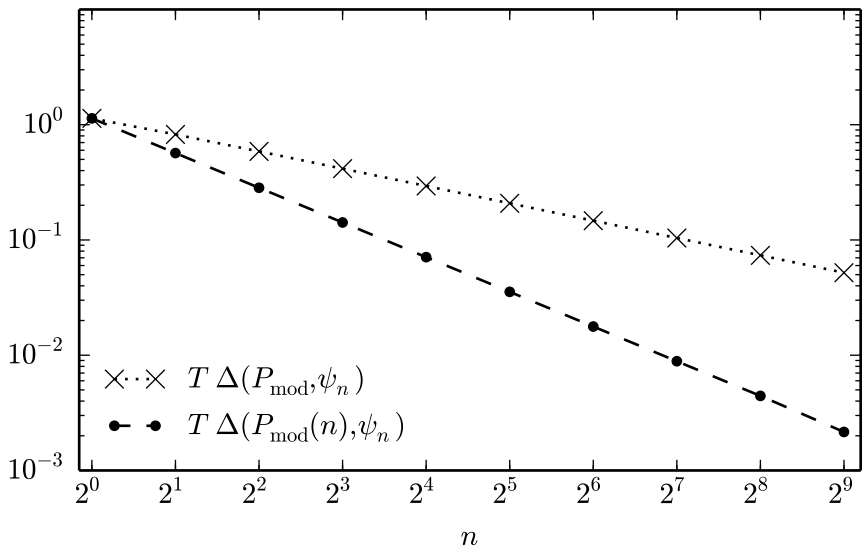

Figure 5.1: The standard deviation of $P_{\mathrm{mod}}(n)$ in state ψ_n is depicted (dots on dashed line) as well as the previously discussed P_{mod} (crosses on dashed line) for easy of comparison. The standard deviations are multiplied by T, removing the dependence on the slit separation.

on $n^{-1/2}$ for P_{mod}). The integration that leads to the second line is straightforward. However, the first line is a very interesting statement that is worth discussing in detail.

Observe that the integration in Eq. (5.4) corresponds to the standard deviation of a half *cosine* pulse. The wavefunction $\widehat{\psi}_n(k)$, however, is substantially more complicated. In Chapter 3 we already discussed that $\Delta(P_{\mathrm{mod}}, \psi_n)$ is independent the fundamental envelope, i.e. independent of the *sinc* function, and this extends immediately to $\Delta(P_{\mathrm{mod}}(n), \psi_n)$. However, Eq. (5.4) states that $\Delta(P_{\mathrm{mod}}(n), \psi_n)$ is independent of the effective envelope, which includes the fundamental envelope. This result precisely meets the conclusions of the discussion of Chapter 4. The mathematical reasoning that leads to Eq. (5.4) is provided in Appendix C.2. The calculation is somewhat tedious for the general case of even slit numbers. A much simpler calculation is required when restricting to slit numbers corresponding to powers of 2, as this allows exploiting the product form. That calculation is provided in Appendix C.1.

The asymptotic behaviour of $\Delta(P_{\mathrm{mod}}(n), \psi_n)$ is depicted in Fig. 5.1 (dots

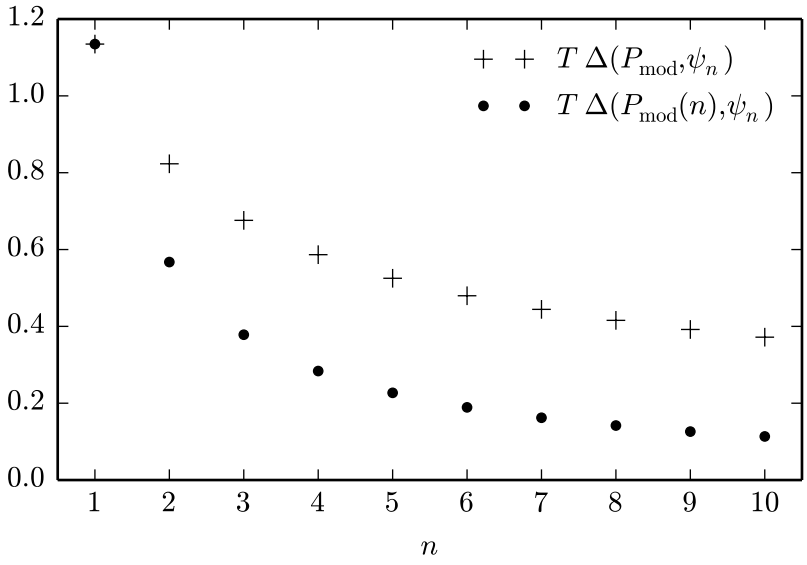

Figure 5.2: The standard deviation of $P_{\mathrm{mod}}(n)$ in state ψ_n is depicted (dots) as well as the previously discussed $P_{\mathrm{mod}}(n)$ for easier comparison. The standard deviations are multiplied by T, removing the dependence on the slit separation.

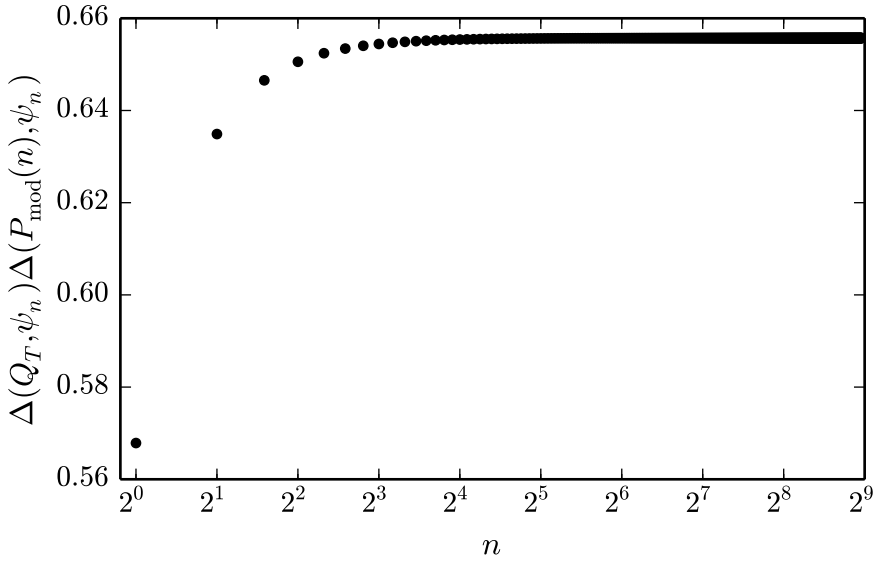

Figure 5.3: Convergence of the uncertainty product (5.6) for uniformly illuminated aperture masks of even slit number.

on dashed line) and in Fig. 5.2 (dots). The resulting asymptotic behaviour of the uncertainty product, Eq. (5.3), is obtained immediately from Eqs. (3.25) and (5.5)

$$\lim_{n\to\infty} \Delta(Q_T, \psi_n)\, \Delta(P_{\mathrm{mod}}(n), \psi_n) = \frac{1}{3}\sqrt{\pi^2 - 6} \approx 0.656\,. \tag{5.6}$$

Asymptotically, we find convergence to a finite value, while the previous uncertainty product of Eq. (3.29) would diverge. The convergent behaviour is illustrated in Fig. 5.3. This is the result of adapting the operator that measures the fringes to the interference setup considered by using the known relationship between the number of illuminated slits and the periodicity of the nodes discussed in the previous section. While the discussion in the previous section was restricted to slit numbers corresponding to powers of 2 only, the expression for $\Delta(P_{\mathrm{mod}}(n), \psi_n)$ holds for all even slit numbers $m = 2n$, i.e. for all n, as is illustrated in Figs. 5.2 and 5.3.

5.2 Uncertainty of joint eigenfunctions of commuting functions of Q and P

The refined uncertainty formulation discussed in the previous section is now applied to a second set of quantum states. These quantum states were constructed in Chapter 2 as eigenfunctions to periodic spectral projections of position and momentum. Here, we parametrise these states as follows:

$$\phi_n(x) = \big[g * (\text{Ш}_T \cdot h_n)\big](x), \tag{5.7a}$$

$$\widehat{\phi}_n(k) = \left[\widehat{g} \cdot \left(\widehat{\text{Ш}}_K * \widehat{h}_n\right)\right](k)\,. \tag{5.7b}$$

Throughout the present text the convolution operation is indicated using the asterisk ($*$). The Dirac comb is defined as

$$\text{Ш}_T(x) = \sum_{j=-\infty}^{\infty} \delta(x - T/2 - jT), \tag{5.8}$$

$$\widehat{\text{Ш}}_K(k) = \frac{\sqrt{2\pi}}{T} \sum_{j=-\infty}^{\infty} (-1)^j \delta(k - jK), \tag{5.9}$$

where δ denotes the delta distribution. Under Fourier transformation, the Dirac comb Ш_T is mapped onto a Dirac comb $\widehat{\text{Ш}}_K$ with reciprocal spacing and a numerical factor. The function g describes the slit shape,

$$g(x) = \text{rec}_a(x), \tag{5.10}$$

while the function $\widehat{h}_n$ is associated with the fringe shape and corresponds to

$$\widehat{h}_n(k) = \begin{cases} \sqrt{2/K_n}\cos \pi k/K_n & \text{for } k \in [-K_n/2, K_n/2] \\ 0 & \text{for } k \notin [-K_n/2, K_n/2] \end{cases}. \tag{5.11}$$

The function $\widehat{h}_n(k)$ is supported on an interval of size K_n, which thus makes a suitable measure of fringe width.

Our parametrisation is such that ϕ_1 corresponds to ψ_1 while for $n \geq 2$, a joint eigenfunction of commuting functions of position and momentum is obtained. These quantum states are eigenstates of periodic position and momentum projectors, which were used earlier to explain the observation of seemingly incompatible properties in Chapter 2. They address the same underlying structure as the uncertainty formulation discussed here: These quantum states are constructed in light of the compatibility of commuting functions position and momentum that naturally occur in multislit experiments, whereas the uncertainty formulation addresses the incompatibility of the observables of multislit interferometry. Hence these states make natural candidates for further examination.

Although both ψ_n and ϕ_n display increasingly finer fringes as n increases, the character of these fringes is very different. See Fig. 5.5 for a direct comparison between ψ_2 and ϕ_2. The difference is found in the effective envelope of ψ_2, i.e. the fact that ψ_2 possesses secondary maxima. In particular, it is the effective envelope of $\widehat{\psi}_2$ that is responsible for the existence of the secondary maxima. However, we already discovered that the effective envelope does not contribute to the fine structure. We conclude immediately that the fringe widths of ψ_n and ϕ_n should be identical. Indeed, this is what we find: $\Delta(P_{\text{mod}}(n), \phi_n)$ can be calculated directly

$$\Delta(P_{\text{mod}}(n), \phi_n) = \left[\frac{2}{K_n}\int_{-K_n/2}^{K_n/2} k^2 \cos\left(\frac{\pi}{K_n}\, k\right)^2 \,\mathrm{d}k\right]^{1/2} \tag{5.12}$$

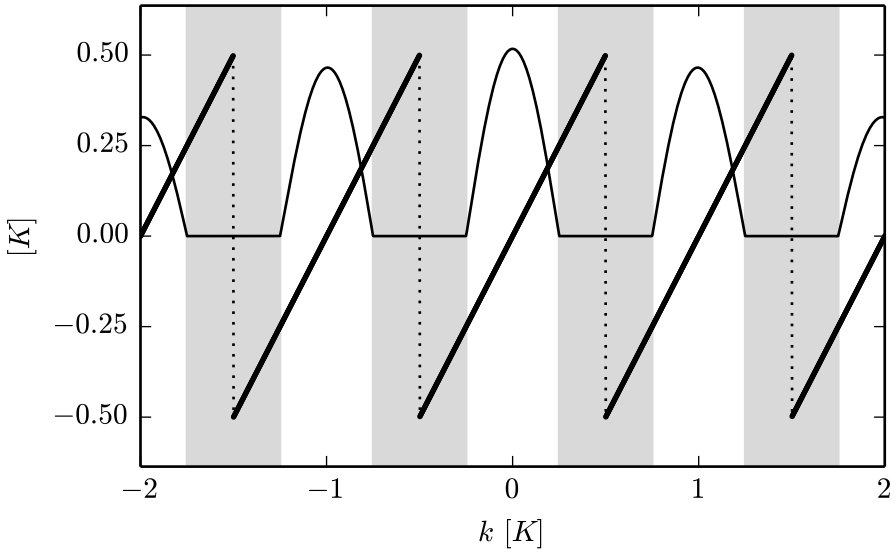

Figure 5.4: The operator P_{mod} and the quantum state ϕ_2 are depicted. This example illustrates that the action of P_{mod} is identical to that of $P_{\mathrm{mod}}(n)$, because only those parts of P_{mod} contribute which are identical to $P_{\mathrm{mod}}(n)$. The other parts do not contribute, because there the wavefunction vanishes. In the depicted example the action of P_{mod} is identical to that of $P_{\mathrm{mod}}(2)$. Note that the wavefunction is not normalised.

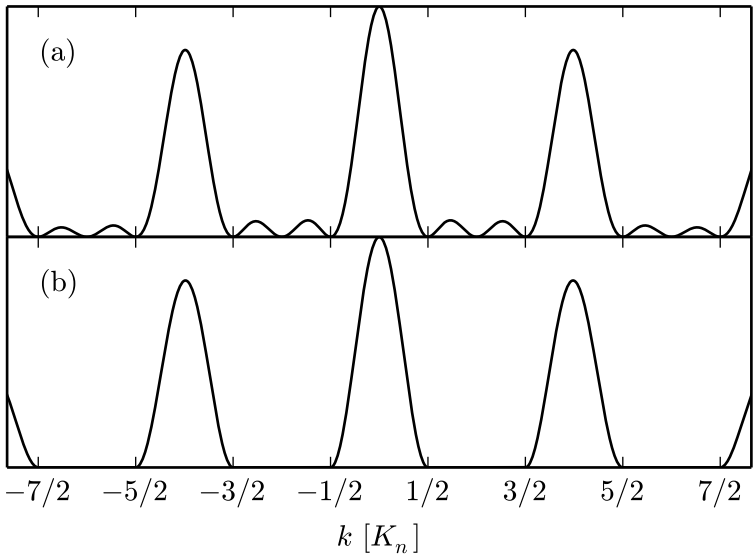

Figure 5.5: A direct comparison of the momentum-space wavefunctions of ψ_2 and ϕ_2. The difference is that ψ_2, depicted in (a), features secondary maxima whereas ϕ_2, depicted in (b), has extended nodes instead. The parameters are chosen such that $a/T = 1/4$.

$$= \frac{K_n}{2\pi}\sqrt{\frac{\pi^2-6}{3}} = \frac{1}{nT}\sqrt{\frac{\pi^2-6}{3}} \tag{5.13}$$

$$= \Delta(P_{\mathrm{mod}}, \phi_n) \tag{5.14}$$

The first equality follows, because a) we assume that the fringes are supported on intervals of size K_n, and b) $\Delta(P_{\mathrm{mod}}, \phi_n)$ can be computed by considering a single interval of periodicity without the envelope. Note that according to Eq. (5.14), there is no benefit from adapting the operator $P_{\mathrm{mod}}(n)$ to the given experimental setup. The operator $P_{\mathrm{mod}}(n)$ is insensitive to the presence of extended nodes, i.e. extended intervals where the wavefunction vanishes. See Fig. 3.1 for an illustration of this point. Finally, observe that the value in Eq. (5.13) is identical to that of Eq. (5.5).

Calculating the standard deviation of Q_T in state ϕ_n is substantially more involved than it was for ψ_n, although the final result is rather simple. Note that the operator Q_T is only sensitive only to the total probability contained in intervals of length T. Let P_j correspond to the probability in the interval $[jT, (j+1)T]$, where j is any integer. The standard deviation of

Q_T in quantum state Ψ is given by

$$\Delta(Q_T, \Psi) = T \left[\sum_{j=-\infty}^{\infty} j^2 \, \mathsf{P}_j - \left(\sum_{j=-\infty}^{\infty} j \, \mathsf{P}_j \right)^2 \right]^{1/2} . \tag{5.15}$$

An aperture mask with infinitesimal slits prepares a quantum state Ψ_δ, indicated by the delta subscript. The variance of Q in state Ψ_δ is given by

$$\Delta(Q, \Psi_\delta) = T \left(\sum_{j=-\infty}^{\infty} (j + 1/2)^2 \, \mathsf{P}_j \right)^{1/2} . \tag{5.16}$$

Following from our assumption of even probability distributions, i.e. we assume that $|\psi(x)|^2 = |\psi(-x)|^2$, the two Eqs. (5.15) and (5.16) are equal,

$$\Delta(Q_T, \psi) = \Delta(Q, \psi_\delta). \tag{5.17}$$

This is shown explicitly in Appendix C.3. While the operator Q_T is insensitive to detailed features of the probability distribution of ψ, the state ψ_δ lacks them. Note that according to Eq. (5.17) the standard deviation $\Delta(Q_T, \psi)$ does not depend on the particular choice of aperture at all.

An explicit expression for $\Delta(Q_T, \phi_n)$ can now be obtained using the equivalence stated in Eq. (5.17), the result of Appendix C.4 and $\widehat{h}_n$ as specified in Eq. (5.11). We find

$$\begin{aligned} \Delta(Q_T, \phi_n) &= \Delta(Q, \phi_{n,\delta}) && (5.18) \\ &= \Delta(Q, \phi_n) - a/12 && (5.19) \\ &= nT/2 && (5.20) \end{aligned}$$

The two subscripts of $\phi_{n,\delta}$ in Eq. (5.18) denote this quantum state as a joint eigenfunction prepared by an aperture mask with infinitesimal slits. Eq. (5.19) follows by the calculation provided in Appendix C.4, while the final result follows from a straightforward calculation of the standard deviation of h_n.

The uncertainty product associated with the state ϕ_n can now be calculated using Eqs. (5.13) and (5.18). We obtain

$$\Delta(Q_T, \phi_n) \, \Delta(P_{\mathrm{mod}}, \phi_n) = \frac{1}{2} \sqrt{\frac{\pi^2 - 6}{3}} \, . \tag{5.21}$$

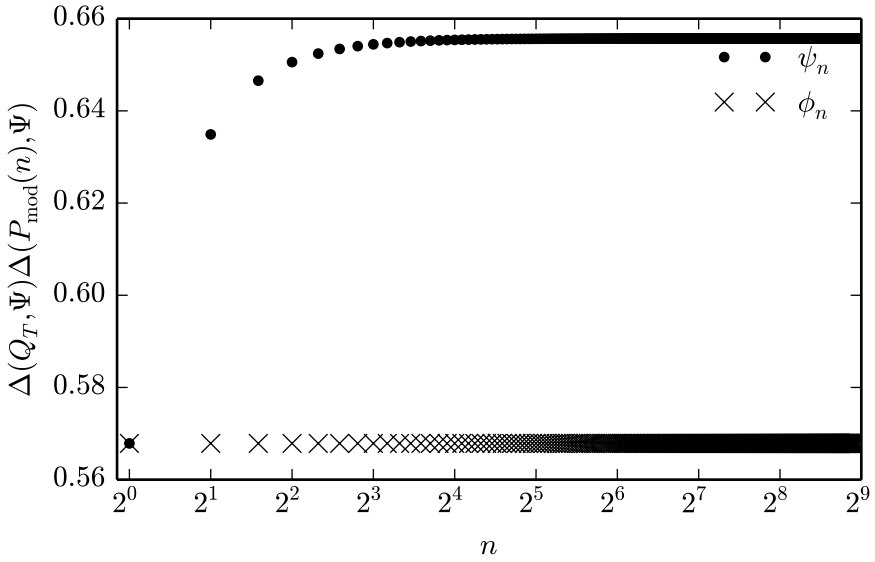

Figure 5.6: The convergence of the uncertainty product of states ψ_n and ϕ_n, Eqs. (5.6) and (5.21) respectively, is depicted.

Evidently this uncertainty formulation assigns the same uncertainty product to ϕ_n irrespective of the particular value of n; see Fig. 5.6, depicting the uncertainty product for a range of values of n. Decreasing the size of the support for each of the fringes, resulting in finer fringes, is precisely reflected by the loss of spatial localisation.

5.3 Conclusion

A successful adaptation of the Heisenberg relation, Eq. (1.11), to multislit interferometry was presented in this chapter.

We started with the formulation of uncertainty proposed by Aharonov *et al.*, which we worked out in Chapter 3, and refined it in order to accommodate for the insights obtained from the discussion of Chapter 4. The modified uncertainty relations employ standard deviations, yet accurately express the complementarity of spatial localisation and fringe width by virtue of the observables involved.

Two detailed applications of this uncertainty relation were presented, investigating two types of multislit states. The first application involved the states ψ_n, prepared through uniform illumination of an aperture mask. The

second application involved the states ϕ_n, which are joint eigenfunctions of commuting functions of position and momentum.

By virtue of the refined operator $P_{\text{mod}}(n)$, we were able to precisely resolve the fringe width of ψ_n. This measure of fringe width not only gives reasonable values, but also shows the expected asymptotic behaviour that we concluded from the discussion of Chapter 4. The uncertainty product starts at a finite value and monotonically converges to a larger value.

We discussed the physical insight regarding the calculation of the standard deviation $\Delta(P_{\text{mod}}(n), \psi_n)$. The arising simplification stems from the fact that the effective envelope has no effect on that calculation. The result is that the only function that determines the fine structure is a simple *cosine*. This analytic result, which is worked out in detail in Appendix C.1 and in Appendix C.2, elegantly expresses the physical argument of Chapter 4.

The application of uncertainty to the states ϕ_n yielded somewhat different results. The fringe width of ψ_n is identical to that of ψ_n. This result was anticipated, because from earlier considerations we concluded that the effective envelope does not affect the fine structure. However, the uncertainty product does not change with n at all, but is the same for all ϕ_n irrespective of the particular value of n. This result is interesting, because the quantum states ϕ_n were constructed in order to express the compatible observations of multislit experiments, while the discussed uncertainty formulation expresses the incompatibility of the observables.

Finally, note that the analysis presented in this chapter does not depend on the particular choice of aperture or the related fundamental envelope at all. This is as it should be, as was pointed out.

Chapter 6

Uncertainty III: Comparison with an alternative uncertainty formulation

In this chapter the utility of an alternative formulation of uncertainty for multislit applications is discussed and compared to the uncertainty formulation of Chapter 5.

This alternative approach was developed by Uffink and Hilgevoord in the context of single- and double-slit experiments. For applications in a more general multislit context, we are required to address a number of arising issues. In particular, it is found that additional consideration is required in order to express the relevant tradeoff in multislit experiments because otherwise additional contributions to the uncertainty product may be introduced. Additionally, one of the underlying concepts is generalised to fit the wider range of cases. Once these issues are resolved, both uncertainty formulations are found to yield the same qualitative results in the example applications, confirming that they independently capture the physical relationship between the relevant observables.

The third part provides a comparison with an alternative uncertainty formulation developed by Uffink and Hilgevoord for single- and double-slit experiments [2]. However, in order to successfully apply their uncertainty formulation to multislit interferometry, arising issues need to be addressed. We generalise an underlying concept to fit the multislit context and find that additional considerations are necessary in order to express the relevant tradeoff. The comparison then becomes straightforward. Many of the results agree qualitatively, independently confirming that the relevant physical structure is captured.

6.1 Introduction

Throughout most of the previous chapters, a modification of the Heisenberg uncertainty relation was discussed. Realising the inadequacy of the Heisenberg relation for single- and double-slit experiments, Uffink and Hilgevoord pursued a different course of action, developing an alternative formulation of uncertainty. According to Ref. [2], part of the motivation was to entirely avoid standard deviations, because Uffink and Hilgevoord were convinced that this measure was not suitable to the given context. Using unusual measures rather than ubiquitous standard deviations, Uffink and Hilgevoord realised an intriguing implementation of the relevant observables.

Uffink and Hilgevoord define two measures to express uncertainty: They define the overall width $\Omega_N(\Psi)$ of a normalised wavefunction $\Psi(x)$ and the mean fringe width $\omega_M(\Psi)$ (in momentum space). They proceed to show that an uncertainty relation exists for these quantities, expressing a tradeoff between spatial localisation on the one hand, and fine structure in momentum space on the other. The same analysis applies independently to $\widehat{\Psi}$ (formally obtained by exchanging Ψ for $\widehat{\Psi}$), and hence $\Omega_N(\widehat{\Psi})\,\omega_M(\widehat{\Psi})$ is bounded from below as well. However, we focus on Ψ in our present investigation.

The overall width $\Omega_N(\Psi)$ of a quantum state Ψ is the smallest interval that contains probability N:

$$\Omega_N(\Psi) = \min\left\{|p_1 - p_2| : \int_{p_1}^{p_2} |\Psi(x)|^2 \,\mathrm{d}x = N\right\} \tag{6.1}$$

The parameter N is a number less than or equal to 1, but chosen close to 1. Note that the value of the overall width necessarily reflects the discreteness of the aperture mask. In the analysis below, particularly of aperture masks with a small number of illuminated slits, a small change in N may lead to notable discontinuous jumps of the overall width.

The fine structure of Ψ is quantified through the mean fringe width $\omega_M(\Psi)$, which is the smallest shift such that the inner product of $\widehat{\Psi}(k)$ and the shifted $\widehat{\Psi}(k-s)$ is associated with a value M:

$$\omega_M(\Psi) = \min\left\{s : \left|\int_{-\infty}^{\infty} \widehat{\Psi}^*(k)\,\widehat{\Psi}(k-s)\,\mathrm{d}k\right| = M\right\} \tag{6.2}$$

The parameter M is chosen with respect to the particular choice of N; see Eq. (6.5) below. Note that $\omega_M(\Psi)$ is defined in terms of the autocorrelation function. Similar approaches are also found in other work, for example Ref. [33]. This measure is conceptually rather different, it quantifies how much the momentum-space wavefunction $\widehat{\Psi}(k)$ deviates from precise values of momentum. The mean fringe width $\omega_M(\Psi)$ is not sensitive to the number of momentum peaks, but only to how sharp they are.

For a normalised quantum state Ψ, Uffink and Hilgevoord proved the existence of a lower bound to the overall width $\Omega_N(\Psi)$ and the mean fringe width $\omega_M(\Psi)$,

$$\Omega_N(\Psi)\,\omega_M(\Psi) \geq 2\arccos\left(\frac{M+1}{N}-1\right), \tag{6.3}$$

with the following two conditions required

$$M^2 + N^2 \geq 1, \tag{6.4}$$

$$M \leq 2N - 1. \tag{6.5}$$

The two conditions on N and M restrict the value range of N significantly. Squaring Eq. (6.5) and substituting it into Eq. (6.4) yields a quadratic for N

$$5N^2 - 4N + 1 \geq 1. \tag{6.6}$$

Solving this equation yields $N \geq 4/5$. The choice $N = 4/5$ is clearly distinguished in Fig. 6.1. However, each of the acceptable pairs (N, M) yields another acceptable value for the uncertainty product.

Uffink and Hilgevoord found that the exact choice of N and M was not important for the applications they considered. We agree that certain results might not depend on N or M. For example, the exact choice of M is entirely irrelevant for an analysis of the double-slit state so long as N is chosen very close to unity. Then, the uncertainty product is approximately equal to the lower bound for any M (strictly true for $N = 1$). In general, though, we arrived at a different conclusion, which is detailed in the analysis of example applications provided below.

Uffink and Hilgevoord state that (in adapted notation)

- $\omega_M(\Psi)$ and $\Omega_N(\Psi)$ are governed by the slit separation T,

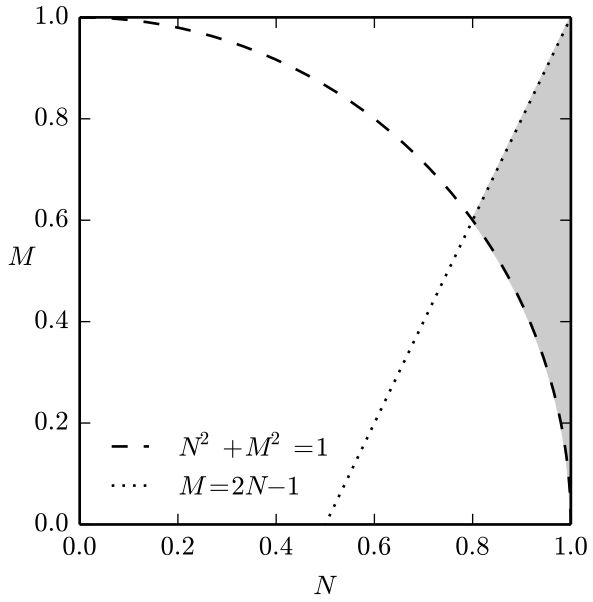

Figure 6.1: The two conditions on the pair (N, M), Eqs. (6.4) and (6.5), are illustrated. The shaded area represents the allowed choices.

- $\omega_M(\widehat{\Psi})$ and $\Omega_N(\widehat{\Psi})$ are governed by the slit width a.

The slit separation T is a mere scaling parameter and, as expected, the value of the uncertainty product is independent of T. This is a consequence of the scaling property of the Fourier transform and follows immediately from the definitions of overall width and mean fringe width: Let us modify the experimental setup, replacing T by $T' = cT$, where c is a positive number. Accordingly, we would describe the experiment in terms of a modified quantum state Ψ'. It follows from Eq. (6.1) that

$$\Omega_N(\Psi') = c\,\Omega_N(\Psi),$$

and it follows from Eq. (6.2) that

$$\omega_M(\widehat{\Psi}') = \omega_M(\widehat{\Psi})/c.$$

The uncertainty product associated with the rescaled experiment remains unchanged

$$\Omega_N(\Psi')\,\omega_M(\widehat{\Psi}') = \Omega_N(\Psi)\,\omega_M(\widehat{\Psi})\,.$$

Only in the double-slit experiment, which Uffink and Hilgevoord considered, the slit separation T is related to the extent of the wavefunction. We generalise the above statement,

- $\omega_M(\Psi)$ and $\Omega_N(\Psi)$ are governed by the fringe width b,
- $\omega_M(\widehat{\Psi})$ and $\Omega_N(\widehat{\Psi})$ are governed by the slit width a.

The fringe width b is equal to K_n for the quantum states considered here.

6.2 Uncertainty of state ψ_n

Any application of this formulation of uncertainty should start with choosing a suitable pair (N, M). Although Uffink and Hilgevoord discussed the mathematical constraints on (N, M) – Eqs. (6.4) and (6.5) – and argued that the precise choice is not important, we found that the results can differ. The correct choice can be made only after careful consideration of the given problem; for our purpose that is the discussion of ψ_n in Chapter 4, and in particular the conclusions of Sec. 4.4.

We choose $N = 1$ for the particular state ψ_n. An expression for the overall width corresponds to the difference between the total number of illuminated slits $m = 2n$ and the first, scaled with the slit separation T and adjusted for the slit width a,

$$\Omega_1(\psi_n) = (2n - 1)\, T + a\,. \tag{6.7}$$

The overall width of state ψ_n depends linearly on n and features an absolute term a. The presence of the absolute term, however, is somewhat unwanted in the context of multislit interferometry as the slit width a is unrelated to interference. Note that its presence stems from matters of consistency: The present uncertainty formulation allows for analysis of single-slit states. Increasing the slit width to $a = T$ results in a single illuminated slit of width $mT = 2nT$, and the overall width must reflect this. Naturally, as the value of $\Omega_1(\psi_n)$ increases, this absolute term is going to become negligible.

The mean fringe width $\omega_M(\psi_n)$ can be calculated and the result is

$$\omega_M(\psi_n) = \min\left\{ s : \left| \frac{1}{n} \operatorname{sinc}\Big(\frac{a}{T} s\Big) f_n(s) \right| = M \right\}. \tag{6.8}$$

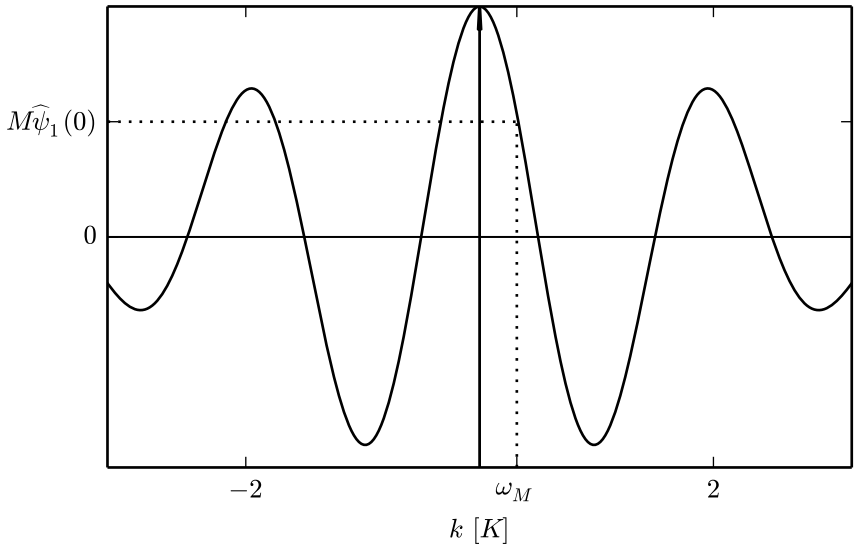

Figure 6.2: An intuitive interpretation of $\omega_M(\psi)$ is illustrated here for this otherwise abstract measure. Considering a typical ($a \ll T$) interference wavefunction $\widehat{\psi}(k)$, then $\omega_M(\psi)$ is approximately half the fringe width of the central peak at a height $0 \leq M\widehat{\psi}(k) \leq \widehat{\psi}(k)$.

The function f_n was defined in Eq. (1.34). The derivation of Eq. (6.8) is provided in Appendix D.1, and an illustration in Fig. 6.2. According to Eq. (6.8), the mean fringe width of ψ_n depends on the slit width a. However, note the following special case

$$\omega_0(\psi_n) = \min\left\{s : \left|\frac{1}{n}\operatorname{sinc}\Big(\frac{a}{T}s\Big) f_n(s)\right| = 0\right\} \tag{6.9}$$

$$= \min\left\{s : \cos\left(2n-1\right)Ts/2 = 0\right\} \tag{6.10}$$

$$= \pi/(nT) = K_n/2\,. \tag{6.11}$$

When $M = 0$, the value of $\omega_0(\psi_n)$ does not depend on a, because $\omega_0(\psi_n)$ depends on the support property of the central fringe only. In fact, $\omega_0(\psi_n)$ is independent of the effective envelope, which distinguishes this particular choice of M and indicates that the desired features are captured. A different choice of M would introduce additional contributions, leading to different asymptotic behaviour. In general, the choice of M (and N) is apparently not as straightforward as Eqs. (6.4) and (6.5) suggest.

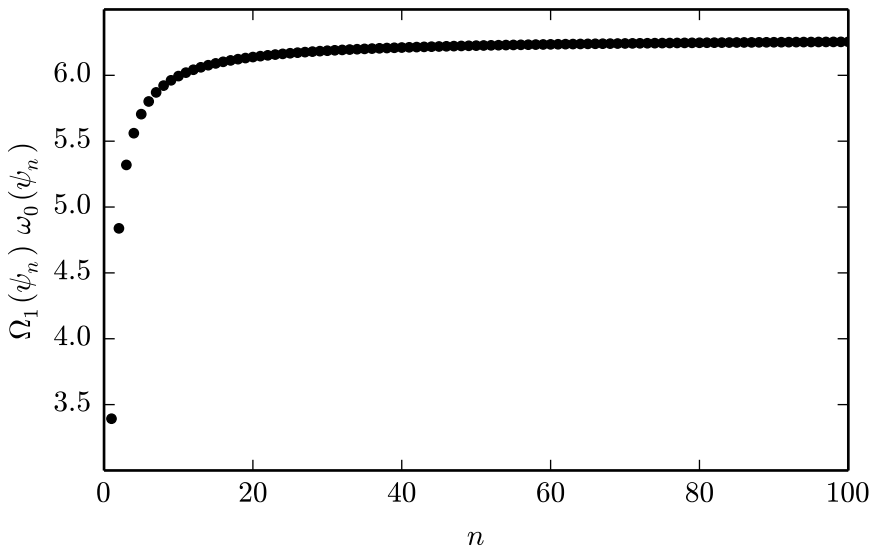

Figure 6.3: Illustration of the uncertainty product given in Eq. (6.12) for states ψ_n. Qualitatively identical behaviour was for the uncertainty formulation based on the work of Aharonov *et al.*, compare Fig. 5.3.

Using Eqs. (6.7) and (6.11), we calculate the uncertainty product

$$\begin{aligned}\Omega_1(\psi_n)\,\omega_0(\psi_n) &= [(2n-1)\,T + a]\,K_n/2 \\ &= 2\pi - \frac{\pi}{n} + \frac{\pi a}{nT}\end{aligned} \tag{6.12}$$

The uncertainty product decomposes naturally into three terms, each of which features different quantities and contributes depending on the respective sign. The third term depends on the ratio of slit width to slit separation (a/T) and expresses the fact that for $a = T$ any change in n would be a scale transformation without physical effect.

The behaviour of the uncertainty product (6.12) is illustrated in Fig. 6.3. We observe that this uncertainty product is smallest for the state ψ_1 and converges to a value of 2π as n increases. The uncertainty product for ψ_1 could be made minimal in the limit of vanishing a/T. The asymptotic behaviour is qualitatively identical to the asymptotic behaviour found for the previously discussed uncertainty formulation; see Fig. 5.3.

6.3 Uncertainty of state ϕ_n

The states ϕ_n have the property that the associated fringes are isolated for $n \geq 2$. This implies that for $n \geq 2$ the mean fringe width $\omega_M(\phi_n)$ depends only on the overlap of a single fringe with its shifted copy. While for $n = 1$ we find the same mean fringe width as we did for ψ_1, because $\phi_1 = \psi_1$, for $n \geq 2$ we use Eq. (5.11) and obtain

$$\omega_M(\phi_n) = \min\Big\{s : \Big|\operatorname{sinc}\Big(\frac{a}{2}s\Big)\Big[\Big(1 - \frac{s}{K_n}\Big)\cos\pi\frac{s}{K_n} + \frac{1}{\pi}\sin\pi\frac{s}{K_n}\Big]\Big| = M\Big\} \tag{6.13}$$

The calculation leading to this result is provided in Appendix D.2. The min condition translates into $s \leq K_n$. Hence, assuming $s \leq K_n$ enables us to simplify the entire expression

$$M = \operatorname{sinc}\Big(\frac{a}{2}\omega_M(\phi_n)\Big)\Big[\Big(1 - \frac{\omega_M(\phi_n)}{K_n}\Big)\cos\pi\frac{\omega_M(\phi_n)}{K_n} + \frac{1}{\pi}\sin\pi\frac{\omega_M(\phi_n)}{K_n}\Big] \tag{6.14}$$

It follows immediately from this result that $\omega_M(\phi_n)$ must be directly proportional to K_n for M to remain approximately constant across n (accurate for $a/T \to 0$). Just as for the previously investigated ψ_n, Eq. (6.8), we find a dependence on a. For $a \ll T$ this dependence becomes negligible numerically, and we ignore it under this assumption henceforth. We set

$$\omega_M(\phi_n) = c_M\, K_n\,. \tag{6.15}$$

The non-negative number c_M determines the particular value of M; c_M is necessarily smaller than or equal to unity. For the states ψ_n we found a similar expression in Eq. (6.11), and conclude $\omega_M(\phi_n) \propto \omega_M(\psi_n)$. We make the arbitrary choice $c_M = 1/2$, which results in $M = 1/\pi$ and gives

$$\omega_{\pi^{-1}}(\phi_n) = K_n/2 = \pi/(nT)\,. \tag{6.16}$$

Regarding the overall width $\Omega_N(\phi_n)$ not much can be said in terms of analytical results. While it is fairly simple to show that $\Omega_N(\phi_n)$ is approximately proportional to n, more concrete results are difficult to obtain. The proportionality follows from a straightforward calculation of the function H

determining the overall width

$$h_n(x) = \frac{1}{\sqrt{2\pi}} \int_{-K_n/2}^{K_n/2} \sqrt{\frac{2}{K_n}} \cos\left(\frac{\pi}{K_n} k\right) \mathrm{e}^{\mathrm{i}\, x k}\ \mathrm{d}k, \tag{6.17}$$

$$= H(K_n x)\,. \tag{6.18}$$

The argument of the function H scales inversely with n, which means that $\Omega_N(\phi_n)$ will approximately scale with n. Our numerical investigation shows that $\Omega_N(\phi_n)$ indeed displays this behaviour in the limit of large n. See Fig. 6.4, which depicts identical qualitative behaviour for three different choices of N. We conclude that

$$\Omega_N(\phi_n) = c_N\, T\, n \qquad \text{for large } n. \tag{6.19}$$

The linear dependence on T follows from the general discussion of this formulation of uncertainty. The numerical factor c_N is non-negative, but otherwise undetermined. Explicit values of c_N are not obtained as easily as for c_M. We approximate the value of c_N using numerical investigations. For example, inspection of the data points in Fig. 6.4 suggests

$$\Omega_{0.99}(\phi_n) \approx 2^{1.25}\, T\, n\,, \tag{6.20}$$

indicated by the dotted line depicted in Fig. 6.4. Using this expression along with the result for $\omega_{\pi^{-1}}(\phi_n)$ in Eq. (6.16), we calculate the asymptotic behaviour of the uncertainty product for the given choices of N and M. We find that asymptotically a precise tradeoff occurs

$$\Omega_{0.99}(\phi_n)\, \omega_{\pi^{-1}}(\phi_n) \approx 7.47 \qquad \text{for large } n. \tag{6.21}$$

The convergence of this uncertainty product is depicted in Fig. 6.5, showing that that the uncertainty product converges to a value of approximately 7.41. This is in good agreement with our prediction, which was based solely on inspection of the data points of Fig. 6.4.

A different choice of a/T would allow for ϕ_1 to reach the lower bound, which is illustrated in Fig. 6.5 by the solid line. It is unclear, however, whether the asymptotic limit or particular values of the uncertainty product could be decreased to meet the lower bound.

A general expression for the uncertainty product is obtained immediately

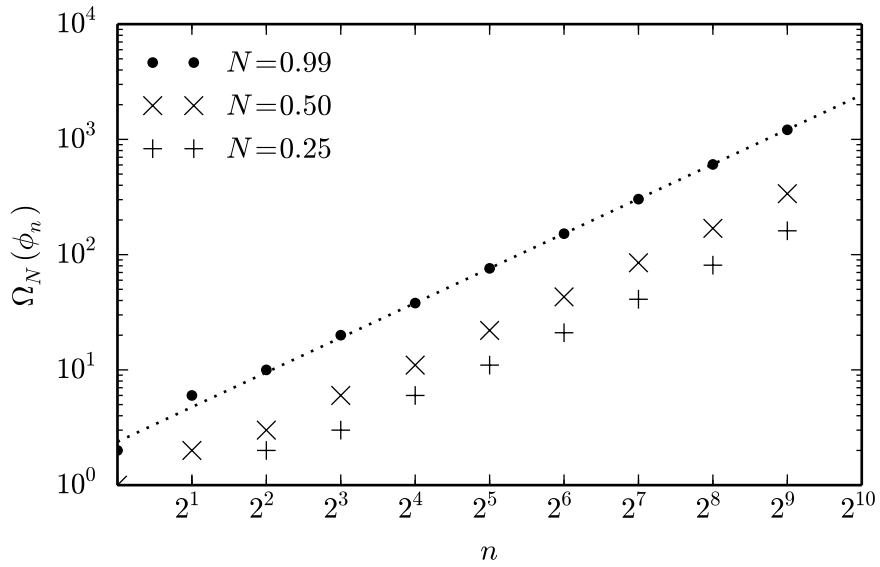

Figure 6.4: The overall width of state ϕ_n is depicted for three choices of N. The numerical calculations show that asymptotically $\Omega_N(\phi_n)$ depends linearly on n. The dotted line corresponds to Eq. (6.20). Observe that $N = 0.25$ and $N = 0.5$ do not make suitable choices according to Eqs. (6.4) and (6.5), but are represented in order to illustrate the mathematical aspects of the overall width.

from Eqs. (6.15) and (6.19),

$$\Omega_N(\phi_n)\,\omega_M(\phi_n) \approx 2\pi\, c_N\, c_M \qquad \text{for large } n\,. \tag{6.22}$$

This is the general form of the asymptotic limit of the uncertainty product for the states ϕ_n. It remains approximately true for small values of n, but no definite statement can be made due to the discrete character of the measures used. It is, in fact, this discreteness that results in the erratic behaviour of the uncertainty product for small values of n.

6.4 Comparison and conclusion

We now compare the results of the uncertainty investigations of the present chapter to those of Chapter 5, discussing the similarities and differences between the two uncertainty formulations. We also address to what extent the general considerations are met that were discussed in Sec. 4.4.

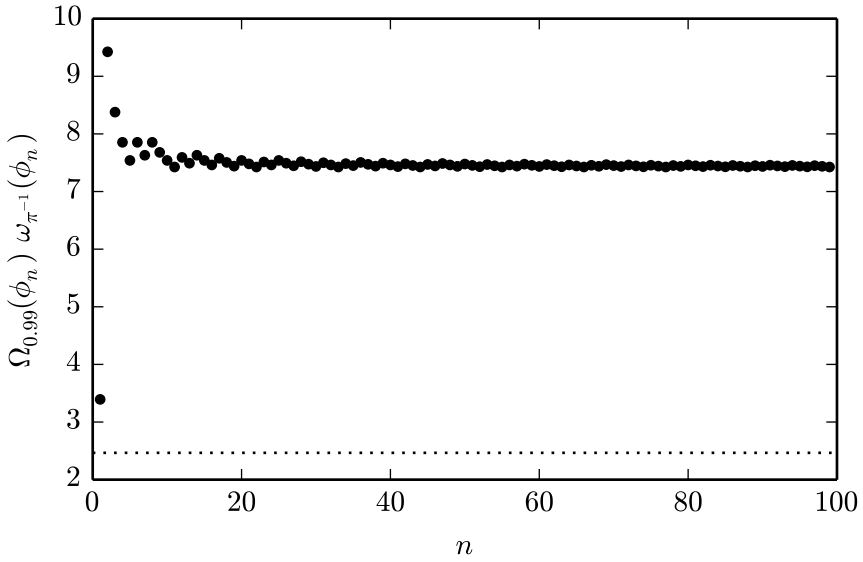

Figure 6.5: Illustration of the uncertainty product given in Eq. (6.21) for states ϕ_n. The dotted line represents the lower bound on the uncertainty product. Compare Fig. 5.6, which illustrates the qualitatively similar behaviour of the uncertainty product (5.6) for large values of n.

The example applications show that both uncertainty formulations yield qualitatively similar results. This is reassuring, independently confirming that the relevant physical structure is captured. However, it is not necessarily straightforward to arrive at this conclusion in general terms, because the two uncertainty formulations appear to be very different. In actual fact, although implemented differently, the measures used describe very similar observables. In particular, both uncertainty formulations feature measures that relate to the width of the fringes. This captures the relevant observable in accordance with the discussion of Chapter 4 and specifically the conclusions of Sec. 4.4; most notably, the fact that there should not be any critical dependence on diffraction. The particular measures employed, though, are rather different. The formulation based on Aharonov *et al.* employs a measure that corresponds to computing the standard deviation of a single fringe while neglecting the effective envelope. The formulation due to Uffink and Hilgevoord is based on the autocorrelation function of the interference wavefunction, and in general features a (possibly negligible) dependence on the fundamental envelope. Yet these two different implementations yield qualit-

atively similar results.

The analysis of the quantum states ψ_n, prepared through uniform illumination of an aperture mask, resulted in qualitatively identical results. Figures 5.3 and 6.3 show that both uncertainty products display the same qualitative behaviour: Starting at a minimal uncertainty product for ψ_1, the uncertainty product converges to some larger, finite value as n increases. However, the uncertainty formulation due to Uffink and Hilgevoord actually allows for the lower bound to be reached in the limit of vanishing slit width. This non-critical dependence on the choice of aperture is actually somewhat unwanted for purely multislit considerations, because it introduces a dependence on diffraction. The measures used in the uncertainty formulation based on Aharonov *et al.* do not depend on the aperture or the related envelope function of the interference pattern.

The second example application involves quantum states ϕ_n, which are characterised by their extended nodes. In this case, for the uncertainty formulation based on Aharonov *et al.* the uncertainty tradeoff is exact and the uncertainty product constant across n. For the formulation of uncertainty due to Uffink and Hilgevoord this is the case only in the limit of large n, because of the discrete quality of the employed measures. This is illustrated in Figs. 5.6 and 6.5. Also note that the measure of fringe width employed by Uffink and Hilgevoord results in a dependence on the slit width. For most considerations this dependence may be negligible with regard to numerical results, yet it poses a qualitative difference. In general, a dependence on the particular aperture is to be expected for this uncertainty formulation, although in some cases a particular parameter choice may remove this dependence (as is the case for ψ_n).

Regarding technical aspects, we found that the formulation of uncertainty due to Uffink and Hilgevoord is computationally more difficult. For our second example application we resorted to numerical analysis in order to obtain an approximate expression for the spatial localisation. (The formulation based on the work of Aharonov *et al.* was not particularly straightforward to apply to this scenario either, but a satisfying analytical result was obtained eventually.) This is further complicated by the two degrees of freedom, N and M. Uffink and Hilgevoord found that the exact choice of N and M is not important to the analysis of single- or double-slit experiments—while adhering to the conditions (6.4) and (6.5), of course. In the context

of multislit experiments, however, we found that additional insight may be required for appropriately choosing (N, M).

Chapter 7

Conclusion

In the preceding chapters a quantum mechanical study of multislit interference experiments was presented. The particular focus of this investigation relates to the compatible and incompatible observables relevant to the given context and a mathematical description thereof. Chapter 2 comprises the first part of this investigation, dealing with compatible observables as illustrated in an experiment reported in 2007 [3]. Chapters 3 to 6 comprise the second part, dealing with the incompatibility of certain observations and the expression of that incompatibility in the form of an uncertainty relation.

More precisely, in Chapter 2 we started from the theoretical results due to Busch and Lahti and developed a quantum mechanical description of the compatible observables in multislit interference experiments. While our results are applicable to all multislit interference experiments and the quantum states prepared therein, we discussed particularly the modified experimental setup reported by Afshar *et al.* in Ref. [3]. The experimental observations of Afshar *et al.* demonstrate the possibility of jointly measuring certain information about the position and the momentum distribution, and match the quantum mechanical description developed here. The presented analysis shows that it is appropriate to consider the quantum states prepared in multislit interference setups as approximations to joint eigenstates of commuting functions of position and momentum. In particular, we constructed and used a class of quantum states which are joint eigenstates of commuting sets of position and momentum.

After concluding the analysis of compatible observables, we studied those measurements which are incompatible. In the context of multisite interfer-

ence experiments Aharonov, Pendleton and Petersen had presented an initial investigation into quantum uncertainty starting from a very similar mathematical structure that we observed in Chapter 2 in relation to compatible observables. This presented a natural connection to our research and became a starting point for an investigation on our part, because although Aharonov *et al.* had proposed a heuristic argument, without developing the argument mathematically they could not provide any concrete results. We showed that their argument can be formalised and indeed leads to a viable uncertainty relation which expresses a tradeoff between the spatial localisation across the multislit aperture mask and the width of the fringes of the interference pattern. Developing this idea further, we obtained a refined uncertainty relation that exhibits the correct asymptotic behaviour in example applications.

Finally, we presented a comparison of this uncertainty formulation with an alternative uncertainty formulation, developed by Uffink and Hilgevoord, which is also suitable for the interferometric context. Although the two formulations are conceptually and mathematically very different, we found that example applications yield qualitatively similar results. This is reassuring, confirming that the relevant physical tradeoff is independently expressed by two alternative formulations. We argued that, although technically implemented differently, the two uncertainty formulations implement effectively similar measures capturing the relevant observables relating to spatial localisation and fringe width. Most notably, both uncertainty formulations employ measures relating to the fringe width. Also, neither uncertainty formulation critically depends on the particular choice of aperture, expressing a clear qualitative difference between the phenomena of diffraction and interference in a quantum mechanical context. (In fact, the uncertainty formulation based on the work of Aharonov *et al.* is entirely independent of the choice of aperture.)

In conclusion, the present investigation appears sufficiently self-contained such that there is no pressing need to pursue further results. However, a technical manuscript containing certain additional results is currently being prepared [22]. Considering the fact that the questions addressed here date back to the advent of quantum mechanics and, in particular, the Bohr-Einstein debate, it may have proved surprising that interesting quantum mechanics still remained to be uncovered.

Appendix A

Calculations of Chapter 2

A.1

The discussion of Sec. 2.3, and in particular the Eqs. (2.5) and (2.6) as well as the explicit construction of Sec. 2.4 involves delta functions. Although this makes for a good heuristic argument, here a different approach is presented that is mathematically rigorous without going into the theory of distributions. While similar to the work of Reiter and Thirring, the result here is more general [21]. We start by choosing a square-integrable function W with support strictly within the interval $(-T/2, T/2)$, and define a periodically-supported function ψ as

$$\psi(x) = \sum_{j=-\infty}^{\infty} c_j \, W(x - jT). \tag{A.1}$$

The terms of this sum are non-overlapping, hence the series converges pointwise. The coefficients c_j are to be determined by further constraints below; here we note that given the square integrability of W, ψ is square integrable if and only if the c_j are square-summable. This entails that the series also converges in norm. Note that

$$\operatorname{supp} \psi = \bigcup_{j=-\infty}^{\infty} \operatorname{supp} (W + jT) \ . \tag{A.2}$$

The Fourier transform of $\psi(x)$ can be computed formally and yields

$$\widehat{\psi}(k) = \frac{1}{\sqrt{2\pi}} \int_{-\infty}^{\infty} \sum_{j=-\infty}^{\infty} c_j \, W(x - jT) \ \exp(\mathrm{i}\, k\, x) \ \mathrm{d}x \tag{A.3}$$

$$= \sum_{j=-\infty}^{\infty} c_j \ \exp(\mathrm{i}\, j\, T\, k) \, \widehat{W}(k) \, . \tag{A.4}$$

The coefficients c_n represent the coefficients of a Fourier series expansion of a periodic function $\widehat{M}_p$ with period $2\pi/T$:

$$\widehat{M}_p(k) = \sum_{j=-\infty}^{\infty} c_j \, \exp\left(\mathrm{i}\, k\, j\, T\right). \tag{A.5}$$

Let $\widehat{M}$ be a function that is supported inside the interval $[-d, d]$ where $0 < d < \pi/T$. We can then specify $\widehat{M}_p$ – and hence the coefficients c_n – so that

$$\widehat{M}_p(k) = \sum_{j=-\infty}^{\infty} \widehat{M}\left(k - \frac{2\pi}{T} j\right). \tag{A.6}$$

This function is supported in a periodic set,

$$\operatorname{supp} \widehat{M}_p \subseteq \bigcup_{j=-\infty}^{\infty} \left[\frac{2\pi}{T} j - d, \frac{2\pi}{T} j + d\right]. \tag{A.7}$$

We thus have that

$$\widehat{\psi}(k) = \widehat{M}_p(k)\, \widehat{W}(k). \tag{A.8}$$

A simple calculation shows that $\widehat{M}$ is square integrable if and only if the c_n are square summable. As noted above, this condition is equivalent to ψ being square integrable. With such a choice of $\widehat{M}$ we can also see directly from the last formula that $\widehat{\psi}$ is square integrable, in line with the Fourier-Plancherel theorem.

A.2

The relation Eq. (2.4) may be used to define a wavefunction ϕ via Eqs. (2.5), (2.6) for square-integrable W, M if W vanishes outside an interval of length strictly less than T, because then the square-integrability condition is met, i.e. if the L^2-norm of $||\phi||$ is finite:

$$||\phi|| = \int_{-\infty}^{\infty} |W * (\text{Ш}_T \cdot M)(x)|^2 \, \mathrm{d}x \tag{A.9}$$

$$= \int \overline{W * \left(\sum_{j=-\infty}^{\infty} \delta((\cdot) - jT)M\right)(x)}\, W * \left(\sum_{j'=-\infty}^{\infty} \delta((\cdot) - j'T)M\right)(x) \, \mathrm{d}x \tag{A.10}$$

$$= \int \overline{W * \Big(\sum_j \delta((\cdot) - jT) M(jT) \Big)(x)} \dots \tag{A.11}$$

$$\dots W * \Big(\sum_{j'} \delta((\cdot) - j'T) M(j'T) \Big)(x) \, \mathrm{d}x \tag{A.12}$$

$$= \int \sum_j \overline{W(x - jT)} \, \overline{M(jT)} \sum_{j'} W(x - j'T) M(j'T) \, \mathrm{d}x \tag{A.13}$$

$$= \sum_j |M(jT)|^2 \int |W(x - jT)|^2 \, \mathrm{d}x = \|W\|^2 \sum_j |M(jT)|^2 \tag{A.14}$$

The last line is obtained due to the localisation property of the function W, which entails that $\overline{W(x - jT)} W(x - j'T) = 0$ if $j \neq j'$. The square integrability of the Fourier transform $\widehat{\psi}$ is ensured by the Fourier-Plancherel theorem.

Appendix B

Calculations of Chapter 3

B.1

Here we show that the value of $\Delta(P_{\mathrm{mod}}, \psi_n)$ is independent of the fundamental envelope, as was claimed in Eq. (3.26).

$$\Delta(P_{\mathrm{mod}}, \psi_n)^2 = \int_{-\infty}^{\infty} P_{\mathrm{mod}}(k)^2 \, \psi_n(k)^2 \, \mathrm{d}k \tag{B.1}$$

We perform the integration using the dimensionless variable κ, which was introduced in Eq. (1.35),

$$= \frac{2^3 a}{T^3 n\pi} \int_{-\infty}^{\infty} P_{\mathrm{mod}}(\kappa)^2 \, \mathrm{sinc}\Big(\frac{a}{T}\kappa\Big)^2 \, f_n(\kappa)^2 \, \mathrm{d}\kappa \,, \tag{B.2}$$

where we are using the shorthand $f_n(\kappa)$, which was introduced in Eq. (1.34). This integral may be decomposed into an infinite sum of integrals over the finite interval K,

$$= \frac{2^3 a}{T^3 n\pi} \sum_{j=-\infty}^{\infty} \int_{\left(j-\frac{1}{2}\right)\pi}^{\left(j+\frac{1}{2}\right)\pi} (\kappa - j\pi)^2 \, \mathrm{sinc}\Big(\frac{a}{T}\kappa\Big)^2 \, f_n(\kappa)^2 \, \mathrm{d}\kappa \,. \tag{B.3}$$

We now substitute $u = \kappa - j\pi$ and immediately exploit the periodicity of the function f_n, i.e. f_n, $f_n(\kappa + j\pi)^2 = f_n(\kappa)^2$,

$$= \frac{2^3 a}{T^3 n\pi} \int_{-\pi/2}^{\pi/2} u^2 \, f_n(u)^2 \sum_{j=-\infty}^{\infty} \mathrm{sinc}\Big(\frac{a}{T}(u + j\pi)\Big)^2 \, \mathrm{d}u. \tag{B.4}$$

The infinite series can be evaluated to T/a using Eq. (11) of Ref. [32]. Note, however, that in the derivation provided in Ref. [34] a factor of $1/\alpha$ missing in both the integral term and the series in Eq. (1). Using this result on

infinite series, we obtain

$$\Delta(P_{\mathrm{mod}},\psi_n)^2 = \frac{2^3 a}{T^3 n\pi}\frac{T}{a}\int_{-\pi/2}^{\pi/2} u^2\, f_n(u)^2 \,\mathrm{d}u \tag{B.5}$$

$$= \frac{2^3}{T^2 n\pi}\int_{-\pi/2}^{\pi/2} u^2\, f_n(u)^2 \,\mathrm{d}u. \tag{B.6}$$

The final expression is indeed equal to Eq. (3.26).

B.2

We show here that $\Delta(P_{\mathrm{mod}},\psi_n)$ in Eq. (3.28) indeed asymptotically goes as $1/\sqrt{n}$. We use the result of Appendix B.1 in order to simplify the necessary integration, which is the same as in Eq. (3.27), but for general m. We calculate

$$\Delta(P_{\mathrm{mod}},\psi_n)^2 = \frac{2}{nK}\left(\frac{2}{T}\right)^3\int_{-\pi/2}^{\pi/2} \kappa^2\, f_n(\kappa)^2 \,\mathrm{d}\kappa \tag{B.7}$$

$$= \frac{8}{n\pi T^2}\int_{-\pi/2}^{\pi/2} \kappa^2\left(\sum_{j=1}^{n}\cos{(2j-1)\kappa}\right)^2 \mathrm{d}\kappa. \tag{B.8}$$

We are again using the dimensionless variable κ. Note that the infinite sum can be evaluated and the square of the *sin* functions reduced using the know identity $(\sin x)^2 = (1-\cos 2x)/2$. Hence we obtain

$$\left(\sum_{j=1}^{n}\cos{(2j-1)\kappa}\right)^2 = \frac{1}{4}\left(\frac{\sin 2n\kappa}{\sin\kappa}\right)^2 \tag{B.9}$$

$$= \frac{1}{4}\frac{1-\cos 4n\kappa}{1-\cos 2\kappa}\,. \tag{B.10}$$

The standard deviation of the first term can be computed analytically

$$\int_{-\pi/2}^{\pi/2}\frac{\kappa^2}{1-\cos 2\kappa}\,\mathrm{d}\kappa = \pi\ln 2\,, \tag{B.11}$$

whereas the second term vanishes in the asymptotic limit,

$$\lim_{n\to\infty}\int_{-\pi/2}^{\pi/2}\frac{\kappa^2}{1-\cos 2\kappa}\cos 4n\kappa\,\mathrm{d}\kappa = 0\,, \tag{B.12}$$

by the Riemann-Lebesgue lemma. Hence, we obtain

$$\Delta(P_{\mathrm{mod}}, \psi_n) \approx \frac{\sqrt{2\ln 2}}{T}\frac{1}{\sqrt{n}} \text{ for large } n, \tag{B.13}$$

analytically confirming the asymptotic behaviour of Eq. (3.28), which was suggested by the numerical investigation depicted in Figs. 3.2 and 3.3.

Appendix C

Calculations of Chapter 5

C.1

The calculation provided here demonstrates that $\Delta(P_{\mathrm{mod}}(n), \psi_n)$ is not only independent of the fundamental envelope, which was shown in Appendix B.1, but is even independent of the effective envelope. The particular calculation included here is for slit number $m = 2^d$, because this particular choice allows exploiting product form. The general calculation is provided in the following section, Appendix C.2. We start with an expression similar to Eq. (B.7), but using $P_{\mathrm{mod}}(n)$ instead of P_{mod}.

$$\Delta(P_{\mathrm{mod}}(n), \psi_n)^2 = \frac{2}{nK} \int_{-K/2}^{K/2} P_{\mathrm{mod}}(n,k)^2 \, f_n(k)^2 \, \mathrm{d}k \tag{C.1}$$

We restrict ourselves to $n = 2^{d-1}$ and substitute a product expansion

$$f_n(k) = n \prod_{j=0}^{d-1} \cos 2^j \frac{T}{2} k \tag{C.2}$$

in place of the sum, giving

$$= \frac{2}{nK} n^2 \int_{-K/2}^{K/2} P_{\mathrm{mod}}(n,k)^2 \prod_{j=0}^{d-1} \cos\left(2^j \frac{T}{2} k\right)^2 \, \mathrm{d}k \tag{C.3}$$

Using the identity $\cos(x)^2 = (1+\cos 2x)/2$, it follows that each of the cosines in the product contributes a factor of $1/2$ from $j = 0$ to $j = d-2$. The resulting integrations including the $\cos 2x$ term are computed over multiples of the periods of the respective cosine and do not contribute. We proceed

explicitly with the case $j = 0$,

$$= \frac{2n}{K}\int_{-K/2}^{K/2} P_{\mathrm{mod}}(n,k)^2 \frac{1}{2}\left[1+\cos 2\frac{T}{2}k\right]\prod_{j=1}^{d-1}\cos\left(2^j\frac{T}{2}k\right)^2 \mathrm{d}k \tag{C.4}$$

$$= \frac{2}{K_n}\frac{1}{2}\int_{-K/2}^{K/2} P_{\mathrm{mod}}(n,k)^2 \prod_{j=1}^{d-1}\cos\left(2^j\frac{T}{2}k\right)^2 \mathrm{d}k \tag{C.5}$$

Repeating this another $d-2$ times contributes $(1/2)^{d-2}$,

$$= \frac{2}{K_n}\frac{1}{2^{d-1}}\int_{-K/2}^{K/2} P_{\mathrm{mod}}(n,k)^2 \cos\left(2^{d-1}\frac{T}{2}k\right)^2 \mathrm{d}k \tag{C.6}$$

$$= \frac{2}{K_n}\frac{1}{n}\int_{-K/2}^{K/2} P_{\mathrm{mod}}(n,k)^2 \cos\left(n\frac{T}{2}k\right)^2 \mathrm{d}k \tag{C.7}$$

We immediately exploit the periodicity of the resulting function, substitute $nT/2 = \pi/K_n$ and use $P_{\mathrm{mod}}(n,k)^2 = k^2$ (on K_n),

$$= \frac{2}{K_n}\frac{1}{n}n\int_{-K_n/2}^{K_n/2} P_{\mathrm{mod}}(n,k)^2 \cos\left(n\frac{T}{2}k\right)^2 \mathrm{d}k \tag{C.8}$$

$$= \frac{2}{K_n}\int_{-K_n/2}^{K_n/2} k^2 \cos\left(\frac{\pi}{K_n}k\right)^2 \mathrm{d}k \tag{C.9}$$

The final expression is indeed equal to Eq. (5.4), although here we only proved the special case $n = 2^{d-1}$.

C.2

The calculation provided here demonstrates that $\Delta(P_{\mathrm{mod}}(n), \psi_n)$ is not only independent of the fundamental envelope, as was shown in Appendix B.1, but is even independent of the effective envelope. This is shown here for the general case, i.e. all even slit numbers $m = 2n$. This calculation is rather tedious and only included for the sake of completeness. The calculation proceeds by considering two cases independently. Depending on whether $n = m/2$ is even or odd, the function f_n is decomposed differently.

C.2.1 First case: even n

The function f_n is now expressed in a suitable form under the assumption that n is an even integer, then we proceed with the calculation of the standard deviation of $P_{\mathrm{mod}}(n)$.

$$f_n(k) = \sum_{j=1}^{n} \cos(2j-1)\frac{\pi k}{K} \tag{C.10}$$
$$= \cos\frac{\pi k}{K} + \cos 3\frac{\pi k}{K} + \cdots + \cos(2n-3)\frac{\pi k}{K} + \cos(2n-1)\frac{\pi k}{K}$$

We now pair the *cosines* as follows and use a trigonometric identity, Eq. (4.8), to express each of the sums of *cosines* as a product,

$$= \left[\cos\frac{\pi k}{K} + \cos(2n-1)\frac{\pi k}{K}\right] + \left[\cos 3\frac{\pi k}{K} + \cos(2n-3)\frac{\pi k}{K}\right] + \ldots \tag{C.11}$$
$$= 2\left[\cos n\frac{\pi k}{K}\cos(n-1)\frac{\pi k}{K}\right] + 2\left[\cos n\frac{\pi k}{K}\cos(n-3)\frac{\pi k}{K}\right] + \ldots \tag{C.12}$$

Notice that a *cosine* with an n in the argument appears in each of the square brackets. Removing this *cosine*, the remaining terms can be expressed in terms of a sum,

$$= 2\cos\frac{\pi k}{K_n}\sum_{j=1}^{n/2}\cos(2j-1)\frac{\pi k}{K} \tag{C.13}$$

(Note that in the final expression we used $K/n = K_n$.) Notice in particular the final expression containing $n/2$, which is only an integer for even n. We proceed to calculate the square of the final expression.

$$\left[2\cos\frac{\pi k}{K_n}\sum_{j=1}^{n/2}\cos(2j-1)\frac{\pi}{K}k\right]^2 = 4\cos\frac{\pi k}{K_n}^2\left[\sum_{j=1}^{n/2}\cos(2j-1)\frac{\pi}{K}k\right]^2 \tag{C.14}$$
$$= 4\cos\left(\frac{\pi k}{K_n}\right)^2\sum_{j=1}^{n/2}\cos(2j-1)\frac{\pi}{K}k^2 \tag{C.15}$$
$$= 2\cos\left(\frac{\pi k}{K_n}\right)^2\sum_{j=1}^{n/2}\left[1+\cos(2j-1)\frac{2\pi k}{K}\right]$$

We now proceed with the actual calculation of the standard deviation of $P_{\mathrm{mod}}(n)$.

$$\Delta(P_{\mathrm{mod}},\psi_n)^2 = \frac{4}{2nK}\int_{-K/2}^{K/2} P_{\mathrm{mod}}(n,k)^2\, f_n(k)^2 \,\mathrm{d}k \tag{C.16}$$
$$= \frac{8}{nK}\int_{-K/2}^{K/2} P_{\mathrm{mod}}(n,k)^2 \cos\frac{\pi k}{K_n}^2 \left[\sum_{j=1}^{n/2}\cos(2j-1)\frac{\pi}{K}k\right]^2 \mathrm{d}k$$

The cross terms of the *cosine* sum integrate to zero, while the sum over squared *cosines* can be simplified,

$$= \frac{4}{nK}\int_{-K/2}^{K/2} P_{\mathrm{mod}}(n,k)^2 \cos\left(\frac{\pi k}{K_n}\right)^2 \sum_{j=1}^{n/2}\left[1+\cos(2j-1)\frac{2\pi k}{K}\right]\mathrm{d}k \tag{C.17}$$
$$= \frac{4}{nK}\int_{-K/2}^{K/2} P_{\mathrm{mod}}(n,k)^2 \cos\left(\frac{\pi k}{K_n}\right)^2 \sum_{j=1}^{n/2} 1 \,\mathrm{d}k \tag{C.18}$$

The sum is easily evaluated, $\sum_{j=1}^{n/2} 1 = n/2$, giving

$$= \frac{2}{K}\int_{-K/2}^{K/2} P_{\mathrm{mod}}(n,k)^2 \cos\left(\frac{\pi k}{K_n}\right)^2 \mathrm{d}k \tag{C.19}$$

The integration can now be restricted to an interval K_n, exploiting the periodicity of both integrands,

$$= \frac{2}{K}n\int_{-K_n/2}^{K_n/2} k^2 \cos\left(\frac{\pi}{K_n}k\right)^2 \mathrm{d}k = \frac{2}{K_n}\int_{-K_n/2}^{K_n/2} k^2 \cos\left(\frac{\pi}{K_n}k\right)^2 \mathrm{d}k \tag{C.20}$$

The final expression is indeed to Eq. (5.5).

C.2.2 Second case: odd n

The function f_n is now expressed in a suitable form under the assumption that n is an odd integer, then we proceed with the calculation of the standard deviation of $P_{\mathrm{mod}}(n)$.

$$f_n(k) = \sum_{j=1}^{n}\cos\left((2j-1)\frac{\pi}{K}k\right) \tag{C.21}$$
$$= \cos\frac{\pi}{K}k + \cos 3\frac{\pi}{K}k + \cdots + \cos n\frac{\pi}{K}k + \cdots + \cos(2n-1)\frac{\pi}{K}k$$

We now pair the *cosines* up and use a trigonometric identity that turns sums of *cosines* into products of *cosines*,

$$= \left[\cos\frac{\pi k}{K} + \cos(2n-1)\frac{\pi k}{K}\right] + \ldots \tag{C.22}$$

$$\cdots + \left[\cos(n-1)\frac{\pi k}{K} + \cos(n+1)\frac{\pi k}{K}\right] + \cos\frac{\pi k}{K_n}$$

$$= 2\left[\cos n\frac{\pi k}{K}\cos(n-1)\frac{\pi k}{K}\right] + \cdots + 2\left[\cos n\frac{\pi k}{K}\cos\frac{\pi k}{K}\right] + \cos\frac{\pi k}{K_n} \tag{C.23}$$

Notice that a *cosine* with an n in the argument appears in each of the square brackets. This naturally simplifies the expression,

$$= 2\cos n\frac{\pi k}{K}\left[\cos(n-1)\frac{\pi k}{K} + \cdots + \cos(n-n+1)\frac{\pi k}{K}\right] + \cos\frac{\pi k}{K_n} \tag{C.24}$$

$$= \cos\frac{\pi k}{K_n}\sum_{j=1}^{n}\cos(n-(2j-1))\frac{\pi k}{K} \tag{C.25}$$

$$= \cos\frac{\pi k}{K_n}\left[1 + 2\sum_{j=1}^{(n-1)/2}\cos 2j\frac{\pi k}{K}\right] \tag{C.26}$$

We now proceed to calculate the standard deviation of $P_{\mathrm{mod}}(n)$ in state ψ_n, where n is assumed to be odd.

$$\Delta(P_{\mathrm{mod}},\psi_n)^2 = \frac{2}{nK}\int_{-K/2}^{K/2} P_{\mathrm{mod}}(n,k)^2\, f_n(k)^2\,\mathrm{d}k \tag{C.27}$$

$$= \frac{2}{nK}\int P_{\mathrm{mod}}(n,k)^2\left(\cos\frac{\pi k}{K_n}\left[1 + 2\sum_{j=1}^{(n-1)/2}\cos 2j\frac{\pi k}{K}\right]\right)^2\mathrm{d}k$$

The cross terms of the *cosines* again integrate to zero, the remaining squares of *cosines* are expressed using a trigonometric identity,

$$= \frac{2}{nK}\int P_{\mathrm{mod}}(n,k)^2\,\cos\left(\frac{\pi k}{K_n}\right)^2\left[1 + 4\sum_{j=1}^{(n-1)/2}\cos\left(2j\frac{\pi}{K}k\right)^2\right]\mathrm{d}k \tag{C.28}$$

$$= \frac{2}{nK}\int_{-K/2}^{K/2} P_{\mathrm{mod}}(n,k)^2\,\cos\left(\frac{\pi k}{K_n}\right)^2\left[1 + 2\sum_{j=1}^{(n-1)/2}\left(1+\cos 4j\frac{\pi}{K}k\right)\right]\mathrm{d}k$$

$$= \frac{2}{nK}\int P_{\mathrm{mod}}(n,k)^2\,\cos\left(\frac{\pi k}{K_n}\right)^2\left[1 + 2\sum_{j=1}^{(n-1)/2}1\right]\mathrm{d}k \tag{C.29}$$

The sum is easily evaluated to $\sum_{j=1}^{(n-1)/2} 1 = (n-1)/2$,

$$= \frac{2}{nK} n \int_{-K/2}^{K/2} P_{\mathrm{mod}}(n,k)^2 \cos\left(\frac{\pi k}{K_n}\right)^2 \mathrm{d}k \tag{C.30}$$

$$= \frac{2}{K} n \int_{-K_n/2}^{K_n/2} k^2 \cos\left(\frac{\pi k}{K_n}\right)^2 \mathrm{d}k = \frac{2}{K_n} \int_{-K_n/2}^{K_n/2} k^2 \cos\left(\frac{\pi}{K_n} k\right)^2 \mathrm{d}k \tag{C.31}$$

The final expression is obtained by reducing the interval over which to evaluate the integral to the minimal period K_n, resulting in a factor of n that is placed in front of the integral. The final expression is indeed to Eq. (5.5). This concludes the proof for all even m.

C.3

Here we show the validity of Eq. (5.17). In order to establish the claim, we use show the equivalence of Eqs. (5.16) and (5.15), i.e. we confirm that

$$\sum_{i=-\infty}^{\infty} i^2 \,\mathsf{P}_j - \left(\sum_{i=-\infty}^{\infty} i \,\mathsf{P}_j \right)^2 = \sum_{i=-\infty}^{\infty} (i+1)^2 \,\mathsf{P}_j \,. \tag{C.32}$$

We do so using the following two results.

$$\sum_{i=-\infty}^{\infty} i \,\mathsf{P}_j = \sum_{i=-\infty}^{-1} i \,\mathsf{P}_j + \sum_{i=0}^{\infty} i \,\mathsf{P}_j = \sum_{i=1}^{\infty} (-i) \mathsf{P}_{i-1} + \sum_{i=0}^{\infty} i \,\mathsf{P}_j \tag{C.33}$$

$$= -\sum_{j=0}^{\infty} (j+1) \mathsf{P}_j + \sum_{i=0}^{\infty} i \,\mathsf{P}_j = \sum_{i=0}^{\infty} \left[i - (i+1) \right] \mathsf{P}_i = -\frac{1}{2} \tag{C.34}$$

This result is obtained assuming symmetric probability distributions, i.e. $|\psi(x)| = |\psi(-x)|$, which entails $\mathsf{P}_j = \mathsf{P}_{-i-1}$. A very similar calculation yields

$$\sum_{i=-\infty}^{\infty} i^2 \,\mathsf{P}_j = 2 \sum_{i=0}^{\infty} i^2 \,\mathsf{P}_j - \frac{1}{2} \tag{C.35}$$

Hence the left-hand side of Eq. (C.32) becomes

$$\sum_{i=-\infty}^{\infty} i^2 \,\mathsf{P}_j - \left(\sum_{i=-\infty}^{\infty} i \,\mathsf{P}_j \right)^2 = 2 \sum_{i=0}^{\infty} i^2 \,\mathsf{P}_j - \frac{3}{4}, \tag{C.36}$$

whereas the right-hand side of Eq. (C.32) becomes

$$\sum_{i=-\infty}^{\infty} (i+1)^2 \,\mathsf{P}_j = 2\sum_{i=0}^{\infty} i^2 \,\mathsf{P}_j - \frac{1}{2} + \left(\frac{-1}{2}\right)^2 + \frac{1}{4} \tag{C.37}$$

$$= 2\sum_{i=0}^{\infty} i^2 \,\mathsf{P}_j - \frac{3}{4}. \tag{C.38}$$

This shows the claimed proportionality of Eqs. (5.15) and (5.16). Note that we assume nothing about the illumination of the aperture, only that it be symmetrical about the origin.

C.4

Here we show how Eq. (5.19) is obtained. In order to simplify notation throughout the following calculation, we denote the limits of integration using $\alpha = jT - a/2$ and $\beta = jT + a/2$ and proceed to calculate

$$\Delta(Q,\Psi) = \sum_{j=1}^{m} \int_{\alpha}^{\beta} \frac{x^2 \mathsf{P}_j}{a}\,\mathrm{d}x - \left(\sum_{j=1}^{m} \int_{\alpha}^{\beta} \frac{x\,\mathsf{P}_j}{a}\,\mathrm{d}x\right)^2 \tag{C.39}$$

$$= \sum_{j=1}^{m} \mathsf{P}_j \int_{\alpha}^{\beta} \frac{x^2}{a}\,\mathrm{d}x - \left(\sum_{j=1}^{m} \mathsf{P}_j \int_{\alpha}^{\beta} \frac{x}{a}\,\mathrm{d}x\right)^2 \tag{C.40}$$

$$= \sum_{j=1}^{m} \mathsf{P}_j \left(\frac{a}{12} + j^2T^2\right) - \left(\sum_{j=1}^{m} \mathsf{P}_j jT\right)^2 \tag{C.41}$$

$$= \sum_{j=1}^{m} \mathsf{P}_j \frac{a}{12} + \sum_{j=1}^{m} \mathsf{P}_j j^2T^2 - \left(\sum_{j=1}^{m} \mathsf{P}_j jT\right)^2 \tag{C.42}$$

Here we use the fact that the probabilities P_j sum to unity in order to simplify the first term. We obtain

$$= \frac{a}{12} + \sum_{j=1}^{m} \mathsf{P}_j j^2T^2 - \left(\sum_{j=1}^{m} \mathsf{P}_j jT\right)^2 \tag{C.43}$$

$$= \frac{a}{12} + \Delta(Q,\Psi_\delta), \tag{C.44}$$

which is the desired result.

Appendix D

Calculations of Chapter 6

D.1

Here we calculate the $\omega_M(\psi_n)$ of Eq. (6.8). We proceed to calculate the autocorrelation function of $\widehat{\psi}_n$, using the dimensionless variable $\kappa = Tk/2$.

$$\int_{-\infty}^{\infty} \widehat{\psi}_n(k)\widehat{\psi}_n(k-s)\,\mathrm{d}k = \frac{2a}{nT\pi}\int \mathrm{sinc}\Big(\frac{a\kappa}{T}\Big)\,\mathrm{sinc}\Big(\frac{a}{T}(\kappa-s)\Big)\,f_n(\kappa)\,f_n(\kappa-s)\,\mathrm{d}\kappa \qquad \text{(D.1)}$$

where we are using the shorthand $f_n(k)$, which was introduced in Eq. (1.34), and the dimensionless variable $\kappa = Tk/2$. This integral may be decomposed into an infinite sum of integrals over the finite interval $K(=\pi$ in units of $\kappa)$,

$$= \frac{2a}{nT\pi}\sum_{j=-\infty}^{\infty}\int_{\left(j-\frac{1}{2}\right)\pi}^{\left(j+\frac{1}{2}\right)\pi} \mathrm{sinc}\Big(\frac{a}{T}\,\kappa\Big)\mathrm{sinc}\Big(\frac{a}{T}(\kappa-s)\Big)\,f_n(\kappa)\,f_n(\kappa-s)\,\mathrm{d}\kappa\,. \qquad \text{(D.2)}$$

We now substitute $u = \kappa - j\pi$ and immediately exploit the periodicity of f_n, i.e. that $f_n(\kappa+j\pi)^2 = f_n(\kappa)^2$,

$$= \frac{2a}{nT\pi}\sum_{j=-\infty}^{\infty}\int_{-\frac{\pi}{2}}^{\frac{\pi}{2}} \mathrm{sinc}\Big(\frac{a}{T}(u+j\pi)\Big)\mathrm{sinc}\Big(\frac{a}{T}(u+j\pi-s)\Big)f_n(u)f_n(u-s)\,\mathrm{d}u$$

$$= \frac{2a}{nT\pi}\int_{-\frac{\pi}{2}}^{\frac{\pi}{2}}\sum_{j=-\infty}^{\infty} \mathrm{sinc}\Big(\frac{a}{T}(u+j\pi)\Big)\mathrm{sinc}\Big(\frac{a}{T}(u+j\pi-s)\Big)f_n(u)f_n(u-s)\,\mathrm{d}u$$

The sum of the two *sinc* functions can be evaluated by means of general result adapted to the particular problem: According to Eq. (13) of Ref. [34],

$$\sum_{j=-\infty}^{\infty}\mathrm{sinc}(\alpha\,(v+j))\,\mathrm{sinc}(\alpha(w+j)) \qquad \text{(D.3)}$$

$$= \int_{-\infty}^{\infty} \operatorname{sinc}(\alpha\,(v+x))\,\operatorname{sinc}(\alpha(w+x))\;\mathrm{d}x \tag{D.4}$$

$$= \frac{\pi}{\alpha}\operatorname{sinc}(\alpha(v-w)) \tag{D.5}$$

The integration of the penultimate line can be evaluated to yield the final expression. Using the definitions

$$v = u/\pi, \qquad w = (u-s)/\pi, \qquad \alpha = a\pi/T\,, \tag{D.6}$$

we return to the expression that is to be evaluated and obtain

$$= \frac{2a}{nT\pi}\frac{T}{a}\operatorname{sinc}\Big(\frac{a}{T}s\Big)\int_{-\pi/2}^{\pi/2} f_n(u)f_n(u-s)\;\mathrm{d}u \tag{D.7}$$

$$= \frac{2}{n\pi}\operatorname{sinc}\Big(\frac{a}{T}s\Big)\int_{-\pi/2}^{\pi/2} f_n(u)f_n(u-s)\;\mathrm{d}u \tag{D.8}$$

$$= \frac{2}{n\pi}\operatorname{sinc}\Big(\frac{a}{T}s\Big)\frac{\pi}{2}f_n(s) = \frac{1}{n}\operatorname{sinc}\Big(\frac{a}{T}s\Big)f_n(s) \tag{D.9}$$

The special case: when $f_n(s) = 0$, there is no dependence on a. In regular units (k) this is the case for $s = \pi/nT$.

D.2

The calculation of $\omega_M(\phi_n)$ in Eq. (6.13) proceeds identically to the calculation provided in Appendix D.1, the only difference being that instead of f_n we consider H_n,

$$\widehat{H}_n(k) = \sum_{j=-\infty}^{\infty} \widehat{h}_n(k - jK)\,. \tag{D.10}$$

We calculate

$$\int_{-\infty}^{\infty} \widehat{\phi}_n(k)\widehat{\phi}_n(k-s)\;\mathrm{d}k \tag{D.11}$$

$$= \frac{2an}{\pi}\int \operatorname{sinc}\Big(\frac{ak}{2}\Big)\operatorname{sinc}\Big(\frac{a}{2}(k-s)\Big)\,H_n(k)\,H_n(k-s)\;\mathrm{d}k.$$

(All normalisation factors are removed from the integral, including those of H_n.) As previously, this integral may be decomposed into an infinite sum of

integrals over the finite interval K,

$$= \frac{2an}{\pi} \sum_{j=-\infty}^{\infty} \int_{\left(j-\frac{1}{2}\right)K}^{\left(j+\frac{1}{2}\right)K} \operatorname{sinc}\Big(\frac{a}{2}\,k\Big) \operatorname{sinc}\Big(\frac{a}{2}(k-s)\Big)\, H_n(k)\, H_n(k-s)\, \mathrm{d}k. \tag{D.12}$$

Upon substituting $u = k - jK$, the periodicity of H_n can be exploited, i.e. we use $H_n(k+jK)^2 = H_n(k)^2$,

$$= \frac{2an}{\pi} \sum_{j} \int_{-\frac{K}{2}}^{\frac{K}{2}} \operatorname{sinc}\Big(\frac{a}{2}(u+jK)\Big) \operatorname{sinc}\Big(\frac{a}{2}(u+jK-s)\Big) H_n(u) H_n(u-s)\ \mathrm{d}u$$

$$= \frac{2an}{\pi} \int_{-\frac{K}{2}}^{\frac{K}{2}} \sum_{j} \operatorname{sinc}\Big(\frac{a}{2}(u+jK)\Big) \operatorname{sinc}\Big(\frac{a}{2}(u+jK-s)\Big) H_n(u) H_n(u-s)\ \mathrm{d}u$$

The sum of the two *sinc* functions is evaluated as in Appendix D.1. We arrive at

$$= \frac{2an}{\pi} \frac{T}{a} \operatorname{sinc}\Big(\frac{a\pi}{T}\frac{s}{K}\Big) \int_{-K/2}^{K/2} H_n(u) H_n(u-s)\ \mathrm{d}u \tag{D.13}$$

$$= \frac{2nT}{\pi} \operatorname{sinc}\Big(\frac{a}{2}s\Big) \int_{-K_n/2}^{K_n/2} H_n(u) H_n(u-s)\ \mathrm{d}u \tag{D.14}$$

$$= \frac{1}{\pi} \operatorname{sinc}\Big(\frac{a}{2}s\Big) \left[\left(\pi - n\frac{T}{2}s\right) \cos n\frac{T}{2}s + \sin n\frac{T}{2}s\right] \tag{D.15}$$

$$= \operatorname{sinc}\Big(\frac{a}{2}s\Big) \left[\left(1 - \frac{s}{K_n}\right) \cos \pi\frac{s}{K_n} + \frac{1}{\pi} \sin \pi\frac{s}{K_n}\right] \tag{D.16}$$

This is the desired expression.

Appendix E

A mathematical observation

This part is somewhat different in its scope, dealing with an interesting mathematical observation. While this observation would serve as an alternative proof for Eq. (4.13), the flavour of this chapter is rather mathematical and the style different in accordance with the different subject matter.

E.1 Powers of 2 and odd numbers

Proposition

Every (positive) odd integer up to 2^d, with $d \in \mathbb{N}$, can be expressed uniquely in the form

$$2^{d-1} + c_{d-2}\, 2^{d-2} + c_{d-3}\, 2^{d-3} + \cdots + c_0\, 2^0 \tag{E.1}$$

with a particular set of coefficients c_n that are either -1 or $+1$.

Proof

This is shown easily using

$$2\cos(A)\cos(B) = \cos(A-B) + \cos(A+B)$$

1. Uniqueness: Each combination of coefficients in Eq. (E.1) results in a unique number. Assume to the contrary that there are two linear combinations that give the same odd number.

$$2^{d-1} + \sum_{i=0}^{d-2} c_i\, 2^i = 2^{d-1} + \sum_{j=0}^{d-2} c'_j\, 2^j$$

   Not all coefficients can be different, because then one number would be the negative of the other. Cancel all the terms that are equal. Arrange the remaining terms so that only positive terms appear by

moving the negative ones to the other side; the resulting sets of terms are denoted N and M. Any such term will have a coefficient of 2, which is henceforth absorbed into the exponent.

$$\sum_{n\in N} 2^{n+1} = \sum_{m\in M} 2^{m+1}$$

Divide by the smallest term. Without loss of generality it is assumed here that the smallest term occurs in the set N.

$$1 + \sum_{n\in N/\min(N)} 2^{n-\min(N)+1} = \sum_{m\in M} 2^{m-\min(N)}$$

That leaves a term +1 on the LHS, making the LHS an odd number. On the other hand, the RHS remains an even number. Contradiction.

2. Oddness: The linear combination of Eq. (E.1) results in odd integers only. All terms are even – and hence their sum is even – apart from $c_0\,2^0$, which is +1 or −1. Hence every linear combination gives an odd number.

3. Onto: There are $d-1$ coefficients, which can take two values. Hence there are 2^{d-1} linear combinations, which fit the 2^{d-1} odd numbers up to 2^d by using the previous results.

Hence there exists a bijection between the odd integers up to 2^d and the linear combinations of powers of two as specified in Eq. (E.1).

E.2 A construction

Observing a connection with binary numbers, it is possible to construct the linear combinations of Eq. (E.1) starting from 1 to 2^d in a manner very similar to constructing the binary expansions. Furthermore, an algorithm is provided for constructing a particular number without the entire construction procedure.

Consider a $d = 5$ system, i.e. $m = 2^d = 32$. In Table E.1, a list the odd numbers less than 2^d, their binary form and their linear combination coefficients is provided.

Starting at 1 and building up the binary form actually corresponds to the same iterative procedure used for obtaining the coefficients, only that the

Table E.1: An alternative representation of odd numbers

number	binary	coefficients
01	00001	$+----$
03	00011	$+---+$
05	00101	$+--+-$
07	00111	$+--++$
09	01001	$+-+--$
11	01011	$+-+-+$
13	01101	$+-++-$
15	01111	$+-+++$
17	10001	$++---$
19	10011	$++--+$
21	10101	$++-+-$
23	10111	$++-++$
25	11001	$+++--$
27	11011	$+++-+$
29	11101	$++++-$
31	11111	$+++++$

initial form for the number 1 is different. Furthermore, it is possible to obtain any single coefficient expansion without performing the entire iteration by means of directly translating a single binary expansion into a coefficient expansion. Working from left to right of the binary expansion, use the following algorithm: If the current digit is a

- 1, this translates into a $+$
- 0, move to the next digit until the current digit is a 1, write $0\ldots01$ as $+-\cdots-$

Then move forward by one digit and repeat the same procedure. An example, the binary expansion 0001 is translated into $+--$.

Appendix F

Numerical calculations

This chapter contains the Python code used to perform the numerical calculations referenced throughout the present text. This code is neither particularly sophisticated nor pleasant to read. It is, however, possible that others might find the availability of it useful.

The programming language Python was used, as it seems to offer an excellent compromise between convenience and performance. This is particularly true of the Enthought distribution of Python, provided through an academic licence, as it includes all the necessary software implemented in a single package.

F.1 The file GlobalDef.py

The file "GlobalDef.py" contains the values of important variables. These values of these variables are stored in a single location so that they can be accessed easily and changed conveniently.

```
1  from numpy import savetxt
2  from os.path import expanduser
3
4  d=10    # max value of d (as in m=2^d)
5  T=2     # slit separation
6  a=0.2     # slit width
7  kmax=5.0*10**3     # half the range of k
8  samps=2**20     # number of sample points
9  dk=2*kmax/samps     # spacing of sample points
10
11 GlobalDef = [d,T,a,samps,kmax,dk]
12
13 routeOut=expanduser("~/Documents/Python/data/...
       ...GlobalDef.txt")
14 savetxt(routeOut,GlobalDef)
```

F.2 Constructing wavefunctions $\widehat{\psi}_n(k)$

The momentum-space wavefunctions $\widehat{\psi}_n(k)$ are constructed and saved for further processing.

```
1  from numpy import linspace,sinc,sqrt,cos,savetxt,...
      ...loadtxt
2  from os.path import expanduser
3  from math import pi
4
5  home = expanduser("~/Documents/Python/data/")
6  routeIn = loadtxt("".join([home,"GlobalDef.txt"]))
7  [d,T,a,samples,kmax,dk] = routeIn
8  d=int(d)
9  samps=int(samples)
10 axis=linspace(-kmax,kmax,samps)
11
12 def psin(k,d): # This is a recursive function.
13     if d == 0:
14         return sqrt(a/(pi*T))*sinc((a/T)*k/pi)
15     else:
16         return sqrt(2)*cos((2**(d-1))*k)*psin(k,d...
              ...-1)
17
18 for j in range(1,d+1):
19     routeOut="".join([home,"Int_prod_",str(j),"....
          ...txt"])
20     savetxt(routeOut,psin(axis,j))
```

F.3 Constructing wavefunctions $\phi_n(k)$

The momentum-space wavefunctions $\widehat{\phi}_n(k)$ are constructed and saved for further processing.

```
1  from numpy import linspace,sinc,sqrt,cos,savetxt,...
      ...loadtxt,array
2  from os.path import expanduser
3  from math import pi
4  from scipy.integrate import simps
5
6  home = expanduser("~/Documents/Python/data/")
7  routeIn=loadtxt("".join([home,"GlobalDef.txt"]))
8  [d,T,a,samples,kmax,dk] = routeIn
9  d=int(d)
10 samps=int(samples)
11 axis=linspace(-kmax,kmax,samps)
12 K=2*pi/T
13
14 def env(k): # the fundamental envelope
15     return sinc((a/T)*k/pi)
16
17 counter=1
18 for b in [2**(-j) for j in range(d)]:
19     data=[]
20     for p in axis:
21         if cos(p)<0:
22             c=-1
23         else:
24             c=1
25         if p%K<K/2*b:
26            data+=[c*cos(p%K/b)]
27         elif p%K>=K-K/2*b:
28             data+=[c*cos((p%K/(1.0*b)-K/(1.0*b)))]
29         else:
30             data+=[0]
31     data2=array(data)
```

```
32      data2*=env(axis)
33      norm=sqrt(simps(data2**2,dx=dk))
34      data2/=norm
35      routeOut="".join([home,"Int_trig_",str(counter...
           ...),".txt"])
36      savetxt(routeOut,data2)
37      counter+=1
```

F.4 Computing $\Delta(P_{\mathrm{mod}}(n), \psi_n)$ and $\Delta(P_{\mathrm{mod}}, \psi_n)$

The standard deviation of the operators $P_{\mathrm{mod}}(n)$ and P_{mod} in state ψ_n is calculated and saved.

```
from numpy import linspace,sinc,sqrt,cos,savetxt,...
   ...loadtxt
from os.path import expanduser
from math import pi
from scipy.signal import sawtooth
from scipy.integrate import simps
home = expanduser("~/Documents/Python/data/")
routeIn=loadtxt("".join([home,"GlobalDef.txt"]))
[d,T,a,samples,kmax,dk] = routeIn
d=int(d)
samps=int(samples)
axis=linspace(-kmax,kmax,samps)

def psin(k,d):
    if d == 0:
        return sqrt(a/(pi*T))*sinc((a/T)*k/pi)
    else:
        return sqrt(2)*cos((2**(d-1))*k)*psin(k,d...
           ...-1)
def saws(k,d): # the operator P_mod(n)
    return pi/2**(d-1)/2*sawtooth(2**(d-1)*2*(k-pi...
       .../2/2**(d-1)))

resAda = [[j,sqrt(simps(psin(axis,j)**2*saws(axis,...
   ...j)**2,dx=dk))] for j in range(1,d+1)]
resReg = [[j,sqrt(simps(psin(axis,j)**2*saws(axis...
   ...,1)**2,dx=dk))] for j in range(1,d+1)]

routeOutReg = "".join([home,"Pmod_prod_reg.txt"])
savetxt(routeOutReg, resReg)
routeOutAda = "".join([home,"Pmod_prod_ada.txt"])
savetxt(routeOutAda, resAda)
```

F.5 Computing $\Delta(P_{\text{mod}}, \phi_n)$

The standard deviation of the operator P_{mod} in state ϕ_n is calculated and saved.

```
1  from numpy import linspace,sqrt,savetxt,loadtxt
2  from os.path import expanduser
3  from math import pi
4  from scipy.signal import sawtooth
5  from scipy.integrate import simps
6
7  home = expanduser("~/Documents/Python/data/")
8  routeIn=loadtxt("".join([home,"GlobalDef.txt"]))
9  [d,T,a,samples,kmax,dk] = routeIn
10 d=int(d)
11 samps=int(samples)
12 axis=linspace(-kmax,kmax,samps)
13
14 def saws(k,d):
15     return pi/2**(d-1)/2*sawtooth(2**(d-1)*2*(k-pi...
          .../2/2**(d-1)))
16
17 FineStructure=[]
18
19 for j in range(1,d+1):
20     routeIn="".join([home,"Int_trig_",str(j),".txt...
          ..."])
21     data = loadtxt(routeIn)**2
22     FineStructure.append([j,sqrt(simps(data*saws(...
          ...axis,1)**2,dx=dk))])
23
24 routeOutReg = "".join([home,"Pmod_trig.txt"])
25 savetxt(routeOutReg, FineStructure)
```

F.6 Computing $\omega_M(\psi_n)$ and $\omega_M(\phi_n)$

The mean fringe widths of the states ψ_n and ϕ_n are computed and saved.

```
1  from numpy import loadtxt, savetxt, linspace
2  from math import pi
3  from os.path import expanduser
4  from scipy.integrate import simps
5
6  home = expanduser("~/Documents/Python/data/")
7  routeIn=loadtxt("".join([home,"GlobalDef.txt"]))
8  [d,T,a,samples,kmax,dk] = routeIn
9  samps=int(samples)
10 d=int(d)
11 axis=linspace(-kmax,kmax,samps)
12
13 MaxiIntFS = pi/2
14 IntFSstep = 15
15
16 pAxisShort = linspace(-kmax,kmax,samps)[samps/2:]
17
18 for case in ['prod','trig']:
19     for j in range(1,d+1):
20         routeIn="".join([home,"Int_",str(case),"_"...
               ...,str(j),".txt"])
21         routeOutProd = "".join([home,"Int_",str(...
               ...case),"_mpw_",str(j),".txt"])
22         data = loadtxt(routeIn)
23         wlist = []
24         prev=10
25         for n in range(0,int(MaxiIntFS/dk),...
               ...IntFSstep):
26             value = simps(data[(n+1):].conjugate()...
                   ...*data[:-(n+1)],dx=dk)
27             if prev<=abs(value):
28                 break
```

```
29              wlist.append([pAxisShort[(n+1)],abs(...
                   ...value)])
30              prev=abs(value)
31          savetxt(routeOutProd, wlist)
```

F.7 Performing the Fourier transform of $\widehat{\psi}_n(k)$ and $\widehat{\phi}_n(k)$

The inverse Fourier transform of the wavefunctions $\widehat{\psi}_n(k)$ and $\widehat{\phi}_n(k)$ is computed and saved.

```
1  from numpy.fft import rfft,fftfreq,fftshift
2  from numpy import loadtxt, savetxt
3  from math import sqrt,pi
4  from os.path import expanduser
5  from scipy.integrate import simps
6  home = expanduser("~/Documents/Python/data/")
7
8  routeIn=loadtxt("".join([home,"GlobalDef.txt"]))
9  [d,T,a,samples,kmax,dk] = routeIn
10 d=int(d)
11 samps=int(samples)
12 N=int(samples)
13 xAxis = fftshift(fftfreq(samps,dk))*2*pi
14 dX=xAxis[samples/2+1]
15
16 for case in ["prod","trig"]:
17     for j in range(1,d+1):
18         routeIn="".join([home,"Int_",str(case),"_"...
               ...,str(j),".txt"])
19         routeOut="".join([home,"Img_",str(case),"_...
               ...",str(j),".txt"])
20         dataIN = loadtxt(routeIn)
21         dataFT = rfft(dataIN)
22         dataFT /= sqrt(simps(abs(dataFT)**2,dx=dX)...
               ...)*sqrt(2)
23         savetxt(routeOut,dataFT.view(float))
```

F.8 Computing $\Delta(Q_T, \psi_n)$ and $\Delta(Q_T, \phi_n)$

The standard deviation of the operator Q_T in states ψ_n and ϕ_n is calculated and saved.

```
1  from numpy import loadtxt,abs,floor,savetxt,...
       ...concatenate
2  from os.path import expanduser
3  from numpy.fft import fftfreq, fftshift
4  from math import pi,sqrt
5  from scipy.integrate import simps
6
7  home = expanduser("~/Documents/Python/data/")
8  routeIn=loadtxt("".join([home,"GlobalDef.txt"]))
9  [d,T,a,samples,kmax,dk] = routeIn
10 d=int(d)
11
12 samples = int(samples)
13 xAxis = fftshift(fftfreq(samples,dk))*2*pi
14 stairs = 2*floor(xAxis/2)
15 stairs2=stairs**2
16
17 for case in ['prod','trig']:
18     QT=[]
19     for j in range(1,1+d):
20         routeInProd = "".join([home,"Img_",str(...
               ...case),"_",str(j),".txt"])
21         temp=abs(loadtxt(routeInProd).view(complex...
               ...))**2
22         data=concatenate((temp[1:-1][::-1]....
               ...conjugate(),temp))
23         data/=simps(data,dx=dk)
24         QT.append([j,sqrt(simps(data*stairs2,dx=dk...
               ...)-simps(data*stairs,dx=dk)**2)])
25     routeOut="".join([home,"QT_",str(case),".txt"...
           ...])
26     savetxt(routeOut,QT)
```

F.9 Computing $\Omega_N(\psi_n)$ and $\Omega_N(\phi_n)$

The overall widths of states ψ_n and ϕ_n are computed and saved.

```
from numpy import loadtxt, savetxt, concatenate,...
   ...linspace
from math import pi
from numpy.fft import fftfreq, fftshift
from os.path import expanduser
from scipy.integrate import simps

home = expanduser("~/Documents/Python/data/")
routeIn=loadtxt("".join([home,"GlobalDef.txt"]))
[d,T,a,samples,kmax,dk] = routeIn
samps=int(samples)
d=int(d)

axis=linspace(-kmax,kmax,samps)
MaxiImgOWliste = [5,20,20,20,20,30,30,30,100,150]
ImgOWstep = 10
xAxis = fftshift(fftfreq(samps,dk)*2*pi)
dX=xAxis[samples/2+1]

p1=samps/2-1
p2=samps/2-1+int(2/2/dX)

def SR3(liste):
    prev=0
    OWs=[]
    for i in range(1,int(MaxiImgOW/2/dX),ImgOWstep...
       ...):
        ow1=simps(liste[p1-i:p1+i],dx=dX)
        ow2=simps(liste[p2-i:p2+i],dx=dX)
        if ow1>ow2:
            if ow1-prev>0.01:
                OWs.append([xAxis[p1+i]-xAxis[p1-i...
                   ...],ow1])
```

```
31                  prev=ow1
32          else:
33              if ow2-prev>0.01:
34                  OWs.append([xAxis[p1+i]-xAxis[p1-i...
                       ...],ow2])
35                  prev=ow2
36      return OWs
37
38  for case in ['prod','trig']:
39      for i in range(1,d+1):
40          MaxiImgOW=MaxiImgOWliste[i-1]
41          routeInProd = "".join([home,"Img_",str(...
               ...case),"_",str(i),".txt"])
42          data0 = loadtxt(routeInProd).view(complex)
43          data = concatenate((data0[1:-1][::-1]....
               ...conjugate(),data0))
44          dataOWs = abs(data)**2
45          routeOutOW = "".join([home,"Img_",str(case...
               ...),"_OW_",str(i),".txt"])
46          savetxt(routeOutOW, SR3(dataOWs))
```

Symbols

- a denotes the slit width
- χ_A is the spectral projector onto the set A, defined on 11
- $\Delta(O, \Psi)$ denotes the standard deviation of the operator O in state Ψ; see Eq. (1.4)
- $\mathcal{F}$ denotes the operator effecting the Fourier transform; see Eq. (1.22)
- $K = 2\pi/T$; defined in Eq. (1.10)
- $K_n = 2\pi/(nT) = 4\pi/(mT)$; defined in Eqs. (1.9)
- K' is introduced following Eq. (2.10)
- $\kappa = Tk/2$, a conveniently rescaled variable; used Chapter 4 and in the Appendix
- $\Omega_N(\Psi)$ denotes the overall width of state Ψ
- $\omega_M(\Psi)$ denotes the mean fringe width of state Ψ; see Eq. (6.2)
- $\mathcal{P}$ denotes the momentum observable
- P denotes the momentum operator
- P_{mod} is the "modular" momentum operator; see Eq. (3.5) and also see Fig. 3.1 (b) for an illustration
- $P_{\text{mod}}(n)$ is the refined "modular" momentum operator; see Eq. (5.2)
- P_K is a coarse momentum observable, defined using Eqs. (3.2) and (3.5)
- $\widehat{\Psi}$ denotes the Fourier transform of Ψ; Eq. (1.22)

- $\mathcal{Q}$ denotes the position observable
- Q denotes the position operator
- Q_{mod} is the "modular" position operator; see Eq. (3.4)
- Q_T is a coarse position observable, defined using Eqs. (3.1) and (3.4); see Fig. 3.1 (a)
- Ш_L denotes the Dirac comb
- $\mathrm{sinc}(x) = (\sin x)/x$
- T denotes the slit separation; see Fig. 1.1
- ζ_d is notation defined in Eq. (4.1) and used throughout Chapter 4

References

[1] Y. Aharonov, H. Pendleton and A. Petersen,
Int. J. Theor. Phys. **2**, 213 (1969).

[2] J. B. M. Uffink and J. Hilgevoord, Found. Phys. **15**, 925 (1985).

[3] S. S. Afshar, E. Flores, K. F. McDonald and E. Knoesel,
Found. Phys. **37**, 295 (2007).

[4] P. Busch and P. J. Lahti, Phys. Lett. A **115**, 259 (1986).

[5] J. C. G. Biniok and P. Busch, Phys. Rev. A **87**, 062116 (2013).

[6] J. C. G. Biniok, P. Busch and J. Kiukas,
Phys. Rev. A **90**, 022115 (2014).

[7] A. Einstein, B. Podolsky and N. Rosen, Phys. Rev. **47**, 777 (1935).

[8] M. F. Pusey, J. Barrett and T. Rudolph, Nat. Phys. **8**, 476 (2012).

[9] D. Bohm, Phys. Rev. **85**, 166 (1952).

[10] H. Everett, Rev. Mod. Phys. **29**, 454 (1957).

[11] J. von Neumann, *Mathematical Foundations of Quantum Mechanics*,
2nd ed. (Princeton University Press, Princeton, 1955), p. 445.

[12] H. Weyl, *Gruppentheorie und Quantenmechanik, 1928*, 1st ed.
(Hirzel, Leipzig, 1929), p. 288.

[13] W. Heisenberg, Zeitschrift für Phys. **43**, 172 (1927).

[14] E. H. Kennard, Zeitschrift für Phys. **44**, 326 (1927).

[15] H. Robertson, Phys. Rev. **34**, 163 (1929).

[16] E. Schrödinger, Phys. Rev (1930).

[17] P. Busch, P. Lahti and R. F. Werner,
Phys. Rev. Lett. **111**, 160405 (2013).

[18] G. Möllenstedt and C. Jönsson, Zeitschrift für Phys. **155**, 472 (1959).

[19] C. Jönsson, Zeitschrift für Phys. **161**, 454 (1961).

[20] M. Arndt, O. Nairz, J. Vos-Andreae, C. Keller, G. van der Zouw and A. Zeilinger, Nature **401**, 680 (1999).

[21] H. Reiter and W. Thirring, Found. Phys. **19**, 1037 (1989).

[22] J. C. G. Biniok, P. Busch and J. Kiukas, unpublished.

[23] C. J. Corcoran and K. A. Pasch,
J. Phys. A. Math. Gen. **37**, L461 (2004).

[24] B.-G. Englert, Phys. Rev. Lett. **77**, 2154 (1996).

[25] Y. Aharonov and D. Rohrlich,
Quantum Paradoxes: Quantum Theory for the Perplexed
(John Wiley & Sons, 2008), p. 299.

[26] J. Tollaksen, Y. Aharonov, A. Casher, T. Kaufherr and S. Nussinov, New J. Phys. **12**, 013023 (2010).

[27] C. Gneiting and K. Hornberger, Phys. Rev. Lett. **106**, 210501 (2011).

[28] D. Judge and J. Lewis, Phys. Lett. (1963).

[29] L. Susskind and J. Glogower, English,
Phys. Discontin. with Vol. 4, no. 1, 1968 (1964).

[30] P. Carruthers and M. M. Nieto, Rev. Mod. Phys. **40**, 411 (1968).

[31] G. Bonneau, J. Faraut and G. Valent, Am. J. Phys. **69**, 322 (2001).

[32] A. B. Bhatia and K. S. Krishnan,
Proc. R. Soc. A Math. Phys. Eng. Sci. **192**, 181 (1948).

[33] H. J. Landau and H. O. Pollak, Bell Syst. Tech. J. **40**, 65 (1961).

[34] R. P. Boas and H. Pollard, Am. Math. Mon. **80**, 18 (1973).